Multiferroic oxide-based thin films applied to magnetic refrigeration

Hamza Bouhani

THÈSE

Pour l'obtention du titre de :

DOCTEUR de L'UNIVERSITÉ DE LORRAINE ET DE L'UNIVERSITÉ MOHAMMED V DE RABAT

Spécialité : Physique

Présenté par :

Hamza BOUHANI

Couches minces à base d'oxyde multiferroïque appliquées à la réfrigération magnétique

---

Thèse publiquement soutenue à Rabat le 03-10-2020 devant le Jury suivant :

M. Abdelmajid AINANE	Professeur, Université de Moulay ismail	Rapporteur
M. Abdelkader OUTZOURHIT	Professeur, Université Cadi AYYAD de Marrakech	Rapporteur
Mme. Hélène FISCHER	Professeur, Université de Lorraine	Examinatrice
M. Abdelilah BENYOUSSEF	Professeur, Académie Hassan II de Rabat	Examinateur
M. Mohamed BALLI	Professeur, Université internationale de Rabat	Examinateur
M. Omar MOUNKACHI	Professeur, Université Mohammed V de Rabat	Invité
M. Abdallah EL KENZ	Professeur, Université Mohammed V de Rabat	Directeur de thèse
M. Stéphane MANGIN	Professeur, Université de Lorraine	Directeur de thèse

Abstract

Energy is essential for humans in everyday life and critical to economic growth and developement progress in industrial sectors. The global energy sources are mostly from fossil resources (e.g oil, coals, gas) being dominant source of local air pollution and emitter of the most dangerous green house gases such as carbon dioxide (CO_2), largely responsible for the ozone layer depletion. In the context of the current shortage of those ressources due to the continuously increase in demands in energy and while fossil reserves will eventually run out, the discovery and development of a low-carbon technologies become critical with the need to decarbonise and reduce our dependency to fossil fuels. One of theses technologies is the magnetic refrigeration based on the magnetocaloric effect (MCE). In this thesis, we have investigated the magnetic and magnetocaloric properties of strongly correlated oxides thin films grown by pulsed laser deposition in view of their portential application in magnetic cooling**.** The obtained results reveal that the magnetic and magnetocaloric properties of $PrVO_3$ (PVO) compounds can be easy tailored by using the thin films approach. Particularly, the coercive magnetic field was dramatically decreased making from the PVO compound a nearly soft magnet in the region where the magnetic entropy change is released as well as a considerable increase in saturation magnetization. Accordingly, a giant magnetocaloric effect is exhibited by PVO thin films grown on LSAT substrate at low temperatures showing the great impact of strain effects. This finding opens the way for the implementations of PVO thin films in some specific applications such as on-chip magnetic cooling of a nanoelectronic device and sensor technology. On the other hand, the DFT calculations have confirmed the ground state and the competition between magnetic interactions under compressive strains in PVO thin films. Our result not only suggests that epitaxial PVO thin films is potential for refrigeration at cryogenic temperatures but may also pave the way to create many novel functionalities in perovskite-type transition metal oxides by control of structural aspects.

The mechanisms leading to the giant anisotropic magnetocaloric effect observed in $HoMn_2O_5$ single crystals are also studied. Both DFT calculations and Monte Carlo simulation allowed us to explore the role of Holmium ions as the main contributor to the MCE as well as the of the importance of the intrinsic anisotropic properties as a promising way to optimize the MCE for magnetic refrigeration application at low temperature regime as well as the implementation of compact and efficient rotary magnetic refrigerators.

KEY-WORDS: Thin films, magnetic refrigeration, magnetocaloric effect, DFT, multiferroic

Résumé

L'énergie est indispensable pour l'homme dans la vie quotidienne et essentielle à la croissance économique et au progrès du développement dans les secteurs industriels. Les sources d'énergie mondiales proviennent principalement de ressources fossiles (pétrole, charbons, gaz) qui sont la principale source de pollution atmosphérique locale et l'émetteur des gaz à effet de serre comme le dioxyde de carbone (CO_2), responsable en grande partie de l'appauvrissement de la couche d'ozone. Dans le contexte de la pénurie actuelle de ces ressources en raison de l'augmentation continue de la demande d'énergie et alors que les réserves fossiles finiront par s'épuiser, la découverte et le développement d'une technologie à faible émission de carbone deviennent critiques avec la nécessité de décarboniser et réduire notre dépendance aux combustibles fossiles. Une de ces technologies est la réfrigération magnétique basée sur l'effet magnétocalorique (MCE). Au cours de cette thèse, nous avons étudié les propriétés magnétiques et magnétocaloriques des films minces d'oxydes fortement corrélés à structure pérovskite deposés par ablation laser pour les applications de la réfrigération magnétique. Les résultats obtenus montrent que les propriétés magnétiques et magnétocaloriques de composés $PrVO_3$ peuvent être facilement modulées en utilisant l'approche des couches minces. En particulier, le champ magnétique coercitif a considérablement diminué faisant à partir du composé PVO un aimant presque doux dans la région où l'entropie magnétique est libérée ainsi qu'une augmentation considérable de l'aimantation de saturation. En conséquence, un effet magnétocalorique géant est présentée par les films minces de PVO déposés sur un substrat de LSAT à basse température montrant l'impact de l'effet des contraintes épitaxiales. D'autre part, les calculs DFT ont confirmé l'état fondamental et la compétition entre les interactions magnétiques sous contraintes de compression dans PVO films minces. Notre résultat suggère non seulement que les couches minces épitaxiales de PVO sont potentielles pour la réfrigération aux températures cryogéniques mais peuvent également ouvrir la voie à créer de nombreuses nouvelles fonctionnalités dans les oxydes perovskite par le contrôle des aspects structurels.

Les mécanismes menant à l'effet magnétocalorique anisotropique géant observé dans

les monocristaux du $HoMn_2O_5$ sont également étudiés. Les calculs DFT et la simulation de Monte Carlo nous ont permis d'explorer le rôle des ions d'Holmium en tant que principal contributeur au MCE ainsi que l'importance des propriétés anisotropes intrinsèques comme moyen prometteur d'optimiser l'EMC pour l'application de la réfrigération magnétique à basse température ainsi que la mise en ¡uvre de réfrigérateurs magnétiques rotatifs compacts et efficaces.

MOTS-CLEFS : Couches minces, réfrigération magnétique, DFT, effect magnétocalorique, multiferroique

Aknowlegdments

Je tiens tout d'abord à remercier sincèrement les membres du jury **Mr Abdelmajid Ainane, Mr Abdelkader Outzourhit, Mme Hélène Fischer, Mr Abdelilah Benyoussef and Mr Mohamed Balli** pour avoir accepté d'examiner mon travail et pour leurs remarques sur le manuscrit.

Par ailleurs, je voudrais remercier tous les membres de l'équipe 101 - nanomagnétisme et Spintronics et de l'équipe LaMCScI - Laboratoire de Matière Condensée et Sciences Interdisciplinaires qui ont fait de ces années de thèse une magnifique expérience. Je tiens tout particulièrement à remercier **Mr Stéphane Mangin**, professeur à l'Université de Lorraine, et **Mr Abdallah El Kenz**, professeur à l'Université Mohammed V de Rabat, pour leur soutien et les conseils qu'ils ont su m'apporter durant ma thèse. Je voudrais leur adresser mes remerciements les plus chaleureux pour la confiance qu'ils m'ont accordée, la rigueur et la qualité avec laquelle ils ont su encadrer mon travail. Il m'ont transmis leur passion et leurs connaissances ainsi que l'esprit critique et scientifique. Les nombreuses discussions que nous avons eues tout au long de ces travaux m'ont permis d'effectuer ce travail de thèse dans de très bonnes conditions. Je leur adresse ici ma sincère et profonde reconnaissance.

Je voudrais exprimer mes remerciements particuliers ainsi que ma profonde gratitude à mon co-direceur **Mr Abdelilah Benyoussef**, membre résident de l'Académie Hassan II des Sciences et Techniques à Rabat, pour son enseignement et son encadrement. Grâce à lui et a l'aide de sa rigueur scientifique et sa large expérience dans le domaine de la physique, j'ai appris les approches d'analyse de la matière condensée et de l'interprétation des résultats et j'ai entamé le chemin de la recherche scientifique. Tout au long de ce mémoire, ses conseils avisés, ses critiques pertinentes et ses qualités humaines m'ont été d'une très grande utilité et ont permis à mon travail d'aboutir et de voir le jour.

Ensuite, je voudrais exprimer aussi toute ma gratitude à **Mr Olivier Copie**, chercheur à l'Institut Jean Lamour, qui a su me familiariser avec les mesures magnétiques des oxydes. Il a été disponible pour répondre à mes nombreuses questions et pour cela je suis trés reconnaissant.

Je remercie particulièrement **Mr Mohamed Balli**, professeur à l'Université International de Rabat, pour la qualité des remarques et les discussions des résultats ainsi que pour son expertise expérimentale. J'ai beaucoup apprecié nos discussions fructueuses via Google Meet.

Je tiens aussi à remercier **Mr Omar Mounkachi**, Professeur à la Faculté des Sciences, Université Mohammed V de Rabat, pour les conseils utils et ses suggestions stimulantes tout au long de ce projet de thèse. Mes remerciements vont par ailleurs à **Mme Halima Zaari** qui n'a cessé d'être disponible pour apporter une aide et une meilleure compréhension théorique. Un grand merci à Dr. Crosby Soon Chang pour son conseil concernant la mesure des propriétés magnétiques.

J'adresse un grand merci à tous les thésards et ex-thésards des deux laboratoires pour leur ambiance chaleureuse et dynamique pendant les années passés: **Ayoub Bourjilat, Mohammed Salah el hadri, Hind Benzidi, Houssam Eddine Kacimi, Boyu Zhang, Kosseila Ait Oukaci, Maryam Massouras, Charles Guillemard, Thibaud Fache**. Je remercie infiniment **Asmaa Endichi** avec qui j'ai partagé tant de bons moments au Maroc comme en France.

Je remercie la Partenariat Hubert-Curien (PHC) Toubkal et l'Agence Univesitaire de la Francophonie pour le support de financement pendant mes recherches en France.

Enfin, et pas des moindres, j'adresse mes sincères remerciements à mes très chers parents. Je vous remercie vivement pour tout le soutien et l'amour que vous me portez depuis mon enfance et j'espère que votre bénédiction m'accompagne toujours. Que ce modeste travail soit l'exaucement de vos v¡ux tant formulés, le fruit de vos innombrables sacrifices, bien que je ne vous en acquitterai jamais assez.

Dedication

I dedicate this manuscript to

My parents

My sisters Mariam, Leila and Salma

To the memory of my grand parents

Contents

General introduction

Energy is essential for humans in everyday life and critical to economic growth and developement progress in industrial sectors. The global energy sources are mostly from fossil resources (e.g oil, coals, gas) being dominant source of local air pollution and emitter of the most dangerous green house gases such as carbon dioxide (CO_2), largely responsible for the ozone layer depletion. In the context of the current shortage of those ressources due to the continuously increase in demands for energy and while fossil reserves will eventually run out, the discovery and development of a low-carbon technologies become critical with the need to decarbonise and reduce our dependency to fossil fuels.

One of the most energy-intensive industries is the refrigeration industry. Refrigeration is a basic need in our everyday life, retail food, household, air-conditioning and transportation sectors. Besides, refrigeration is essential in the production and manufacturing sectors requiring low temperatures to keep food fesh for longer. Indeed, the energy usage for cooling systems is reported to be more than one-fifth of the world global energy consumption clearly demonstrating the powerful impact and importance of refrigeration on the world's energy usage. At present, vapor compression system is the most widely-used refrigeration system which benefit typically from the difference in energy between gas and liquid to provide cooling through an expansion and compression process of a refrigerant fluid giving birth to freon gases such as chlorofluorocarbons (CFCs) and hydrochlor fluorocarbons (HCFCs) known as the major cause of global warming effect. Indeed, according to a recent study [1], HCFCS is predicted to reach 46% of global CO_2 emissions by 2050, presenting major threats for planet earth and forcing key environmental organizations, such as US environmental protection agency (EPA) to announce a protocol aimed at becoming HCFC-free in 2020 [17]. Moreover, conventional system requires high electrical energy consumption to ensure the pressurizing of the refrigerant. This high energy comes with low efficiency since the pressurizing process is irreversible and thus the overall cooling/heating process of the gaz compression system reveal a less than 10% of Carnot cycle efficiency causing a significant waste of energy. Even so this technique is mature and provide relatively low manufacturing costs, it has almost reaches its maximum theoretical

energy efficiency potentiel and no further improvements are possible. In the light of these considerations, the developement of a new innovative and clean refrigeration system that ensure a high efficiency becomes unavoidable.

Nowadays, eyes turned to a solid-state cooling system being a new green technology that could replace conventional vapor compression technique : magnetic refrigeration system. Magnetic refrigeration rely on the reversible thermal phenomena triggered in solids when subjected to a magnetic field and known under the name of the magnetocaloric effect (MCE). It is a potentially low carbon technology [7, 8] whose performance can achieve 60% of Carnot cycle [18]. In fact, the idea of using the magnetic refrigeration as a replacement of conventional gas compressions systems is actually nothing new. For the last 30 years, researchers have been searching for clean materials that can generate a giant magnetocaloric effect cyclically acted upon. And while encouraging materials exists, even to the point that a well designed prototype devices have been deployed at industry shows over the past few years, affodability remains a major obstacle preventing the leap into marketable technology. Actually, the increase interest in magnetic refrigeration is driven also by the future positive market overview. Indeed, according to a 2019 research study [9], the global market magnetic refrigeration is projected to reach 702.20 million USD by 2025 being valued at only 1.14 USD in 2016 offering a huge opportunity to the magnetic refrigeration technology to reach a new level in its development.

Recently, The magnetocaloric effect in manganite-based perovskites exhibiting multiferroic behaviors have become an interesting topic because of the potential application of these oxides in some specific applications such as the liquefaction of hydrogen and and space industry. These manganite perovskites oxides fulfill the necessary conditions for practical applications as they unveil a large corrosion resistance, high electric resistance, low hysteresis and mechanical stability. Conversly, the magnetocaloric potential of the RVO_3vanadates has not yet been explored except the bulk $HoVO_3$. However, perovskite-type vanadium oxides RVO_3 display a great variety of phase transitions associated with a series of charge, spin and orbital ordering phenomena making them interesting candidates from a magnetocaloric point of view.

Today's research activities on magnetocaloric thin films attract a wide interest due to their potential integration in miniaturized electronic devices. This particulary motivated us to investigate using both experimental and theoretical techniques the magnetocaloric in RVO_3 thin films since their behavior strongly depends on the cooperative nature of the Jahn-Teller distortion making them sensitive strain effects. Such structural effects tends to play an important role in tuning the film properties.

This manuscript is devided into four chapters. First, a state of the art of the magnetic

refrigeration and its devlopement over the years and a short review of multiferroic materials will be presented. In the second chapter, all the experimental and theoretical techniques used to fabricate and magnetically characterize the samples as well as the calculations that leads to the study of the magnetocaloric effect are detailed. In the third chapter, we report a combinaison of both experimental and theoretical investigations demonstrating that the magnetic and magnetocaloric properties of $PrVO_3$compounds could be easily tailored by using thin films approach. In the last chapter, the physics behind the giant magnetocaloric effect observed in $HoMn_2O_5$ single crystals are studied using both DFT calculation and Monte Carlo simulation.

Chapter 1

Literature review

1.1 Introduction - what is all about

During the United Nations conference on climate change Paris 2015, the world leaders negotiated to limit climate warming to less than 2řC by 2100. The discussions aimed at avoiding the serious climatic catastrophes in the world and the participants sought to retard greenhouse gases by increasing the use of technologies with zero carbon. One of theses technologies is the magnetic refrigeration which is an emergent, innovating and potentially low carbon technology[7, 8]. Interest for new technology of heating or cooling -and like alternative to conventional compression of the vapor increased considerably during the 15 last years. The principle of the magnetic refrigeration is based on a phenomenon known under the name of magnetocaloric effect (MCE) which is an intrinsic property of certain magnetic materials which results in a change of their thermal state during the variation of their magnetic state induced by an external magnetic field. Currently, Gadolinium Gd is the magnetic material used vast majority of magnetic cooling prototypes, mainly due to its magnetic phase transition taking place at 294 K leading to excellent magnetocaloric properties close to room temperature. However, this metal present multiple disadvantages such as its easy oxidation as well as the limitation of its working temperature range close to the room temperature. In addition, gadolinium cannot be used in large scale applications because of its high cost. These issues have motivated the scientists to search for new less expensive and clean materials with a high magnetocaloric effect under moderate magnetic fields such as intermetallic alloys, perovskites and double perovskites containing manganese and spinels that could be implemented in magnetic refrigeration technology. Therefore, this chapter 1, consists in a state of the art and the fundamental aspects of the magnetic refrigeration as well as the discussion of the several several challenges to be overcome before having devices that are competitive with

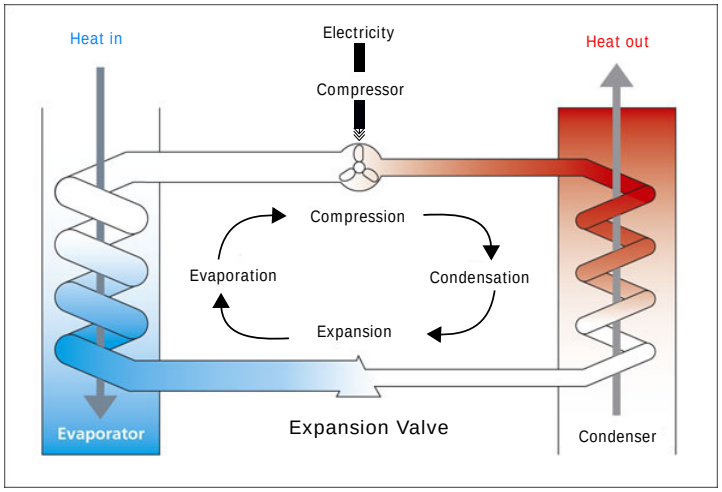

Figure 1.1: Typical vapour compression cycle consisting of four primary components: evaporator, condenser, compressor and expansion valve. Figure adapted from [21]

conventional gas–vapor refrigerants . The fundamental backround of multiferroics and their common features are presented in section 1.2. In section 1.3 and 1.4, the two types of multiferroics are adressed.

1.1.1 Magnetic refrigeration

Brief historic

The origin of the magnetocaloric effect used in magnetic refrigeration goes back more than a century to exactly when a reversible heating of a Nickel sample close to its curie temperature (627 K) when placed in a magnetic field is dicovered by Piccard and Weiss in 1917 [10, 11]. Debeye (1926) [12] and Giaque (1927) [13] independently suggested a possible utilization of this effect at ultra-low temperatures (< 1 K). We had to wait 13 years before the first experimental demonstration of an adiabatic demagnetization of gadolinium sulphate down to 0.24 K by Giauque and MacdDougall [14] followed by the construction of the first magnetic refrigeration system close to room temperature in 1976 using Gadolinium as a magnetic refrigerant.[15]. Since then, the field of room-temperatures magnetic refrigeration has progressed dramatically together with the discovery of giant magnetocaloric materials in the 90's [16] which is of particular interest from an applications development perspective for everyday life.

In contrast to conventional systems where the heating and cooling process is a result

of the compression and expansion of the refrigerant fluid as shown in figure 1.1, magnetic refrigeration based on the magnetocaloric effect consists on heating and cooling when a materials is subjected to an applied magnetic field. Figure 1.2 illustrates the principle of the magnetic refrigeration : when a magnetic field is applied, the materials responds with a change in temperature, the heat is transfered then from or to the refrigerant by the heat exchange fluid at appropriate parts of a magnetic cooling cycle meaning that we can benefit from the magnetocaloric technology in both cooling applications such as refrigeration and heating applications like clothes dryers. Moreover, the reverse magnetocaloric effect can be utilized to generate electricity by recovering the the low-grade waste heat that can converted to electricity using thermomagnetic generators [19, 20].

It is clear that the applied magnetic field tends to align the magnetic spins (represented by arrows) in the refrigerant material. The fact that the increase in temperature by ordering a material might seem counterintuitive for those familiar with the concept of entropy as more order in general means lower temperature. Nevertheless, it is exactly the idea behind magnetic refrigeration since in magnetic materials, one can expect three different contributions to the entropy, a lattice, magnetic and electronic entropy (S_L, S_M and S_E), respectively. S_L and S_E are essentially independent of magnetic fields, whereas S_M is lowered due to ordering of the magnetic spins. That was the intuitive part, high entropy means high disorde, however, when S_M decreases S_L increases in adiabatic conditions. The increase in S_L means an increase in the temperature and that is how the magnetic refrigeration works.

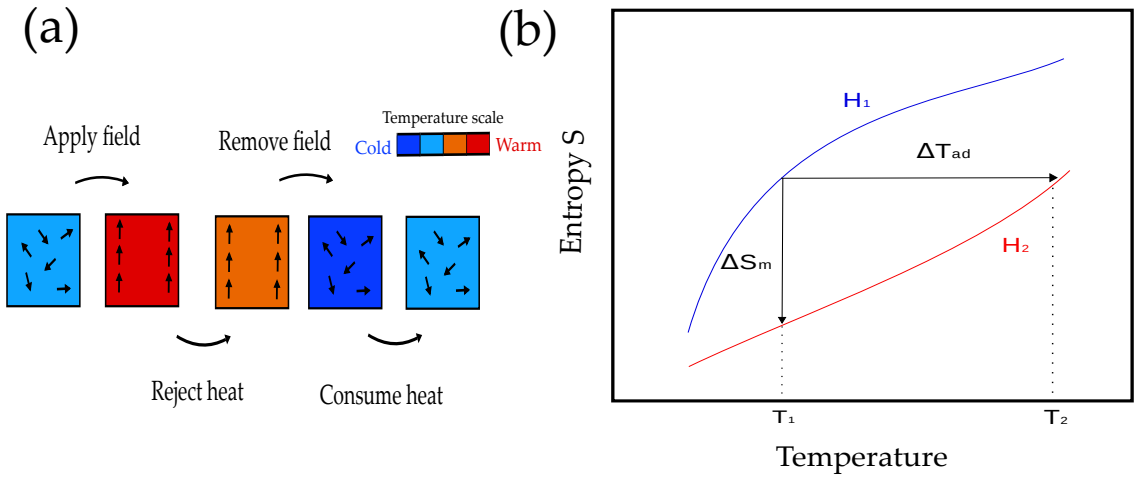

Figure 1.2: Four schematic cycles of refrigeration using magnetic refrigeration (a). The color coding of the refrigerant temperature is shown to the right on the temperature scale. Thermodynamic (TS) diagram demonstrating the magnetocaloric effect by the adiabatic temperature change, $\triangle T_{ad}$, and the isothermal magnetic entropy change, $\triangle S_M$ (b).

In order to use this technique of cooling for something other than the material itself, we need to ensure the transfert of heat from one of of a refrigerator system to the other by applying magnetiziation and demagnetization of the materials in a cyclic process as shown in Fig 1.2.a . The change in temperature of the material when subjected to an applied magnetic field is characteristic of the magnetocaloric effect known as the adiabatic temperature change $\triangle T_{ad}$. The MCE can instead be characterized at constat temperature where the magnetic entropy changes under the application of magnetic field which is known as the isothermal magnetic entropy change $\triangle S_M$ illustrated in Fig 1.2.b.

1.1.2 Thermodynamic Approach of the Magnetocaloric Effect

A general introduction to the thermodynamics of the magnetocaloric effect is given in this section. I will start with describing some aspects of adiabatic cooling and explain how the MCE can be utilized in magnetic cooling by adiabatic demagnetization as well as presenting some basic notions and theories related to magnetocaloric phenomenon.

1.1.2.1 Thermodynamics of Adiabatic Cooling

The principle behind the magnetic refrigeration is the adiabatic demagnetization which is based on the fact that the total entropy, S, of a system is a thermodynamic state function that can be controlled by the the use of external thermodynamic state variables such as temperature (T), pressure (p), and the magnetic field (H) :

$$S = S(T, p, H) \tag{1.1}$$

The change in entropy, dS, can be expressed as follows :

$$dS(T, p, H) = (\frac{\partial S}{\partial T})_{p,H} dT + (\frac{\partial S}{\partial p})_{T,H} dp + (\frac{\partial S}{\partial H})_{p,T} dH \tag{1.2}$$

In general, pressure variations of magnetic refrigerators are too small to play a significant role in the entropy change and can be therefore overlooked. Under isobaric conditions, dS becomes :

$$dS(T) = (\frac{\partial S}{\partial T})_{H} dT + (\frac{\partial S}{\partial H})_{T} dH \tag{1.3}$$

Isothermal entropy change (ΔS) can be induced by keeping the temperature constant and applying a magnetic field (from H_0 to H_1) and can be expressed as follows :

$$\triangle S_{H_0 \to H_1} = S(T, H_1) - S(T, H_0) \tag{1.4}$$

$$= \int_{H_0}^{H_1} (\frac{\partial S(T,H)}{\partial H})_T dH \tag{1.5}$$

Under adiabatic conditions, the entropy is instead kept constant and by applying a magnetic field, a temperature change is induced in the material which is known as the adiabatic temperature change, $\triangle T_{ad}$. Since the total entropy must be conserved, the following must apply:

$$S(T, H_1) - S(T + \triangle T_{ad}, H_0) \tag{1.6}$$

By taking into consideration the definition of heat capacity, C, the entropy can be expressed as follows:

$$C_{conditions} = T\frac{ds}{dT} \rightarrow S = \int \frac{C_p(T)_H}{T}.dT + S_0 \tag{1.7}$$

which under isobaric conditions is expressed as:

$$S(T)_H = -\int \frac{C_p(T)_H}{T}.dT + S_0 \tag{1.8}$$

Differentiating with respect to temperature yields to:

$$(\frac{\partial S(T,H)}{\partial T})_H = -(\frac{C(T,H)}{T})_H \tag{1.9}$$

and since dT can be defined from equation 1.3 and under adiabatic conditions ($dS = \frac{\partial Q}{T} = 0$), dT could be written as follows:

$$dT = (\frac{\partial S}{\partial T})_{p,H}(\frac{\partial S}{\partial H})_{T,p} dH \tag{1.10}$$

By subsequently combining equations 1.9 and 1.10 and integrate from H_1 to H_0 the adiabatic temperature change, ΔT ad , can be expressed

$$\Delta T_{ad}(T,H)_{\Delta H} = \int_{H_0}^{H_1} (\frac{T}{C(T,H)})(\frac{\partial S(T,H)}{\partial H})_T dH \tag{1.11}$$

We note that the change in the applied magnetic field from H_1 to H_0 indicate a demagnetization that yields the adiabatic cooling in a magnetocaloric material.

1.1.2.2 Magnetocaloric Effect and Adiabatic Demagnetization

In order to express the entropy change in terms of the magnetization, M, the relationship between magnetization and entropy need to be introduced. From the thermodynamic Maxwell equations [23]:

$$(\frac{\partial S(T,H)}{\partial H})_T = -(\frac{\partial M(T,H)}{\partial T})_H \tag{1.12}$$

Integrating equation 1.12 from zero field, H_0, to an applied magnetic field, H_1yields

$$\Delta S(T)_{\Delta H} = -\int_{H_0}^{H_1} (\frac{\partial M(T,H)}{\partial T})_H \tag{1.13}$$

the equation indicate that the magnetic entropy change is proportional to both the derivative of magnetization with respect to temperature at constant field and to the magnitude of the field variation.

To express the adiabatic temperature change, $\triangle T_{ad}$, as a function of the magnetization we combine equation 1.11 and 1.12:

$$\triangle T_{ad}(T)_{\Delta H} = \int_{H_0}^{H_1} (\frac{T}{C(T,H)})(\frac{\partial M(T,H)}{\partial H})_H dH \tag{1.14}$$

It is important to note that this relation should be evaluated explicitly along relevant isentrope since the integral is not independent of the integration path. Both magnetization and heat capacity are required for the determination of the adiabatic temperature change , a so-called indirect technique.

1.1.2.3 Entropy and its Dependence on the Magnetic Field

The total entropy of a system can be considered as the sum of magnetic entropy S_M, lattice entropy S_L and electronic entropy S_E [22] which is is valid only in solid systems exhibiting localized electron magnetism:

$$S = S_M(T,H) + S_L(T,H) + S_E(T,H) \tag{1.15}$$

Under isobaric conditions, the entropy of the system depends on both the applied magnetic field H and the temperature T. S_M is associated with the magnetic degree of freedom and can obtained by the free energy of the magnetic sublattice within the mean field approximation:

$$S_M(T,H) = Nk_B\left[ln\frac{sinh(\frac{2J+1}{2J})x}{sinh(\frac{1}{2J}x)} - xB_J(x)\right] \tag{1.16}$$

where x = $\frac{gJ\mu_B H}{k_B T}$, with g being the Landé factor, J the quantum number of angular momentum, k_B the Boltzmann constant and B_J the Brillouin function. By taking into consideration high temperatures and low-field limit, we could write:

$$S_M(T,H) = Nk_B\left[ln(2J+1) - \frac{1}{2}\frac{C_J H^2}{(T-T_C)^2}\right] \tag{1.17}$$

The magnetic entropy will reach its maximal value of $S_M = Nk_B ln(2J+1)$ at the disorder transition. The contribution from electronic entropy $S_E = \gamma T$ where γ is the coefficient of electronic heat capacity can be ignored at high temperatures.

Metals (especially well known 3d magnets such as Fe, V or Co) and in contrast to insulating materials whose magnetism is often described in terms of localised electrons in each atom, have a picture of nearly free electrons. In such itinerant systems, it is common to speak of the entropy of a systemem composed of the phonon S_L and magnetic terms S_M. While the contribution from electronic and lattice entropy is negligible for a second-order transition, it cannot be ignored for a first-order transition due to the discontinuous change of order parameter at the transition temperature.

1.1.3 Classification and phenomenology of magnetocaloric materials

MC materials can be classified according their physical properies in many ways. From a fundamental point of vue, the magnetocaloric effect could be normal or inverse. Normal is when the material heats up upon magnetization and cools down when we demagnetize it and as a result, the magnetic isothermal entropy change is negative (positive) upon magnetization (demagnetization). Inverse MCE is when the material cools down upon magnetization which occur in the case when the temperature derivative of the magnetization is positive [35]. The nature of the magnetic phase transition used to exploit the MCE is a further way of classifying the materials which can be either first- (FOPT) or second-order (SOPT) type phase transition.

1.1.3.1 Magnetic transition order

First order FOPT materials have the advantages of exhibiting large $\triangle S_M$ and $\triangle T_{ad}$ but accompanied by thermal hysteresis causing a strong dependency on the material history which makes both thermodynamic cycles and efficiency losses hard to controle involving

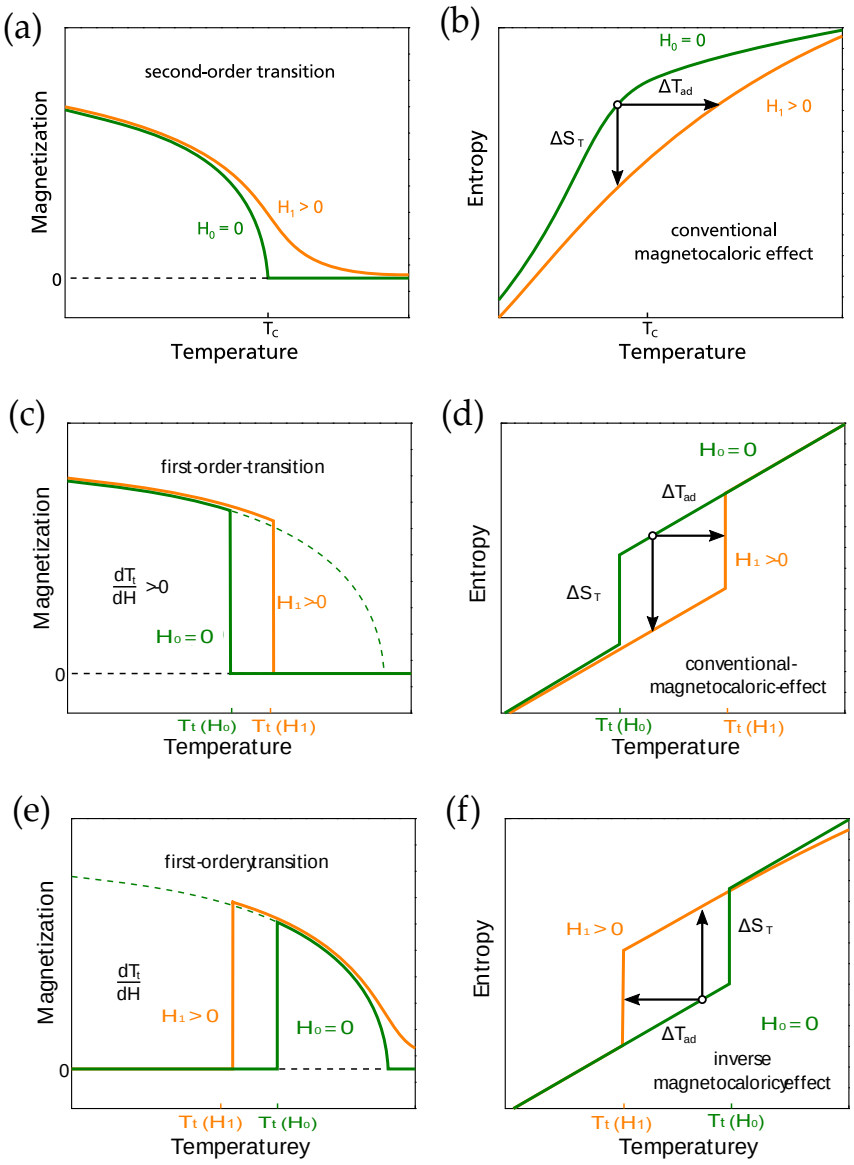

Figure 1.3: Schematic of magnetization as a function of temperature and the total entropy with and without the applied magnetic field of a conventional second-order transition in (a,b), first order transition in both conventional MCE in (c,d) and indirect MCE (e,f).

as well the generation of latent heat and structural changes [24]. FOPT is characterized by a discontinuity in magnetization and the total entropy, a conventional first-order transition is schematically illustrated in figure 1.3(c,d). At low temperatures, the ferromagnetic state is stable and abruptly changes to low magnetization at defined transition temperature Tt. When a magnetic field is applied, H1 > 0, the transition temperature is shifted because the material is stabilized at high magnetization, this being the low temperature phase [32]. In case of conventional MCE, the shift of the transition temperature dTt dH is positive which acts as a driving force of the MCE in such systems, while it is

negative in case of the inverse MCE (figure 1.3(e)). For a inverse MCE, the magnetization of the material causes a decrease of the temperature in adiabatic condition when subjected to an applied magnetic field and an increase of the entropy in the isothermal process (figure1.3(f)). In figure1.3 (e) the ideal behaviour of the temperature dependence of entropy is plotted .

A large variety of different transition types may arise such as metamagnetic transitions which is defined as the transition between two different magnetic structures, eg., ferromagnetic to antiferromagnetic. In many cases field induced metamagnetic can occur together with structural transition giving rise to rich phase diagram.

Second order On the other hand, the magnetocaloric response in SOPT materials is usually smaller compared to most of FOPT materials but operate over a wide range of temperature and do not suffer from thermal hysteresis. In SOPT systems, both the magnetization and the entropy are continious, a shematic of the magnetic behavior of a ferromagnetic material near its curie temperature is presented in figure1.3(a,b). The temperature dependence of magnetization (figure1.3(b)) in zero field , green curve , demonstrate a transition from ferromagnetic to paramagnetic state at a critical temperature called Curie temperature. When subjected to a magnetic field, orange curve, a partial allignement of spins preserve a certain magnetization. In figure1.3(b), the temperature dependence of the total entropy without the application of magnetic field is illustrated as a green curve. The magnetic system become more ordered by the application of a magnetic field due to the alignement of magnetic moments to some extent and the entropy of the system is lowered [33] which is observed in isothermal conditions. Under adiabatic conditions, the total entropy remains constant as the S_L increases to compensate for the decrease in the S_M. For this reason, the material heats up by $\triangle T_{ad}$ when subjected to an applied magnetic field illustrated as a horizontal arrow in figure1.3(b).

1.1.3.2 Employment of Maxwell relation

The magnetocaloric effect in terms of $\triangle T_{ad}$ or $\triangle S_M$ can be determined either directly or indirectly. Direct measurements are ultimately desirable, but can be very challenging, hence it is common practice to use indirect and quasidirect methods to obtain values of isothermal $\triangle S_M$ and adiabatic $\triangle T_{ad}$ from the thermodynamic analysis of experimental data that record the temperature or the magnetic-field dependence of the magnetization magnitude using the well-known Maxwell relation (MR) obtained by integrating equation 1.13. Idealy, the magnetization should be obtained in thermodynamic equilibrium as a single valued function of magnetic field and temperature which may be achieved near

SOPT. Whereas, however, there has been some controversy in the literature regarding the applicability of MR near FOPT [36, 37, 33] with significant hysteresis since the material is assumed to be in equilibrium in order to use MR. The validity of this equation depends on the details of the experimental procedure since it is acceptable to use data obtained after thermal excursion away from the hysteretic regime in strongly hysteretic transitions[25, 26, 27, 28, 29] preventing the occur of the so-called colossal magnetocaloric effect manifesiting in a spurious peak in $\triangle S_M$ calculated by indirect approach [34, 35].

A. Giguère et al [36], have proposed a magnetic analogue of the Clausius-Clapeyron equation which is equivalent to the Maxwell method for FOPT materials allowing the use of non equilibium data without performing thermal excursion away from the hysteretic regime. One typically measures the temperature dependence of magnetization at fixed applied magnetic field, in order to determine the magnetic field dependence of equilibrium transition temperature T_0. $\triangle S_M$ can be obtained using the following equation :

$$\triangle S_M = -\triangle M \frac{dH_c}{dT} \tag{1.18}$$

Where DM is the difference of magnetization between the two phases, while $(\frac{dH_c}{dT})^{-1}$is the change rate of phase transition equilibium temperature with magnetic field.

1.1.4 Selection Criteria

The intensity of the magnetocaloric effect is the most important criterion for the selection of the MC materials. Several promising classes of materials exist with giant MCE and tunable Curie or Neel temperatures covering a wide range of working temperatures. In principle, the two thermodynamic quantities , $\triangle S_M$ and $\triangle T_{ad}$ are the two key parameters that provide a good basis for comparison. Another important parametetr for MCE is the relative cooling power (RCP) which indicate how much heat can be transferred from the cold reservoir to the hot reservoir of a refrigerator describing a thermodynamic cycles. This parameter is defined as the product of the maximum entropy change and the full width at half maximum :

$$RCP = -\delta T_{FWHM}.\triangle S_M \tag{1.19}$$

These parameter are the key to compare the potential of materials in terms of MCE and having large values of those parameters makes them a potential candidate for magnetic refrigeration applications. Nevertheless, these materials must meet certain requirements to bring them to the commercial market:

Hysteresis losses: Matering hysteresis in magnetocaloric materials is the key to maximize the efficiency of magnetic cooling devices. There are multiple strategies to at least partially overcome the hysteresis issue in classes of materials as La-Fe-Si and Heusler materials or even use these material desipite the large hysteresis [37]. A recent study by Gutfleisch O et al demonstrated a possible shift of the transition temperature to room temperature by adding Co to the $La(Fe,Si)_{13}$ accompagnied by a phase transition change from first to second order which tends to reduce the thermal hysteresis. However, this change comes with a reduction of the MCE. The hydrogenation of the base material is another possibility to tune this material properties without a change in the phase transition maintaining, as a result, the large MCE with a small hysteresis. However, high brittleness and poor machinability require binding the material in matrix which tends to decrease the MCE intensity. Another possibility is to use multicaloric cycles in which the thermal hysteresis of a FOPT materials can be exploited which leads to a drastically reduce of quantity of permanent magnets required while increasing the magnetic field strenght [39]. The comprehensive description of all relevent sources of hysteresis, their microscope origins and involvement on various length and time scales will , upon implementation into applications, eventually lead to efficient magnetic refrigeration.

Thermal transport: A key factor to ensure a good heat transfer is the thermal transport which involve the thermal conductivity and specific heat engineering of the material. In fact, a low value of the thermal conductivity slows down the heat transfer through the solide, while high thermal conductivity increases the axial conduction (along the flow direction) which tends to reduce the regenerator performance.

Chemical and mechanical stability: The contact of thermomagnetic material with heat transfer fluid in regenerator means that the stability of material corrosion must be considered. Cyclic performance is very important for the magnetic refrigerant, therefore, a good mechanical stability is essential for determining the long term applicability in a MC device. Noting that when FOPT materials are used, the volume change associated with the phase transition can be significant. This can lead to cracks and other mechanical defects [38].

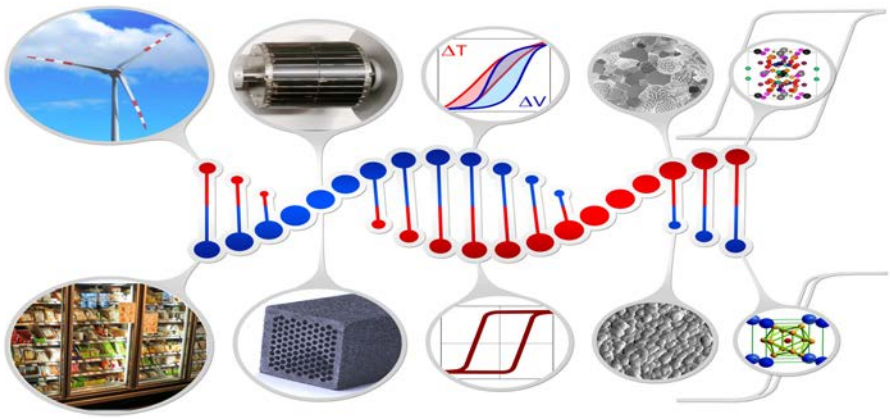

Figure 1.4: The "DNA" of magnets: From the electronic structure to the device implementation [64].

Affordability : Costs remain the real obstacle preventing the leap into marketable technology. Currently, Gadolinium Gd is the only magnetic material used in most prototypes of magnetic cooling, whose temperature of transition is in the vicinity of ambient 294 K. This metal present multiple disadvantages such as its oxidation and its refrigeration limited to the room temperature. Moreover, gadolinium cannot be used in the systems of refrigeration intended for the general public because of the high cost which can exceed the 3500 d'/kg. Therefore, drive down the costs of MC systems is critical to the commercialization of these systems and this could be achieved by searching for new less expensive and clean materials with a high magnetocaloric effect under modest magnetic fields such as intermetallic alloys, perovskites and double perovskites containing manganese and spinels. In fact, being able to produce larger cooling effect in smaller magnetic field is also very important from a practicle point of vue since in most applications, the operating magnetic field must be generated by permanent magnets, which limits the maximu field change to 1-2 T. This encourages researchers from the German Science Foundation (DFG) to start a new Collaborative Research Center (CRC) called "HoMMage" that will begin its first 4 year on January 2020 [64]. These researchers are focused on mastering and designing new magnets for the transformation of energy technologies by understanding smallest detail about what happening within the material. In other words, identifying the "DNA" of the magnet (figure 1.4) and developing new processing methods and strategies for innovative magnet materials.

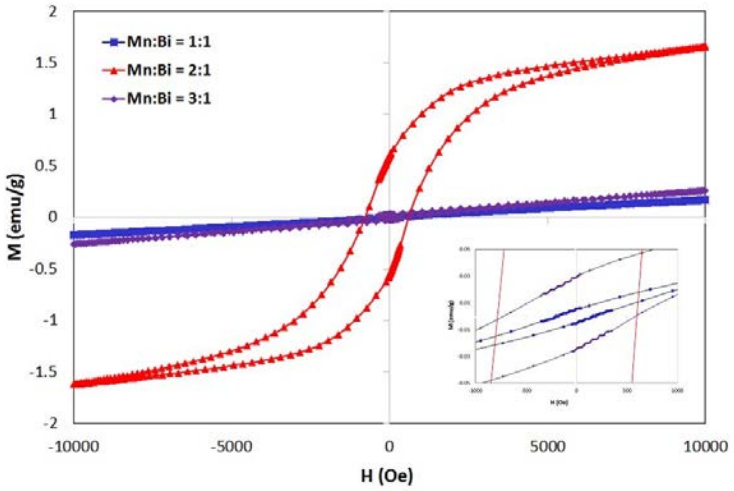

Figure 1.5: Hysteresis loop of MnBi particles under pressure n the ratio Mn:Bi = 1:1, 2:1 and 3:1 after sintering at 1000 řC

Nanostructured permanent magnets are also a good option on the path of inventions and innovations. The concept here is based on the combinaison of nanostructured hard magnetis with soft magnetic materials referred to as hard/soft nanocomposites. The soft phase prevents the hard phase domain wall from moving, and while the rare earth magnets has the maximum energy efficiency and coercive field, the synthesis of rare earth nanostructures is not successful because the typical material lose ferromagnetism when the size is reduced below the superparamagnetic limit as shown in figure1.5. The research on new nanostructure magnet mainly focus on three materials : Iron- Platinium (FePt), Cobalt Carbide (CO_nC,$n = 1 - 6$) and Manganese-Bismute (MnBi) and to resume i will only address the MnBi case.

MANGANESE-BISMUTH (MNBI) is an intermetallic compound and its ferromagnetism is related to the low temperature phase of the hexagonal structure. Due to the magnetocrystalline anisotropy the coercive field of MnBi is very high. In contrast to conventional trend of reducing coercive field when heating (high temperatures), the material has a unique positive temperature coefficient and can be prepared by various processes such as arc melting and solid state sintering. The ball mlling can also improve the coercive field by reducing the particle size. However, in order to reach the desired phase and achieve full industrial productivity, it is necessary to continue research and development.

The great interest in updating the refrigeration technology comes together with the positive feedback about the future global magnetic refrigeration market. According to a recent report, The global magnetic refrigeration market was valued at 1.14 million USD in 2016 and should achieve 702.20 million USD by 2025 [34] which could make the dream of

a totally abandon of conventinal systems a reality.

1.2 Multiferroic materials

1.2.1 Why multiferroics are interesting ?

Schmid first introduced the term 'multiferroic' in 1994. Multiferroic refer to a big class of materials in which two or more kinds of fundamental ferroicities coexist and there are several different ferroic orders:

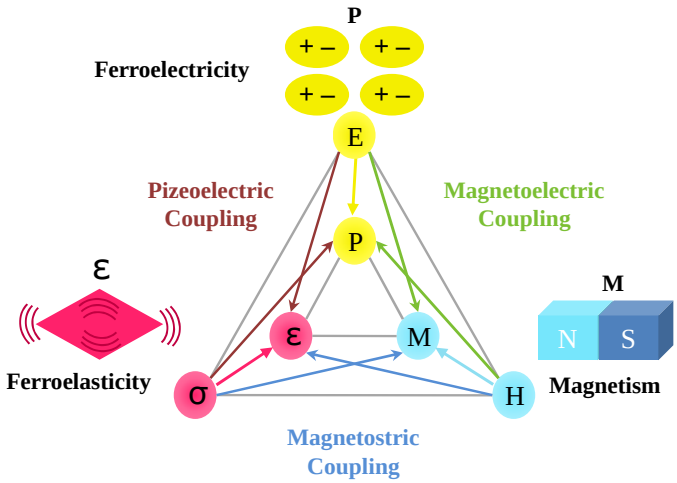

Figure 1.6: The electric field E, magnetic field H, and stress σ control of the electric polarization P, magnetization M, and strain sv, respectively. In a ferroic material, P, M, or e are spontaneously formed to produce ferromagnetism, ferroelectricity, or ferroelasticity, respectively. In a multiferroic, the coexistence of at least two ferroic forms of ordering cause additional interactions. In a magnetoelectric multiferroic, a magnetic field can control P or an electric field can control M [2].

ferromagnetic (magnetization), ferroelectric (polarization) or ferroelastic (strain). The interply between these orders is presented in figure 1.6 offer a good opportunity to bring out novel physical phenomena and designing new multiferroics and new functionalities. Due to this combination of magnetic and dielectric properties together with a possible cross-coupling between these properties, multiferroics have a great potential for applications in the industry and at the same time they raise very interesting rich fundamental physics problems

There are two main motivations for the research of multiferroic materials. The first one is the plenty and representative physics phenomena and mechanisms involved in these materials, such as polarization induced by magnetic order. The other motivation

is the possible applications in the industry including magnetic sensors, magnetoelectric (ME) memory and magnetocaloric effect.

1.2.2 Classifying Multiferroics

Multiferroics form a very diverse category of materials, and there is no unique "theory of multiferroics". Almost all materials need to be studied independently, and the physical mechanism involved is quite different from other multiferroic materials. However, it is very useful to classify multiferroics according to the ferroelectric driving mechanism in the corresponding systems. In particular, there are two major groups of multiferroics, which we call type-1 and type-2 [3]. As presented in figure 1.7, the first group contrains materials in which ferroelectricity and magnetism haeve different origins and they are largerly independently of one another. The ferroelectricity usually occurs at higher temperature compared to that of the magnetism, resulting in considerable spontaneous polarization. Although there is some coupling between ferroelectricity and magnetism in these materials, it is generaly weak. A novel class of multiferroics was discovered at the beginning of this century [4, 5] , where the ferroelectricity is driven by some other electronic mechanism, e.g. "correlation" effects.

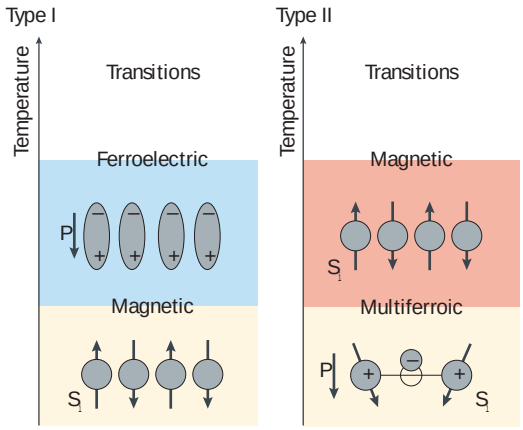

Figure 1.7: Types of multiferroicity. Image adapted from [41]

1.3 Type-I multiferroic : Vanadate RVO_3

1.3.1 Multiferroic structure

As the most promising multiferroic materials one usually considers transition metal perovskites. The first attempts to create multiferroic materials were mostly focused on clas-

sical ferroelectrics, such as BaTiO3 or (PbZr)TiO3 (PZT) taking advantage of their diverse properties. However, after examining hundreds of perovskites [6] and ferroelectric (FE) perovskites [38], it can be concluded that there seems to be incompatibility between magnetism and FE because there is practically no overlap these two properties.

The perovskite materials usually present cubic structure at high temperature with a small B-site cation at the center of an octahedron of oxygen ions and a large A-site cation at the unit cell corners.

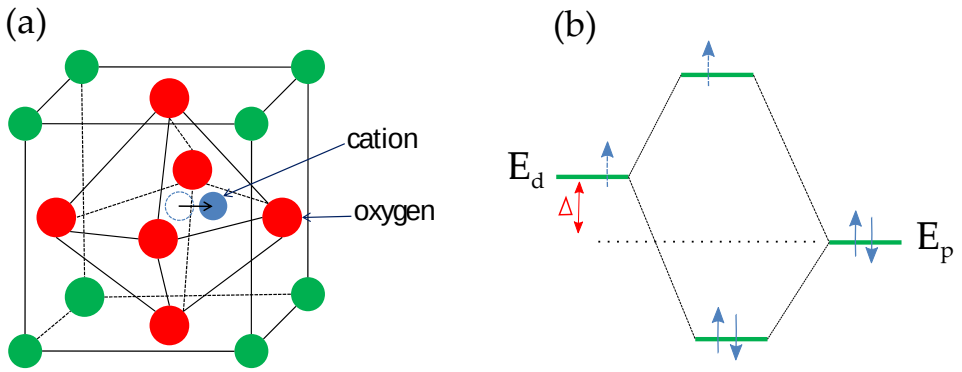

Figure 1.8: Structure of Multiferroic perovskite (a), shift of transition metal ion towards one of the oxygens.(b) schematic energy levels with empty d-level (solid arrows) and with partially filled d-level (dashed arrow).

In particular, these materials undergo a phase transition from a high-temperature, high-symmetry paraelectric phase, to a low-symmetry polarized phase at low temperature accompanied by an off-center shift of the B-site transition metal ions, as presented in figure 1.8(a). The ferroelectricity results from the shift of the B-site ions (V^{3+}) is from the center of O6 octahedra towards one (or three) oxygens forming a strong covalent bonds with the particular oxygen(s) using their empty d states. However , the presence of real d electrons in d^n configurations of magnetic transition perovskites prevents this process [39] which could be described as a second order Jahn-Teller mechanism. The shift of the B-site towards the oxygen that we mentioned above, results in a weakning of the bonds with other oxygens. The hybridization matrix element t_{bd} turns to $t_{pd(1\pm gu)}$. In the linear approximation, the energy can be expressed in this forme $\sim(-t_{pd}^2/\Delta)$ (see figure 1.8(b)), which cancel each other. while the second-order approximation can produce extra energy difference:

$$\delta E = -(t_{pd}(1+gu))^2/\Delta - (t_{pd}(1-gu))^2/\Delta + 2t_{pd}^2/\Delta = -2t_{pd}^2(gu)^2/\Delta \tag{1.20}$$

- u: the distortion

- g : the coupling constant
- $\triangle$: the charge transfer gap

In the following section, we shall give overview on the generel common features in vanadates and a short review on some research done on vanadates so far will be given in chapter 3.

1.3.2 Magnetic configuration

1.3.2.1 Hund rules

Hund's rules are a set of rules that establish the distribution of electrons in orbitals. This is valid in a regime where the crystal field is weak compared to the coulomb interaction between the electrons of the same atom and the spin-orbit interaction $\overrightarrow{L}.\overrightarrow{S}$. The first rule, favoured by spin-orbit coupling, stipulates that the lowest energy atomic state is the one that maximizes the total spin for the electrons in the open subshel. Therefore, it is energetically lessfavoured that two electrons of V^{3+} can occupy the same orbital 3d. So, the electron occupying the orbital dyz or dxz will have a parallel spin to the electron occupying the orbital dxy. The two other rules are less important for the description of the V^{3+} spins, but for information purposes, the second rule states that the electrons are distributed in a way to maximise orbital angular multiplicity. The third rule : if an outermost subshell is half-filled or less, the lowest value level of the total angular momentum J=| L-S | has the lowest in energy. If the outermost subshell is more than half-filled, the level having the larger value of J=L+S has the lowest energy.

1.3.2.2 Super-exchange interactions

The presence of an oxygen atom between two neighbouring magnetic atoms weakens so direct exchange interaction. In these conditions, the super-exchange interaction, which is an antiferromagnetic or ferromagnetic coupling between two next-to-nearest neighbor cations through a non-magnetic anion, becomes important in the description of their interdependence. This interaction was proposed by Hendrik Kramers in 1934 when he noticed that in crystals like MnO, Mn atoms interact with each other even though there are a non-magnetic oxygen atoms between them [48]. Figure 1.9 simplifies this interaction where two electrons neighboring V^{3+} site separated by an oxygen can interfere with each other. Because the interaction depends on the oxygen relative position related to two V^{3+}ions (particulary the V-O-V bond angle), the strength of this interaction is related to the size of the rare earth which distorts oxygen octahedral.

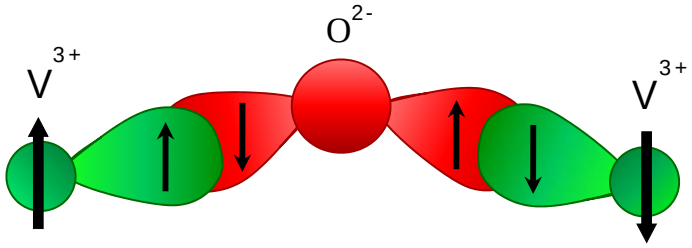

Figure 1.9: The orbital conguration of Vanadium atoms and oxygen by superexchange interaction

The super-exchange interaction is also strongly influenced by the choice of occupied t2g orbitals since it radically changes the electronic overlap between 2p orbitals and t2g orbitals. The properties of this interaction according to the occupied orbitals are described by the Goodenough-Kanamori rules

1.3.2.3 Goodenough-Kanamory rules

Goodenough Kanamori rule is a set of empirical rules proposed by John B. goodenough and junjiro Kanamori in the 1950s, which describes the relationship between super-exchange and and orbital occupation [62, 63]. These rules stipulate that if electrons virtually transfer between two half filled orbitals, the super-exchange is antiferromagnetic and has strong interaction. If the virtual electron transfer is between a half filled orbital and an empty orbital, the supere-xchange will promote the ferromagnetic configuration structure with low interaction. By respecting these rules, we can determine the magnetic order (spin ordering, SO) generated from the orbital structure. First, d_{xy}orbital is half filled. Since the density of states occupying the dxy state is confined to the ab plane, the superexchange interaction between two neighbouring V^{3+} in the same plane always promotes an antiferromagnetic configuration in this plane This orbital, however, plays a minor role in the superexchange along axis c compared to the dyz and dxz orbitals. As a result, this interaction is very sensitive to the orbital order adopted by the V^{3+}. In the case where the occupied orbital remains the same along axis c (C-OO), the V^{3+} spins are aligned antiferromagnetically along this axis. The magnetic moments of the vanadium are then antiferromagnetic independently of the (G-SO) direction. If, on the contrary, the occupied orbital along the axis c are dxz and dyz (G-OO), there is a weak ferromagnetic interaction following this axis [63]. and the magnetic configuration of the V3 spins is then antiferromagnetic in the ab plane and ferromagnetic between planes (C-SO).

To resume, the high dependence of super-exchange interaction on the orbital configuration allows a specific magnetic order to be associated with it. For example, the G-OO/C-

SO and C-OO/G-SO orders are the two possible configurations of low-temperature V3s as shown in figure1.10.

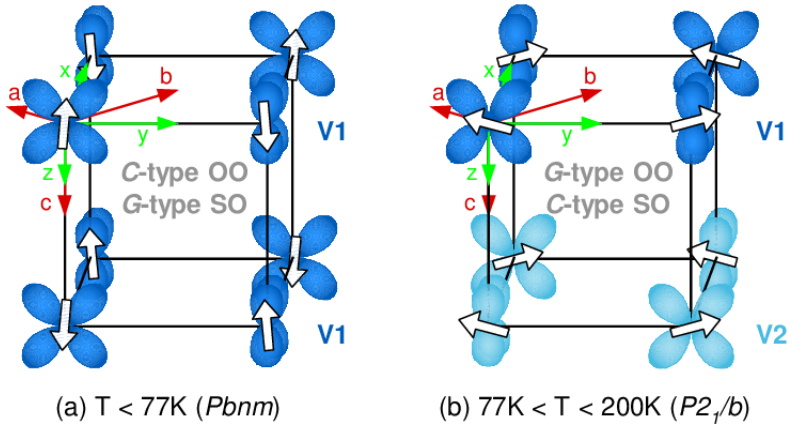

Figure 1.10: Orbital and spin ordering patterns in YVO3 for (a) TS < 77 K and (b) TS < T < TOO = 200 K. The x y orbital is occupied by one electron on each site. The occupation of x z and yz orbitals is C-type below TS and G-type above (see main text for more details). The coordinates of the Pbnm and P21/b crystal systems are given in the upper left corner of each figure [61]

1.3.3 Phase diagram in rare-earth vanadates

The first attempts to compose a phase diagram goes back to 2003 when Miyaska et al published a systematic study of spin and orbitals transitions in most RVO3 using specifric heat measurements [65] which allowed the authors to propose the current reference for all transitions in the vanadates. They have found that Tn increases with incrasing lanthanide ionic radius while the onset temperatures of the orbital oredring increases from Lu to Gd then decreases for larger ions. There are still doubts about the interpretation of lavo3 and cevo3 results for LaVO3 and CeVO3. A report by Ren et al. in 2003 presents the specic heat and single crystal diffraction data (figure 1.11[66]. For LaVO3 a second order transition was observed at T_N=143K and a second order transition at Tt=141K. In CeVO3, a second order transition is found at T_O=154K and a first order transition at TN=134K. According to the authors, the change in structure at T_N is due to an orbital oredring enhanced magnetostrictive distortion and contrary to the report of Miytaska el al, the presence of OO in CeVO3 will be above T_N. For LaVO3, Ren et al propose that the first-order transition at Tt is related to a sudden change in both spin and orbital congurations

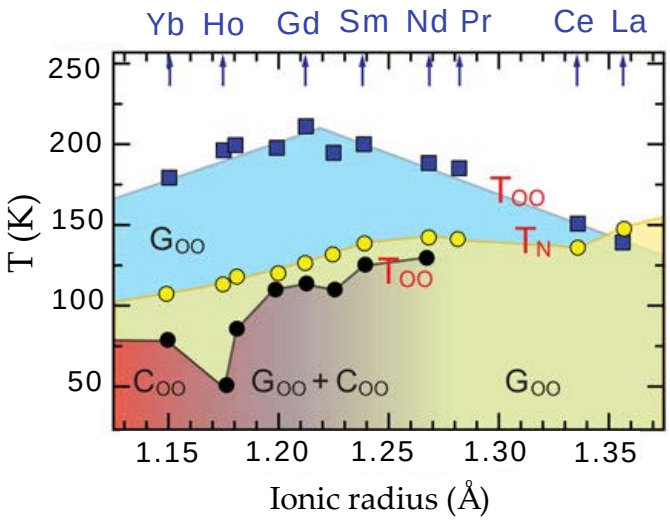

Figure 1.11: Temperature dependence of orbital ordering (subscript OO) and spin ordering (subscript N) versus ionic radius for the rare-earth vanadates (RVO_3)

1.3.4 Quantum versus Jahn teller orbitals physics

At present, the main controversy about vanadate is the description of low energy physics.. In 2001, Khaliullin et al. proposed a quasi-1D spin-orbital model [56] which is at the origin of the discussion. It was pointed out that in order to stabilize the stronger than expected ferromagnetic super-exchange along the c-axis in the C-type magnetic phase, a strong t2g quantum orbital fluctuations must exist ina half-lled system of yz and zx orbitals in RVO3 systems. In this case, JT distortion as well as the C-type magnetic phase should not occur. However, the Jahn-Teller effect would still stabilize the G-type magnetic phase (with C-type OO) at low temperatures. Khaliliullin et al have predicted that orbitals will expand along the c-axis to give a so-called orbital orbital Peierls state when orbital fluctuations are dominant and there is no JT distortion at all. Evidence for an orbital Peierls state [67, 68], where orbitals are dimerised along the c- axis, was obtained by magnetic neutron scattering by Ulrich et al. in YVO3 [69]. This is consistent with Pb11 symmetry observed earlier by Tsvetkov et [72]. In the C-type magnetic phase, the width of the magnon band along the FM c-axis was larger than that in the AFM ab plane. This violates the classical Goodenough-Kanamori rules described in section 1.3.2.3 stating that the ferromagnetic super-exchange interactions are usually weaker than antiferromagnetic interactions. These observations were analyzed using the quasi-1D spin-orbital model, which successfully explains most of the anomalies of the Ts<T<Too phase of YVO3. Most of the subsequent theoretical studies on yvo3 and lavo3 using this model confirmed its validity [71, 70].

It is still controversial whether the lifting of degeneracy of the xz=yz orbitla doublet is controlled by superexchange or is of lattice origin. It seems that the theoretical and experimental work is beneficial to the mechanism of super-exchange [73]. So far, no dimerization phenomenon has been observed in diffraction experiments, howeever, it may be difficult to do so because of the weak lattice coupling of the t2g orbitals as well as the important thermal and quantum fluctuations [69]. several thermal conductivity experiments on vanadate single crystals show that in the ambient temperature phase, above the OO temperature, the crystals conduct like a glass [74]. Due to the existence of spinphonon scattering, OO can only recover a part of the phonon contribution tp the thermal conductivity, which decreases dramatically below Tn. The transition from first order to a high thermal conductivity phase is observed for R<Dy below the transition from C-type to G-type magnetic ordering. Khaliullin pointed out that these results are consistent with the orbital fluctuations model [73]. However, some reports have pointed out that JT orbital physics should not be abandoned when explaining the properties of the G-type OO phase [65, 66]. It is believed that Jahn-taller distortion will lift the orbital degeneracy, and will eliminate the fluctuations of the quantum orbital.. They emphasize that the observed JT distortions in these materials were in fact very strong and should not be ignored. Fang et al reproduced the work of Ulrich [69]et al by considering inequivalent VO2 layers [66]. The significant difference between the exchange coupling strength in successive layers is due to the different magnitude of Jahn-Taller distortions in the two layers. Their calculations show that the anomalous magnetic properties of LaVO3 and YVO3 can be explained using a Jahn-Taller picture. However, optical experiments [65] show that the JT coupling is weak. The nature of vanadate properties is still uncertain,, it is not clear whether quantum orJT orbital physics should be chosen to explain the properties of vanadate. Further experiments are needed.

1.4 Type-II multiferroic: Orthorhombic RMn_2O_5

Type-II multiferroic materials are also called ń magnetic multiferroicż. This last name is because their ferroelectric properties only exist when certain magnetic orders are established. The prototypical example is TbMnO3 in which the first magnetic order appears at $T_{N1} \sim 41$ K, whereas its ferroelectric caracter occur when a second magnetc order arises at $T_{N2} \sim 28$ K [67]. Similar behaviour is also observed in the $TbMn_2O_5$ compound [68]. One can devide this class of materials into two subclasses depending on the microscopic mechanism responsible for ferroelectric caracter. The first subclass includes orthorhombic $RMnO_3$ (R= Tb and Dy) whose ferroelectricity is induced by a non-collinear magnetic

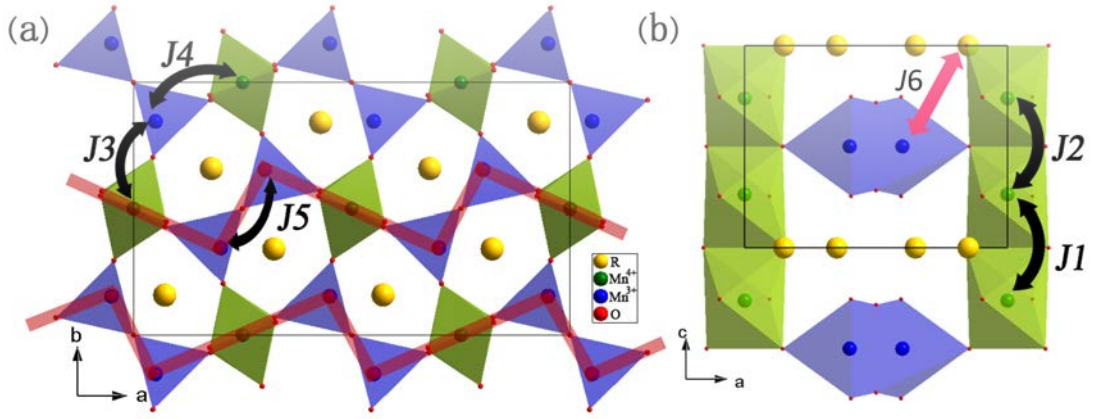

Figure 1.12: Projections of the crystal structure of RMn2O5 along (a) c and (b) b axis. The different exchange interactions Ji are indicated.

order (spiral) and the second subclass brings together those materials whose ferroelectricity is generated by a collinear magnetic order (quasi antiferromagnetic) such as RMn_2O_5 compounds on which we will focus.

RMn_2O_5 are a frustrated magnets whose spin-spin interactions and spin-lattice exclude simple magnetic spin arrangements. The consequences of their frustrated magnetic structures are spectacular. They are mainly manifested in the strong correlation between their magnetic and electrical properties.

1.4.1 General structure

RMn_2O_5 materials have all an orthorhombic structure consistingg of $Mn^{4+}O_6$ octahedral and $Mn^{3+}O_5$bipyramids connected by their edges and corners. This structure is illustrated in figure 1.12. Perfect knowledge of magnetic orders involving Mn3+ and Mn4+ ions is essential for a better understanding of multiferroic features in RMn_2O_5 compounds. Recent studies of these compounds show rich magnetic properties[69]. The majority of these materials present at least four magnetic transitions.

.

The manganeses have two valences, Mn^{4+} and Mn^{3+} , corresponding to two crystallographic sites 4f and 4h, respectively. Mn^{4+} cations have an enviroment of six oxygen octahedral. These octahedra are attached to an edge and form continuous chains along the c axis as shown in figure 1.12. The Mn^{3+} have the environment of five oxygens completing a square pyramids that form $Mn^{3+}O_5$ dimers by edge-sharing. . The chains of octahedra are connected by bipyramids in the ab plane by sharing the oxygen at the summit edge positions. The R^{3+} cations occupy 4g sites. Their environment is complex and

Ion	Name	Site	Position
R^{3+}	R	4g	(x, y, 0)
Mn^{3+}	Mn_1	4f	(x, 0.5, z)
Mn^{4+}	Mn_2	4h	(x, y, 0.5)
O	O_1	4e	(0, 0, z)
O	O_2	4g	(x, y, 0)
O	O_3	4h	(x, y, 0.5)
O	O_4	8i	(x, y, z)

Table 1.1: Pbam cristallographic sites and atomic positions of RMn_2O_5 unit cell

includes 8 oxygen. Along the c axis, there is an alternation of $Mn^{3+}O_5$ pyramids plans, $Mn^{4+}O_6$ octahedral and R^{3+} rare earth. The crystallographic sites and ion coordinates in the unit cell are given in Table 1.1. We will come back to discuss more the general structure and the sequence of magnetic ordering in chapter 4.

1.4.2 Magnetic moments and exchange interactions

1.4.2.1 Magnetic moment

Table 4.4 summarizes the electronic configurations, the value of spins and moments ($-g_J\mu_B J$) of magnetic ions in the case of different R. The ligand field (O^{2-}) of manganese induces a lifting of degeneracy of their 3d orbitals. Figure 1.13 reminds low-field energy levels of d orbitals in a squar pyramidal environment and in an octaedral environment. The filling of these orbitals is done with respect to the Hund rule (see section 1.3.2.1). It should be noted that theMn^{4+} and Mn^{3+} ions have a low anisotropy with an easy magnetization plan in the plane (a,b) (easy axis of the Mn3 follows the apical direction of the pyramid) [30]. Estimating the degeneracy and filling of these orbitals requires further calculations based on specific crystallographic structure since the rare earth environment with 8 first neighbors and the nature of 4f orbitals are quit more complex. As for rare earth, they have a strong anisotropy because of their spin orbit coupling. This anisotropy varies according to the compound and we will see in chapter 4 how this anisotropy will impact the magnetism and magnetocaloric properties in $HoMn_2O_5$.

1.4.3 Exchange interactions

There are five types of exchange interactions in the RMn_2O_5 structure. Exchanges paths between the magnetic moments of Mn are described by the $J_{i=1->5}$ constants and are shown in Figure 1.12

Rare earth	Configuration	Spin(S)	Measured moment (μ_B)
La^{3+}	$4f^0$	0	diamagnetic
Ce^{3+}	$4f^1$	1/2	2.4
Pr^{3+}	$4f^2$	1	3.5
Tb^{3+}	$4f^8$	3	9.5
Ho^{3+}	$4f^{10}$	2	10.4
Yb^{3+}	$4f^{13}$	1/2	4.5
Lu^{3+}	$4f^{14}$	0	diamagnetic

Table 1.2: Electronic configurations, spin and magnetic moment of some R^{3+}rare earth

In ab plane, three nonequivalent exchange interactions are: J_5, the interaction between Mn^{3+} spin, J_4 and J_3 whicfh are the interactions between Mn^{3+} and Mn^{4+} is oriented according to a and b directions, respectively. The main contribution of these constants is the superexchange between manganeses through their common(s) oxygen (s), these couplings are antiferromagnetic (AF). In the ab plane,the crystallographic structure forms zigzag bipyramids $Mn^{3+}O_5$ and $Mn^{4+}O_6$ octahedra chains. AF exchange interactions along these chains are J_5 and J_4 and they are dominant in the magnetic structure. The chains are magnetically coupled along b by J_3. Since all J_3 couplings cannot be satisfied, there is magnetic frustration. In the Pbam group, the terms of exchange by J3 cancel out two to two in the magnetic energy of the fundamental state.

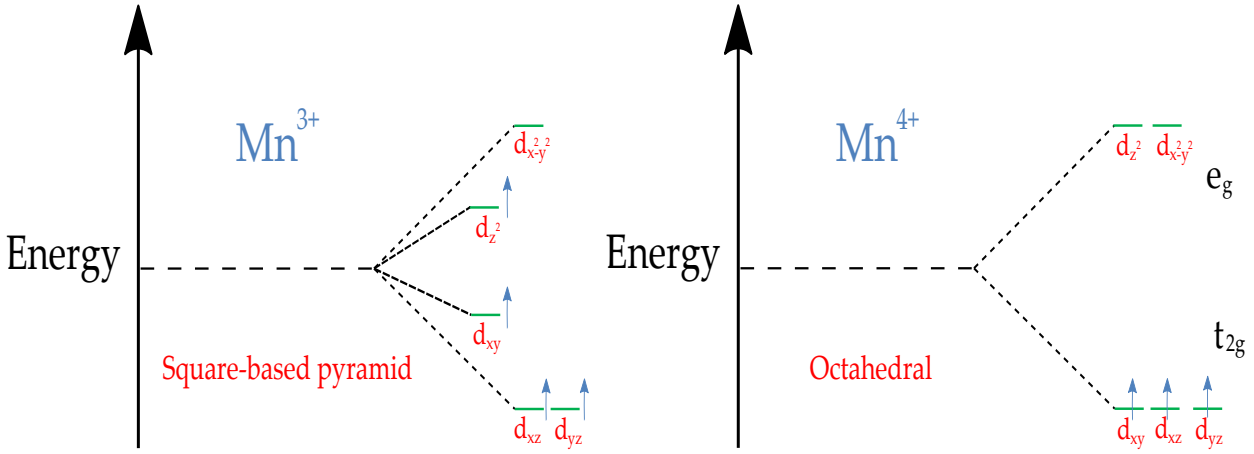

Figure 1.13: Energy level and filling of 3d manganese orbitals in pyramidal (left) octahedral (right) environment

According to c, two AF super exchange constants describe correlation between Mn^{4+}: J_2 across plans Mn^{3+} and J_1 across R^{3+} plans, however, these constants of exchange are frustrated. In particular, J_2 is frustrated by the presence of J_4 and J_3. It is shown, however, that the order between The Mn^{4+} spins connected by $J2$ is ferromagnetic[32]. As for J_1,

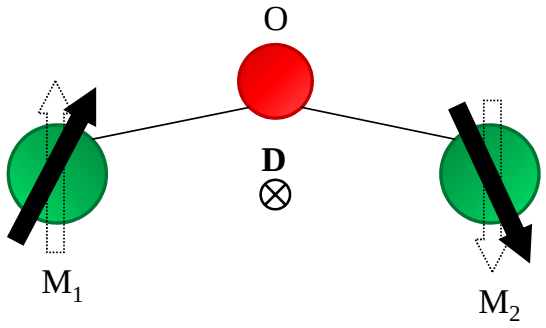

Figure 1.14: Dzyaloshinskii - Moriya Interaction in system consisting of two magnetic ions of vanadium and a diamagnetic ion O. DM vector D is non-zero because the geometric center of [M_1, M_2] is not the center of inversion of the system. D is dependent on the position of O and promotes a canting of the spins of vanadium atoms..

the interaction is frustrated by the presence of coupling with the rare earths.

1.4.4 Dzyaloshinskii-Moriya interaction

The Dzyaloshinskii-Moriya interaction is a relativistic correction of the superexchange. Dzyaloshinskii-Moriya theory (DM) [60]was developed in 1958 in the purpose to the low magnetic moment in the antiferromagnetic Fe2O3 material. Dzyaloshinskii shows that if the spins are collinear and parallel to the axis of symmetry, the later remains remains unchanged while there is a ferromagnetic component if If the spins are not collinear. an antisymmetric exchange interaction term is then introduced in the free energy:

$$D.(S_1 \times S_2) \tag{1.21}$$

- where D is the Dzyaloshinskii-Moriya vector
- $S_1$and S_2 are spins of the magnetic atoms

A canting of the spins is favored giving birth to a low ferromagnetic moment. In 1960, T. Moriya developed a microscopic theory of this interaction. It showed that spin-orbit coupling is responsible on this interaction by adding an antisymmetric component. In addition, t. Moriya pointed out that in the system of two magnetic atoms $M_1$and M_1(such as $RMnO_3$and RMn_2O_5), when the middle of the two atoms is not the system inversion center, D will not be zero. Thus, D depends on the position of the Oxygen ion. As shown in Figure 1.11, DM interaction is related to system symmetry and promotes non-collinear alignment of the magnetic moments.

1.5 Outline of the thesis

The perovskite-type vanadium oxides RVO3 display a great variety of phase transitions associated with a series of charge, spin and orbital ordering phenomena which present a good opportunity to tune their magnetocaloric effect. Nonetheless, their potential for magnetic cooling application has not yet been explored except for bulk $HoVO_3$. Therefore, our aim in this thesis is to explore and tune the magnetocaloric effect in highly epitaxial $PrVO_3$ thin films. First, we will introduce in chapter 2 the experimental tools and the theoretical methods used in this thesis to fabricate and characterize the oxide thin films and to calculate the magnetocaloric effect. Therereafter, chapter 4 focuses on the investigations of the strain and thickness-dependent magnetic and magnetocaloric properties of the studied PrVO3 thin films. We report a combinaison of both experimental and theoretical studies revealing outstanding magnetocaloric performance for magnetic cooling at cryogenic temperatures. Finally, in chapter 4, the mechanisms behind the giant magnetocakiruc effect in $HoMn_2O_5$ single crystals were studied using both DFT calculation and Monte Carlo simulation.

.

Bibliography

[1] G. Velders, D. Fahey, J. Daniel, M. McFarland and S. Andersen, Proc. Natl. Acad. Sci., vol. 106, p. 10949, 2009.

[2] O. Tegus, E. Br£uck, K. H. J. Buschow, and F. R. de Boer, Nature 415, 150 2002

[3] A. Fujita, S. Fujieda, Y. Hasegawa, and K. Fukamichi, Phys. Rev. B 67, 104416 2003

[4] https://www.kennethresearch.com/sample-request-10059802

[5] P. Weiss and A. Piccard, J. Phys. (Paris), vol. 7, p. 103, 1917.

[6] P. Weiss and A. Piccard, Comptes Rendus, vol. 166, p. 352, 1918.

[7] P. Debye, Ann. Physik., vol. 81, p. 1154, 1926.

[8] W. Giauque, J. Amer. Chem. Soc., vol. 49, p. 1864, 1927.

[9] W. Giauque and D. MacDougall, Phy. Rev., vol. 43, p. 768, 1933.

[10] G.V. Brown, J. Appl. Phys., vol. 47, p. 3673, 1976.

[11] Pecharsky V K and Gschneidner K A J 1997 Phys. Rev. Lett. 78 4494–4497

[12] Federal Register / Vol. 74, No. 239 / Tuesday, December 15, 2009 / Rules and Regulations

[13] B.F. Yu et al. / International Journal of Refrigeration 26 (2003) 622–636

[14] T. Christiaanse and E. Brück, Metall. Mater. Trans. E, vol. 1, p. 36, 2014.

[15] R. A. Kishore and S. PriyaSustainable, Energy Fuels, 1, 1899 2017

[16] image credits to lmari Karonen, wikipedia

[17] A.M. Tishin and Y.I. Spichkin. The Magnetocaloric Effect and its Applications. Institute of Physics Publishing, Temple Back, Bristol, UK, 2003

[18] A.H. Morrish. The Physical Principles of Magnetism. John Wiley & Sons, Inc., 1965

[19] KA Gschneidner Jr and VK Pecharsky. ńThirty years of near room temperature magnetic cooling: Where we are today and future prospectsż. In: International journal of refrigeration 31 (2008), pp. 945–961

[20] Tishin, A. M. & Spichkin, Y. I. The Magnetocaloric Effect and its Applications (Institute of Physics, 2003)

[21] Moore, J. D., Skokov, K. P., Liu, J. & Gutfleisch, O. Procedure for numerical integration of the magnetocaloric effect. J. Appl. Phys. 112, 063920 (2012).

[22] Moya, X. et al. Giant electrocaloric strength in single-crystal BaTiO3. Adv. Mater. 25, 1360–1365 (2013).

[23] Moya, X. et al. Giant and reversible extrinsic magnetocaloric effects in La0.7Ca0.3MnO3 films due to strain. Nature Mater. 12, 52–58 (2013).

[24] Moya, X., Kar-Narayan, S. & Mathur, N. D. Caloric materials near ferroic phase transitions. Nat. Mater. 13, 439–450 (2014)

[25] Caron, L. et al. On the determination of the magnetic entropy change in materials with first-order transitions. J. Magn. Magn. Mater. 321, 3559–3566 (2009)

[26] Das, M., S. Roy, and P. Mandal. Physical Review B 96.17 (2017): 174405.

[27] Karaca HE, Karaman I, Basaran B, Ren Y, Chumlyakov YI, Maier HJ. 2009Magnetic field-induced phase transformation in NiMnCoIn magnetic shape-memory alloys—a new actuation mechanism with large work output. Adv. Funct. Mater. 19, 983–998

[28] Gottschall T. 2016On the magnetocaloric properties of Heusler compounds: reversible, time- and size-dependent effects of the martensitic phase transition. PhD thesis, Technische Universitt Darmstadt, Fachbereich Material- und Geowissenschaften, Darmstadt, Germany

[29] https://www.kennethresearch.com/sample-request-10059802

[30]] P. J. von Ranke , N. A. de Oliveira , B. P. Alho , E. J. R. Plaza , V. S. R. de Sousa , L. Caron , M. S. Reis , J. Phys.: Condens. Matter 2009 , 21 , 056004

[31] A. Giguère , M. Földeàki , B. Ravi Gopal , R. Chahine , T. K. Bose , A. Frydman , J. A. Barclay , Phys. Rev. Lett. 1999 , 83 , 2262 .

[32] L. Tocado , E. Palacios , R. Burriel , J. Appl. Phys. 2009 , 105 , 093918 .

[33] M. Balli, D. Fruchart, D. Gignoux, and R. Zach, Appl. Phys. Lett. 95, 072509 (2009).

[34] L. Tocado , E. Palacios , R. Burriel , J. Appl. Phys. 2009 , 105 , 093918 .

[35] A. de Campos, D. L. Rocco, A. Carvalho, G. Magnus, L. Caron, A. A. Coelho, S. Gama, L. M. D. Silva, F. C. G. Gandra, A. O. D. Santos, L. P. Cardoso, P. J. von Ranke, and N. A. de Oliveira, Nature Mater. 5, 802 (2006)

[36] A. Giguère , M. Földeàki , B. Ravi Gopal , R. Chahine , T. K. Bose , A. Frydman , J. A. Barclay , Phys. Rev. Lett. 1999 , 83 , 2262

[37] Gutfleisch O., Gottschall T., Fries M., Benke D., Radulov I., Skokov K. P., Wende H., Gruner M., Acet M., Entel P. and Farle M. Mastering hysteresis in magnetocaloric materials374Philosophical Transactions of the Royal Society A: Mathematical, Physical and Engineering Sciences

[38] J. Lyubina , R. Schäfer , N. Martin , L. Schultz , O. Gutfl eisch , Adv. Mater. 2010 , 22 , 3735

[39] T. Gottschall, A. Grácia-Condal, M. Fries, A. Taubel, L. Pfeuffer, L. Mañosa, A. Planes, K. P. Skokov, O. Gutfleisch, Nat. Mater. 2018, 17, 929

[40] N. A. Spaldin. "MATERIALS SCIENCE: The Renaissance of Magnetoelectric Multiferroics." In: Science (80-.). 309.5733 (2005), pp. 391–392

[41] B. B. Van Aken, J. P. Rivera, H. Schmid, et al. "Observation of ferrotoroidic domains." In: Nature 449.7163 (2007), pp. 702–705

[42] D. Khomskii. "Trend: Classifying multiferroics: Mechanisms and effects." In: Physics (College. Park. Md). 2 (2009), p. 20 (cit. on pp. 5, 15)

[43] T. Kimura, T. Goto, H. Shintani, et al. "Magnetic control of ferroelectric polarization." In: Nature 426.6962 (2003),

[44] N. Hur, S. Park, P. A. Sharma, et al. "Electric polarization reversal and memory in a multiferroic material induced by magnetic field." In: Nature 429.6990 (2004), pp. 392–395.

[45] J. B. Goodenough and J. M. Longo. "Landolt-Brönstein, Numerical Data and Functional Relationships in Science and Technology, New Series." In: Springer, Berlin III.4 (1970)

[46] T. Mitsui. "Landolt-Brönstein, Numerical Data and Functional Relationships in Science and Technology, New Series." In: Springer, Berlin 16(1) (1981)

[47] N. A. Hill. "Why Are There so Few Magnetic Ferroelectrics?" In: J. Phys. Chem. B 104.29 (2000), pp. 6694–6709.

[48] Kramers, H. A. (1934). L'interaction entre les atomes magnetogenes dans un cristal paramagnetique. Physica, 1, 182192.

[49] Dzyaloshinsky, I. (1958). A thermodynamic theory of a weak ferromagnetism of antiferromagnetics. Journal of Physics and Chemistry of Solids, 4(4), 241 255.

[50] G. R. Blake, T. T. M. Palstra, Y. Ren, A. A. Nugroho, et A. A. Menovsky. Physical Review Letters 8724(24), 5501–5508 (2001)

[51] J. Kanamori. J. Phys. Chem. Solids 10, 87 (1959).

[52] J.B. Goodenough. Phys. Rev. 100, 564 (1955).

[53] TU Darmstadt, Functional Materials/prspics/Piqza.de

[54] S. Miyasaka, Y. Okimoto, M. Iwama, Y. Tokura; Physical Review B 68 (2003)

[55] Y. Ren, A. A. Nugroho, A. A. Menovsky, J. Strempfer, U. Rutt, F. Iga, T. Takabatake, C. W. Kimball; Physical Review B 67, 014107 (2003)

[56] G. Khaliullin, P. Horsch, A. M. Oles; Physical Review Letters 86, 3879 (2001)

[57] Y. Yamashita, N. Shibata, K. Ueda; Physical Review B 58, 9114 (1998)

[58] F. Mila, B. Frischmuth, A. Deppeler, M. Troyer; Physical Review Letters 82, 3697 (1999)

[59] C. Ulrich, G. Khaliullin, J. Sirker, M. Reehuis, M. Ohl, S. Miyasaka, Y. Tokura, B. Keimer; Physical Review Letters 91, 257202 (2003)

[60] J. Sirker, G. Khaliullin; Physical Review B 67 (2003)

[61] S. Miyashita, A. Kawaguchi, N. Kawakami, G. Khaliullin; Physical Review B 69 (2004)

[62] A. A. Tsvetkov, F. P. Mena, P. H. M. van Loosdrecht, D. v. der Marel, Y. Ren, A. A. Nugroho, A. A. Menovsky, I. S. Elmov, G. A. Sawatzky; Physical Review B 69, 075110 (2004)

[63] G. Khaliullin; Progress of Theoretical Physics Supplement 155{202 (2005)

[64] J. Q. Yan, J. S. Zhou, J. B. Goodenough; Physical Review Letters 93, 235901 (2004)

[65] Y. Motome, H. Seo, Z. Fang, N. Nagaosa; Physical Review Letters 90 (2003)

[66] Z. Fang, N. Nagaosa; Physical Review Letters 93, 176404 (2004)

[67] T. Kimura, T. Goto, H. Shintani, K. Ishizaka, T. Arima, et Y. Tokura. Magnetic control of ferroelectric polarization. Nature 426, 55-58 (2003)

[68] N. Hur, S. Park, P. Sharma, J. Ahn, S. Guha, and S.-W. Cheong. Electric polarization reversal and memory in a multiferroic material induced by magnetic fields. Nature 429, 392 (2004)

[69] Y.Noda et al. Mangetic and ferroelectric properties of multiferroic RMn2O5. J. Phys : Condens. Matter 20, 434206 (2008)

Chapter 2

Experimental and theoretical techniques

This chapter describes the experimental methods and the theoretical approaches I used in this thesis for the sample elaboration and the study of the magnetic and magnetocaloric properties. First, i will introduce in section 2.1 the techniques used to grow and characterize the oxide thin films. Section 2.2 will cover the computational methods performed to investigate the structure, magnetic and magnetocaloric properties of the studied materials.

2.1 Sample elaboration and characterization

2.1.1 Sample elaboration

Several thin film deposition techniques are available including molecular beam epixaty, atomic layer deposition, DC magnetron sputtering ans so forth. to elaborate our samples, Pulsed laser deposition (PLD) was carred out by (team..). It is a conceptually simple technique: an intense pulsed laser beam (typically 10-30 ns) passes through the optical window of a vacuum chamber and is focused on a target that can be solid or liquid. The energy is partially absorbed and if the energy density (fluence) is greater than the clagging threshold of the material, the laser-material interaction results in the creation of a plasma consisting of partially ionized species directed perpendicularly on the surface of the target. A substrate is placed in front of the target at a certain distance from it and the plasma species condense there. This is followed by the nucleation and growth of the film.

Despite its promising aspects and simplicity, this technique was not indisputable success until 1987[1] and the development of short pulse lasers of very high energy density. Applied in the field of the deposit of thin films of superconductors at high critical temperature, it then proved its effectiveness and originality. This work has undoubtedly con-

tributed to the dissemination of this technique in the scientific community, which has since given rise to a large number of publications related to laser ablation and LDP. Although its industrial development remains limited, it is still a very interesting technique for the synthesis of new materials and nanoarchitectures that pave the way for new scientific advances in the field of physics and Technologies.

The main advantages of this technique are the ability to obtain high-density films, with controlled setchiometrics, in a relatively simple way compared to other methods of vacuum deposits and without external contamination. Whereas every technique has limitations, this one could not be the excaption. the inconvenient of PLD technique is the restriction to small substrate areas of $\sim 2cm^2$and the large kinetic energy of some plume species which affecting the substrate negatively (re-sputtering). The studied epitaxial films were grown by on two different substrates (001)-oriented(La,Sr)(Al,Ta)O_3 (LSAT) with a thickness of 41.7 nm, and on (001)-oriented SrTiO_3 (STO) with a thickness of 100 nm. A KrF excimer laser (= 248 nm) with repetition rate of 2 Hz and laser fluence of 2 J/cm2 was focused on stoichiometric ceramic targets. All the flms used in this study were deposited at an optimum growth temperature (T_G) of 650 C and under oxygen partial pressure (P_{o_2}) of 10^6mbar.

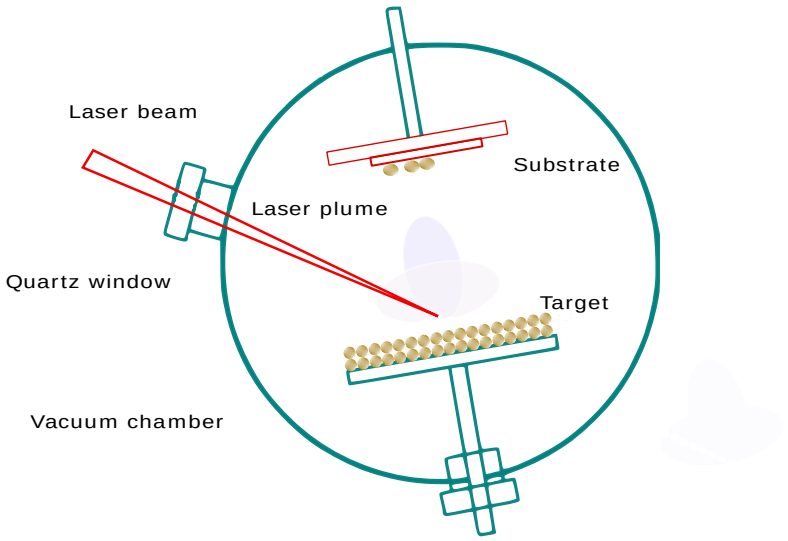

Figure 2.1: Schematic of pulsed laser depositon (PLD)

2.1.2 Magnetic characterization

In this thesis, the magnetic characterizations of the deposited thim films have been performed using VSM (vibrating sample magnetometer)[7]. This technique aims at oscillating the sample within uniform magnetic field which induce an electrical voltage in the

detective coils proportional to to the magnetization of the sample. Different models of VSM are available, Superconducting Quantum Interference Device (SQUID) (shown in Figx) is the most adapted model to a specific type of materials of which at least one dimensions is nanometric or for bulk materials/powders of very low magnetization. This device allow to measure low magnetic signals with a sensitivity that can reach 10^{-8} emu. It equipped with a superconducting coil allowing the application of magnetic fields ranging from -7 to 7 Tesla and the control the temperature of the sample is possible from 2 K to 1000 K . The key magnetic parameters enabling us to understand the magnetism and the magnetocaloric effect of the studied samples such as the saturation magnetization, the effective anisotropy or the coercivity are extracted successfully.

Figure 2.2: MPMS SQUID VSM from Quantum Design

2.2 Ab initio calculations

Because of the complexity of some systems, research scientists are more and more oriented toward the use of theoretical calculations to interpret the data relating to the experimentation. In addition, the theoretical calculations are used to predict the behavior and the properties at a resolution and lenght scale currently inacessible to experiments and in very difficult conditions such as the zones of pressure and extreme temperetures. Indeed, computer apporaches help to synthetize systems efficiently, to stock and to search the data of physical entities, as well as to envisage new materials difficult to test making the research life easier for scientists. Throughout this thesis, i have used density functional

theory (DFT) and Monte Carlo simulation to study the magnetic and magnetocaloric effect of oxide materials.

2.2.1 Introduction to ab initio calculations

The study at the quantum level of the electronic, magnetic and other properties of a periodic crystal is one of the most traditional subjects of solid state physics. At present, a lot of theoretical schemes have been proposed to understand and interpret experimental measurements. In the atomic scale, several numerical simulations are based on an empirical description of correlations between atoms. This approach seems well adapted to the study of the ionic materials, rare gases, or to any other material in which electronic states do not depend on the local arrangement of atoms. On the contrary, this theory is very limited for other type of material and precisely metals for which the energy redistribution of electrons in response to the rearrangements of atoms is impossible to describe by simple physical models because the equations of states become more and more complicated to solve and as a result it was necessary to search for other formalisms that describe better the properties of a system. A realistic treatment of metals must then necessarily go through an approach based on an explicit description of the electronic structure which gives birht to the theory of density functional theory (DFT). In this subsection, an introduction to ab initio calculations and the basic concepts behind it will be given.

2.2.2 Quantum many-body systems

From the microscopic point of view a solid can be seen as a collection of heavy, positively charged nuclei (n) and lighter, negatively charged electrons (e). The nuclei and electrons are treated as electromagnetically interacting point charges and the exact nonrelativistic many-body hamiltonian for this system becomes:

$$\begin{aligned} H = -\frac{\hbar}{2}^2 \sum_i \frac{\nabla^2_{\vec{Ri}}}{M_i} - \frac{\hbar}{2}^2 \sum_i \frac{\nabla^2_{\vec{r_i}}}{m_e} - \frac{1}{4\pi\varepsilon_0} \sum_{ij} \frac{e^2 Z_i}{\left|\overrightarrow{R_i} - \overrightarrow{r_j}\right|} \\ + \frac{1}{8\pi\varepsilon_0} \sum_{i\neq j} \frac{e^2}{\left|\overrightarrow{r_i} - \overrightarrow{r_j}\right|} + \frac{1}{8\pi\varepsilon_0} \sum_{i\neq j} \frac{e^2 Z_i Z_j}{\left|\overrightarrow{R_i} - \overrightarrow{R_j}\right|} \end{aligned} \tag{2.1}$$

M_i is the mass of the nucleus at R positioned at $\overrightarrow{R_i}$ .The electrons have mass m_e and are positioned at$\overrightarrow{r_i}$. The first and second term correspond to the kinetic energy operator of the nuclei and of the electrons respectively. The remaining terms describe the Coulomb interaction between electrons and nuclei, among electrons and among nuclei respectively.

To know the state (wave functions $\psi(\overrightarrow{R},\overrightarrow{r})$, avec $\overrightarrow{R} = \overrightarrow{R_1} + ...\overrightarrow{R_i}$ et $\overrightarrow{r} = \overrightarrow{r_1} + ...\overrightarrow{r_j}$) of this system the corresponding Schrodinger equation has to be solved:

$$H\psi(\overrightarrow{R},\overrightarrow{r}) = E\psi(\overrightarrow{R},\overrightarrow{r}) \tag{2.2}$$

Unfortunately, due to the high degree of complexity it requires the introduction of some appoximations to facilitate the calculations and to solve the Schrodinger equation.

2.2.3 The Born-Oppenheimer approximation

In 1927, the two physicists Max Born and Robert Oppenheimer developed an approach to quantum theory describing molecules, called the Born-Oppenheimer approximation. The purpose of this approximation is to simplify and solve the Schrodinger equation. In fact, electrons and atomic nuclei have very different masses and the magnitude of the electromagnetic forces acting on them are same. As a result, the electronic motion ($\approx 10^6$m/s) and nuclear motion ($\approx 10^3$m/s) can be separated leading to a molecular wave function depending on the electorn positions (nuclear positons are fixed). The assumption of instananeous equilibrium for every nuclear configuration implies that the electron wave function is a solution of equation 1.1

$$H = \underbrace{-\hbar^2 \sum_i \frac{\nabla^2_{\overrightarrow{r_i}}}{m_e}}_{T_e} \underbrace{- \frac{1}{4\pi\varepsilon_0} \sum_{ij} \frac{e^2 Z_i}{\left|\overrightarrow{R_i} - \overrightarrow{r_j}\right|}}_{V_{ext}} + \underbrace{\frac{1}{8\pi\varepsilon_0} \sum_{i\neq j} \frac{e^2}{\left|\overrightarrow{r_i} - \overrightarrow{r_j}\right|}}_{V_e} + \underbrace{\frac{1}{8\pi\varepsilon_0} \sum_{i\neq j} \frac{e^2 Z_i Z_j}{\left|\overrightarrow{R_i} - \overrightarrow{R_j}\right|}}_{V_{NN}} \tag{2.3}$$

As already mentioned, this approximation is intended to simplify the Schrodinger equation and therfore reduce the variables to describe the wave function. Considering the immobility of the nuclei, the nuclear repulsion term (V_{NN}) become negligible and the hamiltonian can be written in the following reduced form :

$$H_e = \underbrace{-\hbar^2 \sum_i \frac{\nabla^2_{\overrightarrow{r_i}}}{m_e}}_{T_e} \underbrace{- \frac{1}{4\pi\varepsilon_0} \sum_{ij} \frac{e^2 Z_i}{\left|\overrightarrow{R_i} - \overrightarrow{r_j}\right|}}_{V_{ext}} + \underbrace{\frac{1}{8\pi\varepsilon_0} \sum_{i\neq j} \frac{e^2}{\left|\overrightarrow{r_i} - \overrightarrow{r_j}\right|}}_{V_e} \tag{2.4}$$

The new equation called the electron hamiltonian since $H = H_e + V_{NN}$, the kinetic energy of the electrons is represented by T_e term, V_{ext} represents the electronic repulsion and V_e is the electron-nucleus interaction. Henceforth, electronic motion and the nuclear motion can be separated.

2.2.4 Density functional theory

Despite the fact that the resolution of the Schrödinger equation is simplified and reduced to the behavior of electrons, it is still very complex to solve because of the electron-electron interactions and therefore the intervention of other complementary approximations will be necessary. The Hartree-Fock (HF) approximation is one of the most important ways to deal with that problem, this method is based on an important element which is Pauli exclusion principle, this principle means that two fermions cannot occupy the same quantum state leading us to consider the anti-symmetry of the wave function that will be described by the Slater determinant. This method is, however, quite complex to solve for solids due to the presence of the exchange potentiel taking into account the anti-symmetry of the wave function. The resolution of Schrodiner equation was beyond human reach until discovery of Hohenberg [10], Kohn and sham [11] that leads to a remarkable reduction in difficulty giving birth to the density functional theory (DFT). In principle, the only input required for DFT calculations is the most basic informations related to the system: atomic species and atomic positions.

2.2.4.1 The theorems of Hohenberg and Kohn

The Hohenberg and Kohn [10] approach is linked to any system consisting of electrons moving under the influence of external potential. It aims to make the DFT an exact theory for many-body systems and is based on two theorems that state:

First theorem The total energy of a particle system is expressed as a unique functional of total density (r) [xxx]. In other words, there is unique link between the external potentiel and electronic density. Therefore, the hamiltonian operator is determined only by electronic density and from that operator the properties of the system can be calculated.

Second theorem A universal functional for the energy in terms of the density $\rho\left(\overrightarrow{r}\right)$ can be defined for any V_{ext}. The exact ground state energy of the system is the global minimu that corresponds to the exact ground state density. The ground state energy $H[\rho] = E_{V_{ext}}[\rho]$ is of the form :

$$E_{V_{ext}}[\rho] = \langle\psi|T+V|\psi\rangle + \langle\psi|V_{ext}|\psi\rangle \tag{2.5}$$

$$= F_{H.K}[\rho] + \int \rho(\overrightarrow{r}).d\overrightarrow{r}V_{ext}\left(\overrightarrow{r}\right) \tag{2.6}$$

Where the Hohenberg and Kohn density functional is universal for any many-electron system.

In principle, the problem boils down to minimization of the total energy of the system by respecting the variations of the density governed by the constraint on the number of particules. At this stage, the dft allows the reformulation of the problem and not so solve it considering the lack of knowledge of the H-K density functional $F_{H,K}$.

2.2.4.2 The Kohn-Sham equations

Kohn and Sham [11] made an important step towards applicability of DFT by replacing the actual system of interacting particles with a imaginary system that does not interact and has the same electronic density as the real system. In this case the kinetic energy operator will be known and the density functional $F_{H,K}$.takes the following form :

$$F_{HK}[\rho] = T_0[\rho] + V_H[\rho] + \underbrace{V_c[\rho] + V_x[\rho]}_{V_{xc}[\rho]} \tag{2.7}$$

where $T_0[\rho]$ is the kinetic energy functional for noninteracting system and $V_H[\rho]$ is the Hartree contribution, which describes the interaction with the field obtained by averaging over the positions of the remaining electrons. Supposing that we know the exchange-correlation functional $V_{xc}[\rho]$, we can now write :

$$E_{v_{ext}}[\rho] = T_0[\rho] + V_H[\rho] + V_{xc}[\rho] + V_{ext}[\rho] \tag{2.8}$$

meaning that nonininteracting particles energy is submitted to two external potentials $V_{ext}[\rho]$and $V_{xc}[\rho]$,with corresponding K-S hamiltonian:

$$H_{KS} = T_0 + V_H + V_{xc} + V_{ext} \tag{2.9}$$

$$= \frac{\hbar}{2m_e}^2 \nabla_i^2 + \frac{e^2}{4\pi\varepsilon_0} \int \frac{\rho(\vec{r})}{|\vec{r} - \overrightarrow{r}|} d\vec{r} + V_{xc} + V_{ext} \tag{2.10}$$

ith the exchange-correlation associated to the functional derivative:

$$V_{xc} = \frac{\partial V_{xc}[\rho]}{\partial \rho} \tag{2.11}$$

Following K-S theorem and for a system of N electron, the exact ground state density $\rho(\vec{r})$ is :

$$\rho\left(\overrightarrow{r}\right) = \sum_{i=1}^{N} \psi_i^*(\overrightarrow{r})\psi_i(\overrightarrow{r}) \tag{2.12}$$

where $\psi_i(\overrightarrow{r})$ represents the single-particle wave functions being the N lowest energy solutions of the K-S equation

$$H_{KS}\psi_i(\overrightarrow{r}) = \epsilon_i\psi_i(\overrightarrow{r}) \tag{2.13}$$

Now, the only remaining parameter enabling us to solve the Schrodinger like single particle equation is the exchange-correlation functional. Nevertheless, this functional can be submitted to approximations in order to be calculated.

2.2.4.3 The exchange-correlation functional

The effectiveness of the Kohn-Sham approach depends entirely on the ability to calculate as precisely as possible V_{XC}. Given the fact that the exact expression is not known, the simplest formulation of this potential is obtained in the context of local density apporixmation (LDA) and generalized gradient approximation (GGA).

LDA [11, 12, 13, 14]defines the the exchange correlation functional as :

$$V_{xc}^{LDA}[\rho] = \int \rho(\vec{r})\,\varepsilon_{xc}(\rho(\vec{r}))d\vec{r} \tag{2.14}$$

The point of departure of this approximation is based on the fact that we can assimilate the inhomogeneous gas (real) with a homogenous gas with the same density r(r) for the calculation of the energy of the exchange-correlation by electron[10]. It is quite clear that in this approximation, it is assumed that the spatial fluctuations of the electronic density in the real gas are slow, this can sometimes be quite imprecise. For this reason, a significant improvement is to take into account the variations of $\rho(\vec{r})$ including precisely the density gradient to calculate V_{XC}:

$$V_{xc}^{GGA}[\rho] = \int \rho(\vec{r})\,\varepsilon_{xc}\left[\rho(r), |\nabla\rho(r)|\right] d\vec{r} \tag{2.15}$$

Using this approximation, namely GGA [15, 16, 17], the results are rather better. The lattices parameters calculated with GGA match quite well with experiment in most cases and for many magnetic systems it predicts the ground state perfectly while the LDA gives values in general 1-4% smaller than the experimental and fails also in predicting the real ground state for many systems. Overall, GGA is considered to be an improvement of the LDA.

DFT+U even though exact DFT allow the obtaining of the ground state properties correctly, Both apprixmations are not successful for all systems. In fact, LDA and GGA approximationa are not able to correctly describe the electronic structure and thus the conduction properties of strongly correlated materialss due to the well-localized d(f) electrons and a sizable energy gap between occupied and unoccupied subbands. The DFT+U [17, 18] correction can be introduced to treat the strong on-site Coulomb interactions of the localised 3d and 4f electrons explicitly with an additional Hubbard term. In this thesis, the materials studied are strongly correlated systems which makes the use of DFT+U of great benefits.

2.2.5 Solving the equations

At this level, the final task to accomplish is solving the resulting Kohn-Shame equation :

$$\underbrace{(-\frac{\hbar}{2m_e}^2\nabla_m^2 + \frac{e^2}{4\pi\varepsilon_0}\int\frac{\rho(\vec{r})}{|\vec{r}-\vec{r}|}d\vec{r} + V_{xc} + V_{ext})}_{H_{KC}}\psi_m(\vec{r}) = \epsilon_m\psi_m(\vec{r}) \tag{2.16}$$

Expanding the one-electron functions over a limited basis set $\phi^b_{p_{p=1..P}}$ is a major key to obtain the final solution, :

$$\psi_m = \sum_{p=1}^{p} c_p^m \phi_p^b \tag{2.17}$$

In principle the idea was to reduce the integro differential equation system to a matrix eigenvalue problem. Certain approximations helped further on to simplify the problem giving rise to powerful computational methods like Pseudopotentiel, APW and it derivative LAPW to be discussed in some detail below.

2.2.5.1 The pseudopotentiel basis set

The purpose of this method is to take into account only valence electrons since most physical and chemical properties of solids are less depending on the core electrons assumed to be frozen [19]. In this approach, the correlation between electron-ion in metals is expressed according to a so-called pseudo-potentiel which acts on a set of pseudo wave functions rather than on the real valence wave functions.

Several different pseudopotentials are available, such as : projected augmented waves (PAW), orthogonalised plane wave (OPW) and ultra-soft pseudopotentials (USPP). For the simulation of oxide thin films, the projected augmented wave (PAW) method proposed by

Bloch , and implemented in VASP (Vienna Ab initio Simulaiton Package) software is used. The wave functions of all electrons ψ^{AL} is now wrriten as follows:

$$|\psi^{AE}>=|\psi_{\nu}^{PS}>+\sum_{\mathrm{i}} c_i(|\ \varphi_i^{AE}>-|\varphi_i^{PS}>) \tag{2.18}$$

where ψ_{ν}^{PS} refers to the valence electrons pseudo-function, φ_i are the local functions defined in the space centered in atoms core. ψ_{ν}^{PS}can be written as follows :

$$\psi_{\nu}^{PS}=\sum_{i}<\rho_i\mid\psi_{\nu}^{PS}>\varphi_{\nu}^{PS} \tag{2.19}$$

The all electrons wave functions can be now written as :

$$|\psi^{AE}>=|\psi_{\nu}^{PS}>+\sum_{\mathrm{i}}|\varphi_i^{PS}><\rho_i\mid\psi_{\nu}^{PS}>+\sum_{\mathrm{i}}|\varphi_i^{AE}><\rho_i\mid\psi_{\nu}^{PS}>) \tag{2.20}$$

2.2.5.2 The LAPW basis set

The LAPW (Linearized Augmented Plane Wave), developed by Andersen [24], is fundamentally an improvement of the APW (Augmented plane waves) method developed by Slater [23]which ensures the continuity of the potential on the surface of the " muffin-tin " sphere (S_{MT}) , the potential is developed in as follows:

$$V(r)=\begin{cases}\sum_{lm} V_{lm}Y_{lm}(r) & \vec{r}\in S_{MT}\\ \sum_k V_k^{ikr} & \vec{r}\notin S_{MT}\end{cases} \tag{2.21}$$

Before describing the LAPW method, we will remind the basics of APW method. Slater considers that the space is divided into two types of region (Fig): near nuclei and away from them. Far away from nuclei, the region has a potential and a wave function similar to those of an isolated atom (the potentiel varies strongly). Close to nuclei, electrons behave as if they were in free atoms and therefore, the APW basis function is written as folllows:

$$\varphi(\vec{r},E)=\begin{cases}\frac{1}{\sqrt{V}}e^{i(\vec{k}+\vec{K}).\vec{r}} & \vec{r}\in I\\ \sum_{l,m} A_{lm}^{\alpha,\vec{k}+\vec{K}}u_l^{\alpha}(r_i,E)\,Y_{lm}^{l}(r_i\quad) & \vec{r}\in S_{MT}\end{cases} \tag{2.22}$$

with $\vec{k}$ a vector in the first Brillouin zone, I(interstitial region) is the region between the spheres,$\vec{K}$ a reciprocal lattice vector and V the unit cell volume. The $Y_{lm}^{l}(r_i)$ are spherical harmonics with {l,m} an angular momentum index and $\vec{r_i}=\vec{r}-\vec{r_\alpha}$ where the $\vec{r_\alpha}$ is the atomic position within the unit cell of α.$A_{lm}^{\alpha,\vec{k}+\vec{K}}$ are expansion coefficients and $u_l^{\alpha}(r_i,E)$ is a

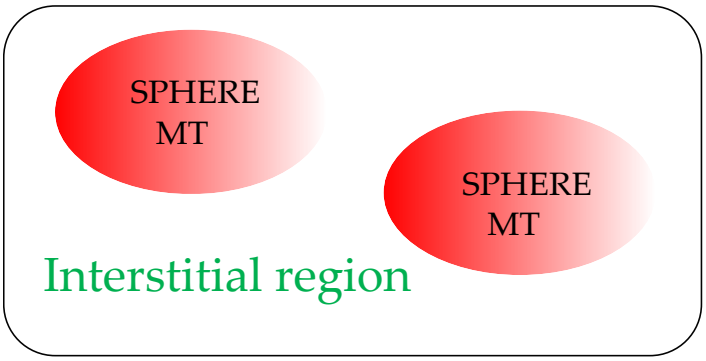

Figure 2.3: Partition of the unit cell in atomic spheres and in interstitial region

solution of the radial Schrodinger equation with spherical averaged crystal potential V(r) centered at atom.

The lack of variational freedom to deal with deviations of the band energy $\epsilon^{n}_{\overrightarrow{k}}$ from the trial value of E is a real problem since we need in APW method to costruct the $u^{\alpha}_{l}(r_i, E)$ function using the eigenvalue $\epsilon^{n}_{\overrightarrow{k}}$ of the searched eigenstate $\psi^{n}_{\overrightarrow{k}}$ for E which is uknown. LAPW method[24, 7, 26] is considered as a solution to this problem since the basis functions here have an expansion in spherical harmonics inside S_{MT} and plane waves in interstitial region. A part in the LAPW basis function is the muffin-tin region, which is the augmentation, is has been replaced by a linear combinaison first function u^{α}_{l} and its derivative $\dot{u}^{\alpha}_{l}$ calculated at a fixed energy E_0.

$$\varphi(\vec{r}, E) = \begin{cases} \frac{1}{\sqrt{V}} e^{i(\vec{k}+\vec{K}).\vec{r}} & \vec{r} \in I \\ \sum_{l,m}[A^{\alpha,\vec{k}+\vec{K}}_{lm} u^{\alpha}_{l}(r_i, E_0) + B^{\alpha,\vec{k}+\vec{K}}_{lm} \dot{u}^{\alpha}_{l}(r_i, E_0)]Y^{l}_{lm}(r_i \quad) & \vec{r} \in S_{MT} \end{cases} \tag{2.23}$$

This method is implemented in Wien2k-code (more details in APPENDIX 1) developed by Peter Blaha and Karlheinz Schwarz [27]that i used for the investigations of structural and magnetic properties in RMn2O5 materials.

2.3 Monte Carlo simulation

The notion of Monte Carlo simulation saw the light during the end of the second world war, it was used in the frameword of the US Manhattan project for the development of nuclear weapons. Thus, this century was a witness to the birth of first programmable computer. The main idea was to simulate using computers a stochastic phenomenon using random numbers as a statistical approach (random fluctuation of a system from one

state to another). In fact, the probability of detecting a system in a 'a' state during the simulation is equivalent to the weight of that state in the real system. This imposes the choice of a rule that manages the passage from one state to another during the simulation.

2.3.1 Theoretical models

Spin systems play a fundamental role in classical and quantum statistical mechanics especially to explain magnetism. Several spin models developed depend essentially on degrees of freedom and other terms of interaction in the Hamiltonian. Indeed, classical spin models include discrete models such as the *Potts model* and the *Ising model*, or continuous models such as the two-dimensional unit vectors of the *XY model*, the three-dimensional unit vectors of the classical *Heisenberg model*, and the *Blume-Emery Griffiths Model* [28]. In the following, i will describe the thre models used in this thesis.

Heisenberg model The classical Heisenberg model [29]is the case where spins takes values in the two-dimensional sphere. It is one of the models used in statistical physics to describe the ferromagnetism and other phenomena. In addition, the Heisenberg model is a model studied in statistical mechanics and specially utilized in the phase transitions study of magnetic systems, in which the spins are mechanically treated in a quantum way. In this model, the spins are represented by vectors with three components or by two variables of spherical coordinates θ and ϕ.

$$H = -J \sum_{<i,j>} (S_i)(S_j) - H \sum_{<i,j>} S_i)(S_j) \tag{2.24}$$

Where J is the exchnage interaction coupling and H is the external magnetic field.

Ising model The ising model is derived from Heisenberg model taking into consideration a strong uniaxial anisotropy. Only the Si projections along the axis of easy magnetization is then relevent. The ising Hamiltonian in the presence of an external magnetic field is given by :

$$H = -J \sum_{<i,j>} (S_i)(S_j) - H \sum_{i=1}^{N} (S_i) \tag{2.25}$$

Where J represents the exchange interactions coupling between first nearest neighbor noted <i,j> beween $S_i = \pm 1$ spins.

XY model The classical XY model is an important model studied extensively in statistical physics. This model is also derived from the Heisenberg model to which a strong planar anisotropy is added and studied for the particular case of the N-vector model (N = 2) where spins takes values in the unit cell. The Hamiltonian corresponding to this model is given by :

$$H = -J \sum_{<i,j>} cos(\theta_i - \theta_j) \tag{2.26}$$

where o varies between [0, 2π].

2.3.2 Basic of Monte Carlo simulation

The next step after choosing the model is In the following, we will define the steps of the metropolis algorithm. In order to introduce this algorithm in a simple way we will take the case of the Ising model.

2.3.3 Metropolis algorithm

This algorithm was invented by Nicholas Metropolis and his teammates in 1953 in the interest of calculating the equation of states of molecule mixtures in interactions [144]. Ergodicity and detailed balance are the two important conditions that stochastic Markov chain has to fulfill in order to converge to thermodynamic equilibrium. Metropolis algorithm consists in generating a Markov chain of spins configuartion: the displacement of a particle from a state x to a new state y $P(x \rightarrow y)$ is governed by a certain probability. Before describing the steps of this algorithm, is useful to define some basic concepts and some variables to allow the reader to assimilate all steps.

h is a random variable belonging to] 0, 1].

N is the number of spins of the system N = L^2or L^3,where L is the total number of spins.

The Monte Carlo cycle is a variable that depends on the size of the system, it is equal to N.

Monte Carlo cyle required to visite each site once on average.

Before constructing algorithm the parametres of the studied sytstème are fixed. In order to introduce this algorithm in a simple way, we will take the case of the ising model and we use the corresponding Hamiltonian described in equation x.

J is taken as a unit of energy (J=1), T is a variable in a J/K_B unit and the spin can take two distinct values ±1.

1. The first step consists in generating an initial configuration randomly. To achieve this, we choose randomly a number h over set of numbers uniformly distributed over the interval]0, 1]. If h belongs to]0, $\frac{1}{2}$], a number +1 (spin up) is associated for the first element of the system. If h belongs to]$\frac{1}{2}$, 1] then we associate -1 (spin down) for the the first element of the of the system. We proceed in the same manner until all the sites of the system are visited.

2. The second step is to visit a site at a random. To do so, we generate a random number α from the]0, 1] interval which will be multiplied by N so that $\alpha\times$N belong to [0, N−1]. We take then the integer part of $\alpha\times$N c so that this number coincides with a site of the system.

3. Once the spin (S_i) is chosen, we calculate its energy of interaction with the first four neighbors. we then calculate the difference in energy $\triangle E = E(S_i) - E(-S_i)$ between the current spin state (S_i) and state after its reversal.

- If $\triangle E \prec 0$: The change of the spin state is accepted which is in accordance with the principle of energy minimization.
- If $\triangle E \succ 0$: Another random number is then generated and compared to the Boltzmann factor $e^{(-\frac{\triangle E}{k_B \cdot T})}$.

If the random number is less than this Boltzmann factor, we accept the change in the state of the spin, otherwise, we leave its state as it is. We proceede in the same manner to complete the first Monte Carlo cycle, we then measure and accumulate the values of E, M, E^2, M^2, etc. The second Monte Carlo cycle begins with the final configuration of the first cycle, we operate in the same way until we finish all the MC cycles to obtain the statistical avergae of the quantities. We note that the precision on the average values increases with the increase in the number Monte Carlo steps.

Summary

In this chapter, we outlined the experimental techniques and the two theoretical simulation methods used in our research: the Ab-initio calculation and the Monte Carlo simulation. The first is based on different theoretical approaches, in particular the theory of density functional theory (DFT) for the resolution of the Schroedinger equation. The use of DFT theory allowed us to determine the fundamental state of the system studied. The second method is the Monte Carlo simulation whose main idea is the use of randomness

to solve problems that could in principle be deterministic. Monte Carlo method will help us to calculate the magnetic and magneticaloric properties of the studied materials.

Bibliography

[1] D. Dijkamp, et al. Appl. Phys. Lett, 51 (1987), p. 619

[2] S. Foner, "Versatile and sensitive vibrating-sample magnetometer," Review on scientific instruments, vol. 30, pp. 548-557, 1959.

[3] Anisimov V I, Zaanen J and Andersen O K 1991 Phys. Rev. B 44 943

[4] P. Hohenberg and W. Kohn, Inhomogeneous electron gas, Phys. Rev. 136 (1964), B864.

[5] W. Kohn and L.J. Sham, Self-Consistent Equations Including Exchange and Correlation Effects, Phys. Rev. 140 (1965), A1133.

[6] U. von Barth and L. Hedin, A local exchange-correlation potential for the spin polarized case., J. Phys. C: Solid State Phys. 5 (1972), 1629.

[7] D. M. Ceperley and B. J. Alder, Ground State of the Electron Gas by a Stochastic Method, Phys. Rev. Lett. 45 (1980), 566.

[8] S. H. Vosko, L. Wilk, and M. Nusair, Accurate spin-dependent electron liquid correlation energies for local spin density calculations: a critical analysis, Can. J. Phys. 58 (1980), 1200.

[9] J.P. Perdew and Y. Wang, Accurate and simple density functional for the electronic exchange energy: Generalized gradient approximation, Phys. Rev. B 33 (1986), 8800.

[10] J.P. Perdew and Y. Wang, Accurate and simple analytic representation of the electron-gas correlation energy, Phys. Rev. B 45 (1992), 13244

[11] J.P. Perdew, K. Burke, and M. Ernzerhof, Generalized Gradient Approximation Made Simple, Phys. Rev. Lett. 77 (1996), 3865.

[12] Anisimov V I, Zaanen J and Andersen O K 1991 Phys. Rev. B 44 943

[13] Anisimov V I, Aryasetiawan F and Lichtenstein A I 1997 J. Phys.: Condens. Matter 9 767

[14] Richard Martin, Electronic structure, Basic theory and practical methods, Cambridge University press, USA, 2004

[15] P. E. Blöch. Phys. Rev. B, 50, 17953, (1994).

[16] G. Kresse and J. Furthmüller. Phys. Rev. B, 54, 11169, (1996).

[17] G. Kresse and D. Joubert, Phys. Rev. 59 , 1758 (1999).

[18] J. C. Slater, Wave Functions in a Periodic Potential, Phys. Rev. 51 (1937), 846.

[19] O. K. Andersen, Linear methods in band theory, Phys. Rev. B 12 (1975), 3060.

[20] D. J. Singh, Planewaves, Pseudopotentials and the LAPW method, Kluwer Academic Publishers, Boston, 1994.

[21] D.D. Koelling and G. O. Arbman, Use of energy derivative of the radial solution in an augmented plane wave method: application to copper, J. Phys. F: Met. Phys. 5 (1975), 2041.

[22] Blaha, K. Schwarz, G.K.H. Madsen, D. Kvasnicka, J. Luitz, in:WIEN2K: An Augmented Plane Wave Plus Local Orbitals Program for Calculating Crystal Properties, Ed. K. Schwarz, Vienna Technological University, Vienna, Austria(2001).

[23] Hadjiagapiou, A. Ioannis. Phys. A:Statistical Mechanics and its Applications 390.7 (2011): 1279-1288.

[24] Yvon. La théorie du ferromagnétisme et le modèle Heisenberg. J. Phys. Radium, (1952), 13 (10), pp.488-489.

Chapter 3

Magnetocaloric effect in oxyde thin films

3.1 Introduction

Recently, The magnetocaloric effect in manganite-based perovskites exhibiting multiferroic behaviors have become an interesting topic because of the potential application of these oxides in some specific applications such as the liquefaction of hydrogen and and space industry. These manganite perovskites oxides fulfill the necessary conditions for practical applications as they unveil a large corrosion resistance, high eletric resistance, low hysteresis and mechanical stability [1, 7]. Conversly, the magnetocaloric potential of the RVO_3 vanadates has not yet been explored except for bulk $HoVO_3$ [8]. However, perovskite-type vanadium oxides RVO_3 display a great variety of phase transitions associated with a series of charge, spin and orbital ordering phenomena making them interesting candidates from a magnetocaloric point of view. Today's research activity in magnetic refrigeration is focused more on thin films structure since it is easy to fabricate into electornics miniature structure for device applications [9, 10, 11, 12, 13] which gives us another reason to investigate the MCE in RVO_3 films since their behavior depends of the cooperative nature of the Jahn-Teller distortion making these materials susceptible to strain in addition to the biaxial strain induced due to the lattice mistmach between the substrate and the film which tends to play an important role in tuning film properties.

Recently, O.copie et al [14]have demonstrated the possibility of controling the content of oxygen vacancies in epitaxial $PrVO_3$ (PVO) thin films grown on SrTiO_3 (STO) substrate to controle their magnetic properties by producing tensile strain. In this work, we focus mainly on exploring and tuning the magnetic and magnetocaloric properties of high quality epitaxial PVO thin films by applying a compressive strain via a proper choice of substrate.

First, we give a short overview of the miniaturization (from micro- to nanoscale) of

different structures of the most important MC materials of the ABO_3 serie. we highlight in this section3.2 the main motivation for exploring the size-reduction both from the technological and the purely scientific point of vue and stress the general consequences on the magnetic and magnetocaloric properties in ABO_3 perovskites..As going along the innovations published so far, the major challenges that have been overcome and those that still need to be tackled will be identified. Second, we investigated the magnetic and magnetocaloric properties in epitaxial $PrVO_3$ films. It consists in exploring the magnetic and caloric properties of epitaxial $PrVO_3$ oxide thin films emerging new features and combine/ couple complex phenomena in order to tune the MCE in oxide thin films.

3.2 Research progress in rare earth perovskite oxide magnetocaloric materials : From micro to nanoscale

Twenty years ago, the magnetic refrigeration field has completely changed after the discovery of the giant magnetocaloric effect at ambient temperature demonstrating the potential of magnetic cooling at room temperature and preparing the start of a race for setting the beginning of a race for the best magnetocaloric material over a wide range of temperatures. Since then, hundreds of different bulk materials have been studied in depth. However, only a small part of these materials has a huge MCE. In the past decade, due to their interest in these materials, their research scope has expanded to the micro and nano level.

3.2.1 ABO_3 perovskites

Oxides perovskites family presents a strong interplay between spin and lattice degrees of freedom. Scientists are interested in their versatility which enables them to obtain a wide range of research and applications in modern technological devices. I will illustrate the interesting physical and magnetocaloric properties a few oxide films for magnetic refrigeration application. ABO_3 perovskites are one of the most interesting materials, their rich and complex magnetic properties are mainly due to the new bonding geometries and their electronic states nature. Therefore, nanostructured oxides thin films can lead explorationg and controle of the exchange interaction lengths on an atomic level which is fundamental for the emergence of new features.

As seen in Chapter1, In a cubic unit cell, the perovskite materials usually present cubic structure at high temperature with a small B-site cation at the center of an octahedron of oxygen ions and a large A-site cation at the unit cell corners (see Figure1.8).This arrange-

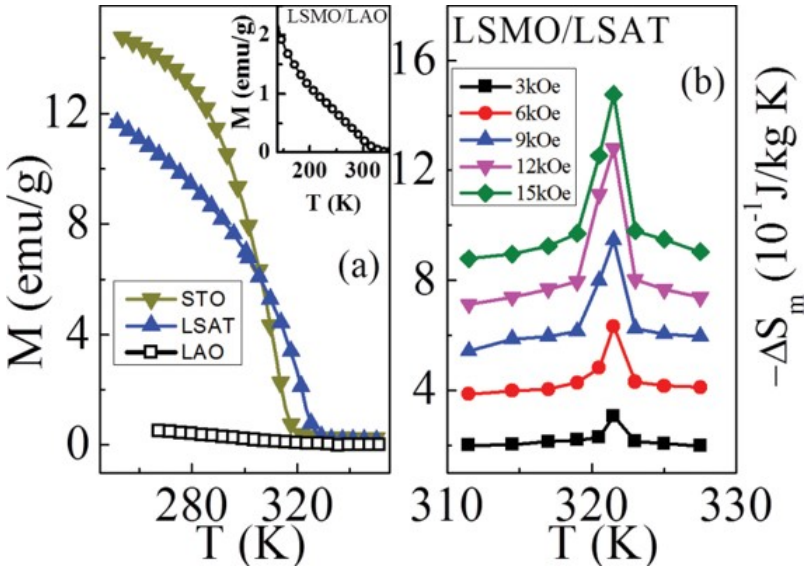

Figure 3.1: (a) Temperature dependence of magnetization for LSMO/STO, LSMO/LSAT, and LSMO/LAO under a field of 50 Oe, in the temperature range 250–350 K and (b) DSm for LSMO/LSAT in the temperature range 310 K , T , 327 K, under a field change of 1.5 T. . [29]

ment can also be considered as a set of octahedra, where the "B" atoms lie in the center and are coordinated by six O atoms lying in the vertices [15]. The geometry plays an important role on the magnetism, namely, the B–O–B network, which forms a perfectly cubic ABO_3 unit cell with 180° B–O–B bond angles. The A–O and B–O bond lengths are such that the Goldschmidt tolerance factor is 1.0 [16] For a large number of magnetic oxides, it is constrained to 0.71–1, where the coordination between atoms and constraints of three-dimensional connectivity are accommodated by cooperative distortions such as tilts and rotations of the constituent octahedra [17] . Hence, the pseudocubic structures, such as orthorhombic, tetragonal, or rhombohedra symmetries are observed for low distortions. In addition, the change of B-O-B bond angle results in multiple competing magnetic interactions exchange which are mediated through these bonds. Another important factor is the oxidation state of B atom, which also has a great influence on the nature of magnetic state. In the single magnetic state case, this mechanism is called super-exchange weak ferromagnetic state described by the Goodenough-Kanamori-Anderson (GKA) rules [18, 19, 20]explained in detail in section1.3.2.3. Another key parameter to be considered is the existence of structural distortions which may lead to the emergence of JT effect, which in return responsible for the division of crystal field splitting and therefore, the mediation of magnetic state.

Based on the scale reduction studies of this materials system, amajor success has been

achieved in 1994 by Jin et al [21]when they have grown $La_{0.67}Ca_{0.33}MnO_3$ by pulsed laser deposition. They observed a negative isotropic magnetoresistance effect three orders of magnitude larger than the typical value observed in some superlattice films. being as high as 127,000% near 77 K and approximately 1300% near ambient temperature. In addition, In addition, a detailed report by Lampen et al [22] highlighted the impact of reduced dimensionality on the magnetic and magnetocaloric properties of a FM material when they deposited a of 150 nm thick LSMO films on MgO substrates by PLD and two typical 15 and 33 nm sized sol-gel powders, they noticed that the size reduction tends to broaden the and shift the magnetic transition to a lower temperature accompagnied by a dercrease in M_s and $\triangle S_M$ pointing out a weakening of the first order nature of the transition in the nanocrystalline samples.

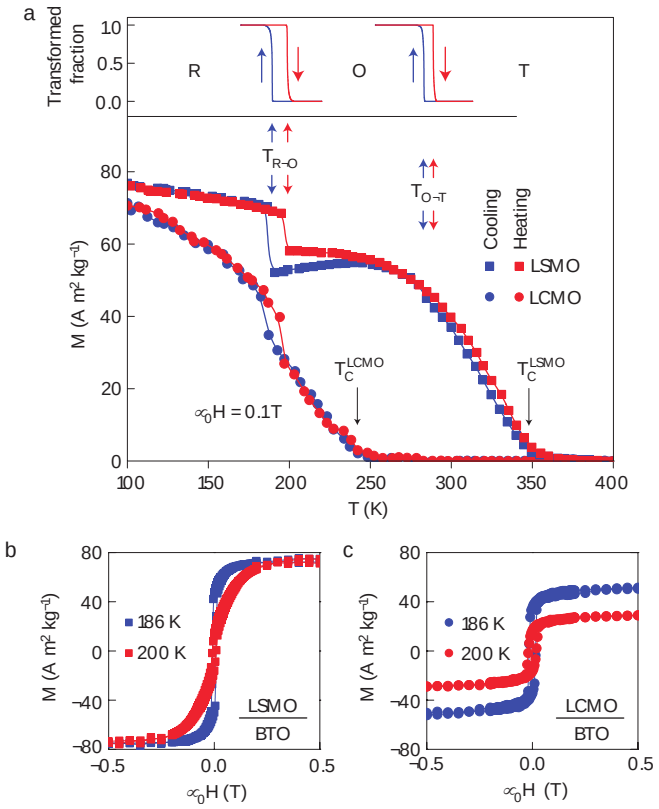

Figure 3.2: M(T) of LSMO/BTO and LCMO/BTO: (a) M(T) measured on cooling (blue circles, LCMO; blue squares, LSMO) and heating (red circles, LCMO; red squares, LSMO), showing magnetic jumps near TR-O ; 200 K below film TC ; 350 K (LSMO) and TC ; 240 K (LCMO). (b) M(H) for LSMO/BTO and (c) LCMO/BTO. [9]

When it comes to the magnetocaloric effect, Wang et al [23]were the first to study it in $La_{0.78}Ag_{0.22}MnO_3$ thin film deposited by laser pulsed deposition (PLD) in 2002 reporting $\triangle S_M$ = 2.22 J/(kg K) at ambient temperature under a magnetic field of 10 kOe. In

2009, the MCE in $La_{0.75}Ba_{0.1}M_{0.15}MnO_3$ thin films has been studied in depth, and the obtained values are as follows: $\triangle S_M$ = 1.72 and 2.44 J/(kg. K.), respectively, under a magnetic field change of 5 and 20 kOe.[24] In 2011, Prellier et al [25]grew a series of ($La_{0.7}Sr_{0.3}MnO_3/SrRuO_3$) superlattices with different interlayer thicknesses of SRO layers.The finite size effect reduced T_c of $La_{0.7}Sr0.3MnO3$ layer and produces a room temperature MCE while the working temperature ranges were enlarged, the isothermal entropy change values remained similar to the values in polycrystalline $La_{0.7}Sr0.3MnO3$. As a result, the RCPs were significantly enhanced. This innovative study shows that the artificial oxide superlattices/multilayers can provide an alternative pathway in the search for efficient nanoscale refrigerator [26, 28].

A major breakthrough has been cleverly engineered and carried out experimentally by Moya et al [9] in 2013 when they create a giant and reversible extrinsic magnetocaloric effects in epitaxial films of the ferromagnetic manganite$La_{0.7}Ca_{0.3}MnO_3$ using strain mediated feedback from $BaTiO_3$ substrates near a FOPT as shown in Figure3.2. This extrinsic effect led to a significant increase of DSm max up to 9 J/(kg K), ten times higher than the intrinsic effect observed in the La0.7Ca0.3MnO3 thin film 0.7 J/(kg K) for the same applied magnetic field of DH of 1T. In the same year, the role of substrate induced compressive and tensile strain in the LSMO thin-films on $\triangle S_M$ and RCP has been highlighted and the possibility of achieving a near room temperature MCE with RCP as high as bulk samples is demonstrated in LSMO/STO thin-films (see Figure 3.1[29]. Giri et al [30]deposited epitaxial $Sm_{0.55}Sr_{0.45}MnO_3$ thin films on 001-oriented LAO, LSAT and STO single crystal substrates by PLD technique. They demonstrated that is possible to tune the MCE by the lattice strain induced by the different substrates.

More recently, Jia et al (2019) have successfully grown epitaxial $GdCoO_3$ on top of the (001)-oriented LaAlO3 substrate using simple polymer assisted deposition (PAD) method. They found a giant magnetocaloric effect at cryogenic temperatures as n $\triangle S_M$ reaches 58,56 (J/kg.K) with a magnetic field of 70 kOe[31]

3.3 $PrVO_3$: An inhomogeneous antiferromagnetic material with random field

3.3.1 Bulk and film magnetic properties

$PrVO_3$(PVO) belongs to the family of rare earth perovskite vanadates. At room temperature, bulk PVO adopts an orthorhombic Pbnm crystal structure with a = 5.487A,b = 5.564A and c = 7.78A as lattice parameters resulting from cooperative distortion of the VO_6 oc-

tahedra along the [-001] direction of the ideal cubic unit cell [32]. PVO single crystal has shown an orbital order transition (OO) at T_{oo}= 155 K and than followed by the antiferromagnetic magnetic spin ordering (SO) transition at T_{SO}= 132 K . An additional transition has been observed by L.Tung in the ordering region with the glassylike behaviour [32], a feature which is usually expected only for disorder systems. The author observed a stairlike behavior in the hysteresis loops at a temperature below 3 K as shown in figure 3.3(a) and high values of the remanent magnetiztion (M_r) along all the axes and suggested that the PVO should be considered as a disorder (or inhomogenous) antiferromagneti with random fields. L.Thung proposed many possible machanisms of the stairlike behavior of the hysteresis curves based on domain propagation and growth involving the pinning of the domain wall by defects which has been invoked to explain this behavior in the $SmCo_{3.5}Cu_{1.5}$ antiferromagnet [37].

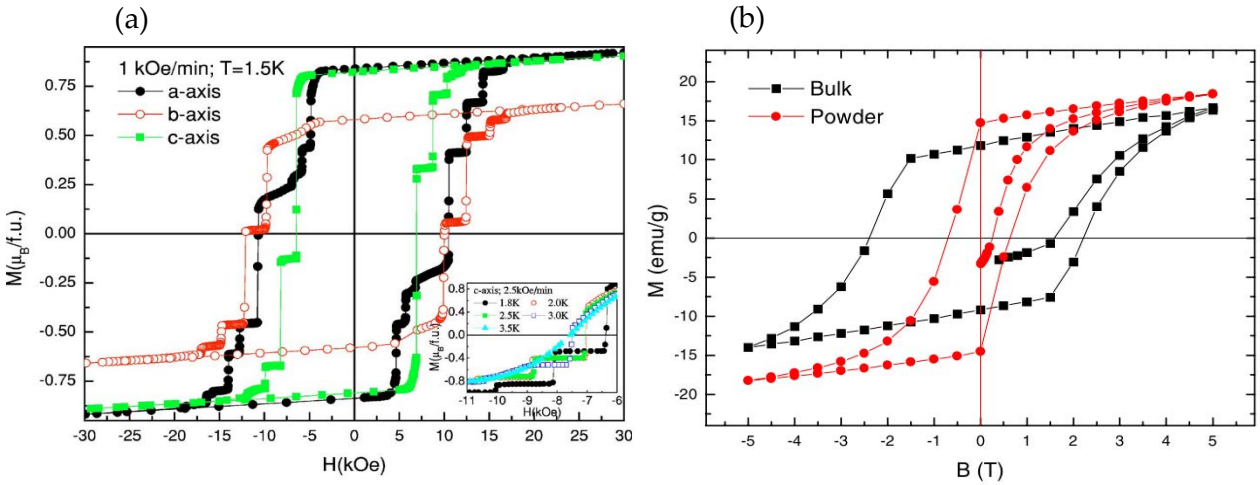

Figure 3.3: (a) The curves of hysteresis at 1.5 K along the main axes of $PrVO_3$ single crystal studied in ref [14]. The inset shows the hysteresis curves at different temperatures along the c axis. (b) The hysteresis loops at 5 K of the powder (Red) and the sintered bulk $PrVO_3$ studied in ref [15]. Figures adapted from [14, 15]

Another possible mechanism is based on the presence random fields (RF) [33, 34, 35, 36] observed in other disorder systems. According to this mechanism, the flipping of domains at some applied magnetic field may force the neighboring domains to flip as well in the same direction leading to avalanche of domain flips. In systems with no random fields, the local fields at each crystallographic site are identical so the spins or all the domains will flip at the same time creating to a single step at the switching field. The stairlike behavior is also a characterestic of antiferromagnetic structures with a dispersion of metamagnetic field transitions [37]. According to the same author, only V^{3+}ions are responsible for the magnetism in $PrVO_3$ as the Pr^{3+} are in a non magnetic statre provided that the exhchange

interaction is weak and considering the splitting of the J gound state multiplet into nine singlets for Pr^{3+} under the effect of the crystal field as a consequence to the low symmetry of the compoound (orthorhombic at ambient temperature and monoclinic below T_{SO}.

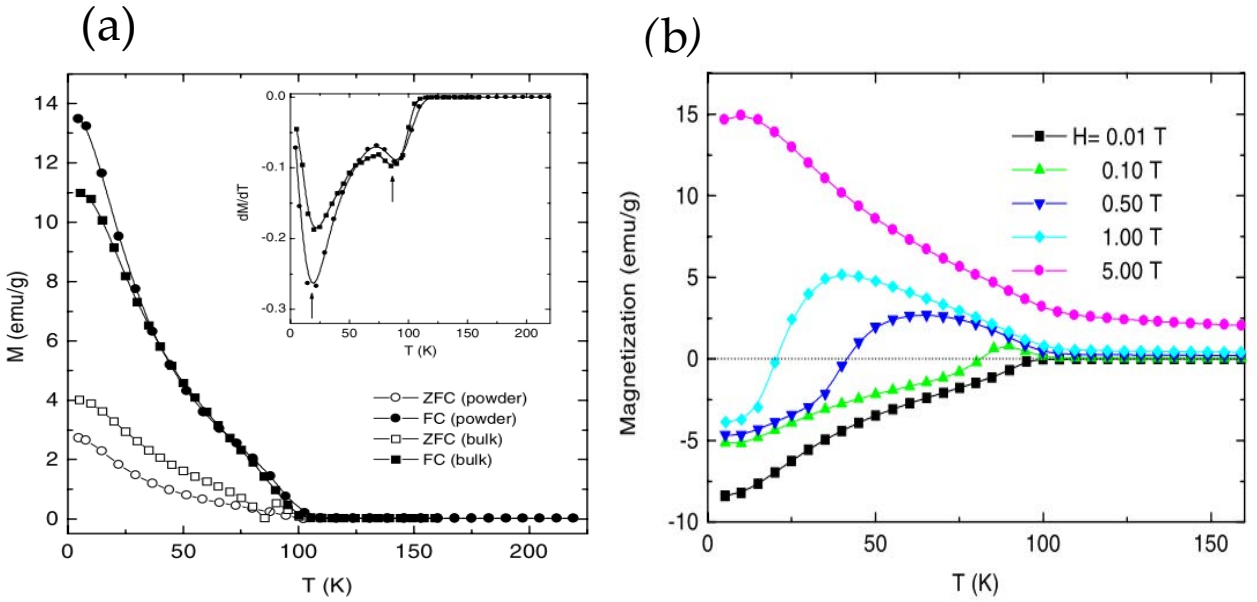

Figure 3.4: (a) The curves of magnetization versus temperature of the powder (circle) and the sintered bulk (square) $PrVO_3$ in an applied magnetic field of 0.05 T measured on warming as samples are zero-field cooling (ZFC) and field-cooled (FC). Inset shows the differentiation of the temperature dependent magnetization under field cooling. (b) Temperature dependence of magnetization of the sintered bulk $PrVO_3$ under different applied magnetic field in ZFC conditions. Figures adapted from [15]

In another work, Whang et al [33] reported a high coercivity of 2.4 T at low temperatures (5 K) in the sintered bulk and 0.7 T for the powder with low spontaneous magnetization ≃15 emu.g^{-1}, ie. 0.65μ_B/f.u (see figure3.3(b)) much lower than the ionic theoretical moment, which indicates a canted antiferromagnetic configuration for both the V and Pr sublattice [34, 35, 36]. Table 3.1 summarize the magnetic properties of the free ions.

Recently, O.copie et al [14] have demonstrated the possibility of controling the content of oxygen vacancies in epitaxial $PrVO_3$ (PVO) thin films grown on SrTiO_3 (STO) substrate to controle their magnetic properties by producing tensile strain.

The authors presented a direct comparison of magnnetic properties of PVO in bulk and thin form. They measured T_N =85 K in the PVO film whereas a magnetic signal arises around T_N = 135 K due to the ordering of the canted V^{3+} spins in the bulk form as seen in figure 3.5.

Ion	Pr^{3+}	V^{3+}
Spin magnetic moment (S)	1	1
Orbital magnetic moment (L)	5	3
Total moment (J=| L-S |)	4	3/2
Lande g-factor =1+$\frac{J(J+1)+S(S+1)-L(L+1)}{2\times J(J+1)}$	$4/5\mu_B$	$1.418\mu_B$
Total magnetic moment ($\mu_T = g \times J \times \mu_B$)	$3.2\mu_B$	$2.11\mu_B$
Effective magnetic moment	$3.58\mu_B$	$2.83\mu_B$
	$u_{eff}(PrVO^3)$ =	$4.56\mu_B$

Table 3.1: Magnetic properties of Pr^{3+} and V^{3+}

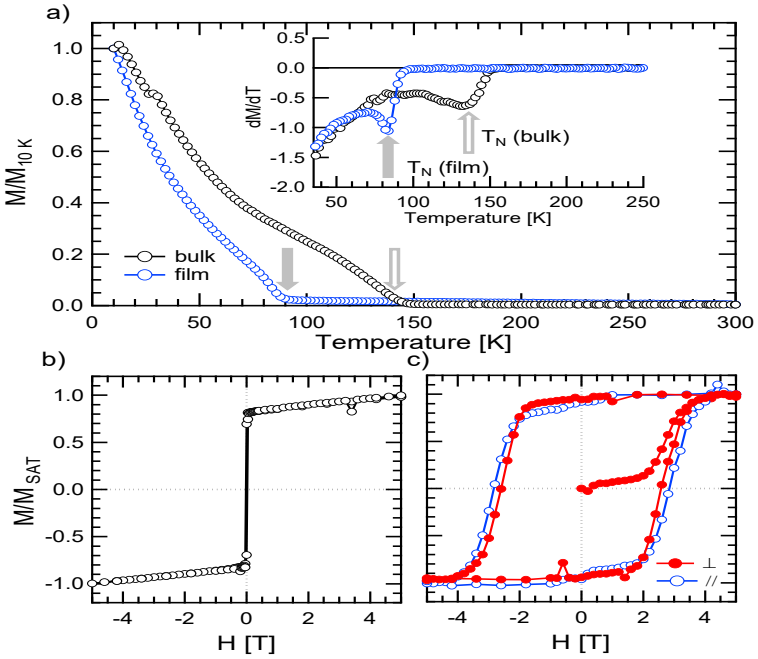

Figure 3.5: (a) Normalized magnetization (M/M10K) as a function of temperature for bulk and thin film PVO under an applied magnetic field of 50 Oe. Inset: first derivative of the tmagnetization versus temperature. (b) Normalized magnetization (M/MSAT) as a function of the magnetic field for bulk PVO, measured at 10 K. (c) Normalized magnetization (M/MSAT) as a function of the magnetic field for PVO thin film, measured at 10 K with a magnetic field applied out of plane. Figure taken from [14]

On the other hand, the hysteresis curve of PVO film, after substraction of the diamagnetic substrate contribution, is characterized by a larger coercivity as shown in Figure 3.5c with Hc ≈ 2.8 T and with very close remanence and saturation magnetization values ~ 0.27 and 0.29$\mu_B/f.u$ respectively. On can conclude that the magnetic properties of $PrVO_3$ films grown on $SrTiO_3$ seems analogous to a hard ferromagnetic-like behavior as reported previously[38].

3.4 Strain-induced giant magnetocaloric effect in epitaxial $PrVO_3$ thin films

In this section3.4, we present a study of the thickness and substrate effect on the magnetic and magnetocaloric properties of strongly correlated epitaxial $PrVO_3$ films.

3.4.1 Outline of the experiments

EXPERIMENTS: The epitaxial $PrVO_3$ films were grown by pulsed-laser deposition (PLD) on two different cubic substrates, namely, (001)-oriented $(La, Sr)(Al, Ta)O_3$ (LSAT) and (001)-oriented $SrTiO_3$ cubic substrates. Their in and out-of-plane lattice parameter are found to be 3.868 Å and 3.95 Å with a thickness of 41.7 nm for the LSAT film while those of the STO film are 3.905 Å and 3.92 Å with a thickness of 100 nm. A KrF excimer laser (λ = 248 nm) with repetition rate of 2 Hz and laser fluence of $\sim$ 2 J/cm2 was focused on stoichiometric ceramic targets. All the films used in this study were deposited at an optimum growth temperature (T_G) of 650 °C and under oxygen partial pressure (P_{o_2}) of 10^{-6} bar.

In ZFC measurements our sample was cooled to the desired temperature without the application of a magnetic field, then data were collected while heating under magnetic field. For the FC process, the sample was cooled in the presence of an external magnetic field to the desired temperature. We performed two modes, field cooled cooling (FCC) and field cooled warming (FCW) where data are collected during the cooling and heating processes, respectively. . The in-plane and out-of-plane magnetizations were performed by using the Quantum Design SQUID-VSM. Each hysteresis loop was measured after a 150 K excursion above the Néel temperature and corrected by subtracting the diamagnetic contribution arising from the substrate.

3.4.2 Magnetic characterization

3.4.2.1 $PrVO_3$ (100nm) deposited on 001-oriented $SrTiO_3$ (STO) substrate

As mentioned in the outline of the experiments, our samples were heated above T_N and cooled down to the desired temperature before each run to ensure a perfect demagnetization since PVO has a magnetic hysteresis. To investigate the the strain effect on magnetic properties of PVO films, the temperature dependence of magnetization was measured under an applied magnetic field of 50 Oe for a 100 nm thick PVO deposited on STO substrate

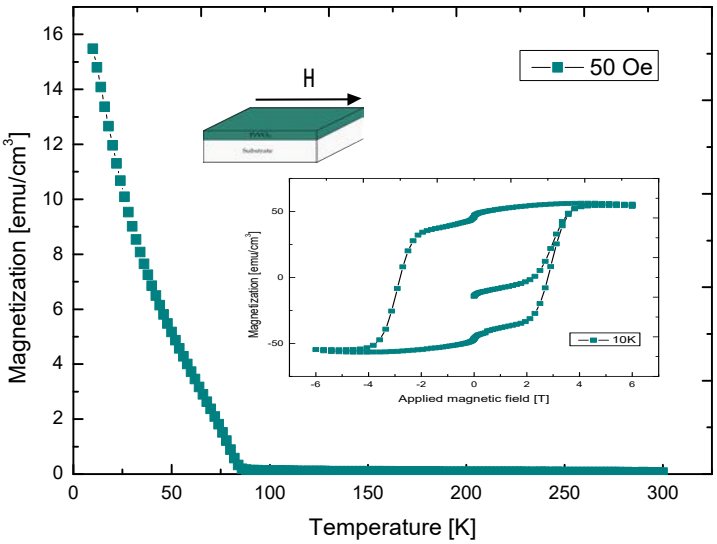

Figure 3.6: Magnetization dependence of temperature for PVO film on STO substrate performed at an in-plane applied magnetic field of 50 Oe. Inset displays the magnetic hysteresis loops measured at 10 K after substracting the diamagnetic contribution of the substrate and the holder.

as shown in figure 3.6. A hard-ferromagnetic behavior below 80 K is observed semilar to that reported previously in ref [14, 38].

In fact, the S-shape of magnetization depicts a metamagnetic transition which is defined as the transition between antiferromagnetic (AF) and ferromagnetic (F) configurations of spins under the effect of magnetic fields or temperature change[39]. The intrinsic coercivity is $\sim$ 2.8 T while the remanence magnetization is $\sim$ 48 emu/cm^3. The magnetization saturation is found to be $\sim$ 54 emu/cm^3 being equivalent to 0.291 μ_B/f.u at 10 K. The presence of soft component can be seen at a magnetic field of $\sim$ 0.2 T indicated by the shape of MH loop caused by the magnetic field induced transition which is absent for higher temperatures as observed earlier [2].The high coercivity might come form the pinning mechanism due to the microstructure as well as the film unit cell orientation compared to the in-plane and out-of plane magnetic field direction. On the other hand, we observed a reduction of T_N compared to bulk PVO ($T_N \simeq$ 140 K) which could be explained by the distortion of the film lattice caused by the epitaxial strain[41]. XRD reveals that the pseudocubic volume of PVO unit cell when deposited on a STO substrate ($\simeq 60.91A^3$) is larger than its equivalent of the bulk ($\simeq 58.86A^3$)[38]. As a result, the volume expansion decrease the transfert integral which tends to reduce the neighbor exchange interactions as the magnetic interactions in this system are governed by superexchange mechanism. We note that we did not observed a significant magnetic anisotropy by comparing the magnetic measurement with magnetic fields applied in and out of the sample plane.

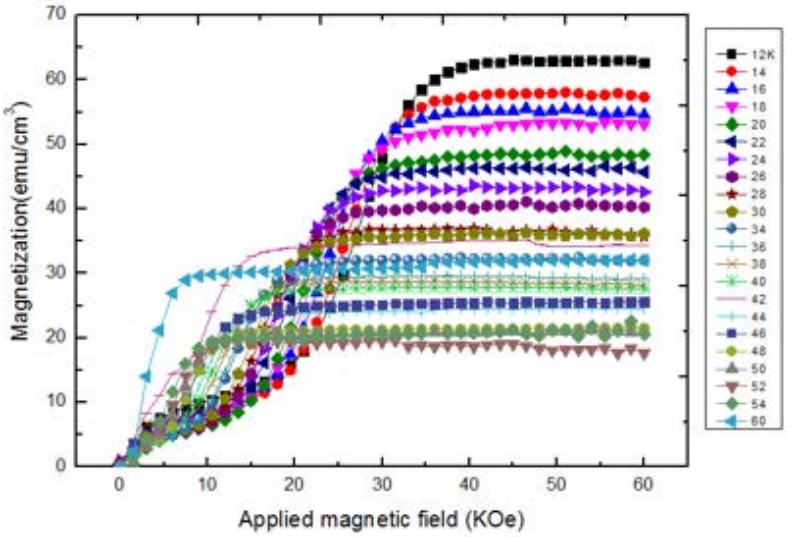

Figure 3.7: Magnetization isotherms of PVO film deposited on a (001)-oriented STO substrate in the temperature range of 10-60 K when subjected to in-plane magnetic field. Each loop was measured after a 30K excursion above T_N to ensure that the demagnetization of the sample is successful and corrected for diamagnetic background signal.

3.4.2.2 $PrVO_3$ (41.7nm) deposited on 001-oriented $(La, Sr)(Al, Ta)O3$ ($LSAT$) substrate

We now applied a compressive strain by growing a 41.7 nm thick PVO on 001-oriented LSAT substrate. Figure3.8.b displays the isothermal magnetization for two different orientations measured up to 6 T and recorded at 10 K. Suprisingly, a strong magnetic anisotropy is observed. As shown, the magnetization saturation is markedly enhanced when compared to PVO/STO, reaching about $\simeq$ 900 emu/cm^3 and $\simeq$ 785 emu/cm^3 at 3 K for H$\perp$ (Figure 3.8, $\perp$ symbol) and H// (Figure 3.8b, // symbol), respectively. At 10 K, the corresponding magnetization saturations are about $\simeq$ 402 $emu/cm^3$and $\simeq$ 305 emu/cm^3, respectively. These values are much larger than those of PVO/STO as can be clearly seen from inset of Figure 3.6. In addition, the coercive field is largely reduced to attain about 0.3 T and 1.1 T for hysteretic loops performed in plane and out of plane, respectively. More surprisingly, the coercive field decreases dramatically at 3 K reaching only 0.05 T for magnetic fields applied within the films plane as shown in Figure 3.9a. This markedly contrasts with the conventional magnets in which usually the thermal excitations lead to the reduction of coercivity. This contrast could be attributed to FM and AFM couplings or/and the spin and orbital transitions usually leading to stair-like hysteresis observed in bulk PrVO_3[32]. The enhancement of coercivity when heating may also be attributed to the stress induced magnetic anisotropy due to the relaxation of the surface stress reported for various magnetic thin films[3, 4]. It is worth noting that for the LSAT substrate, the PVO out-of-plane

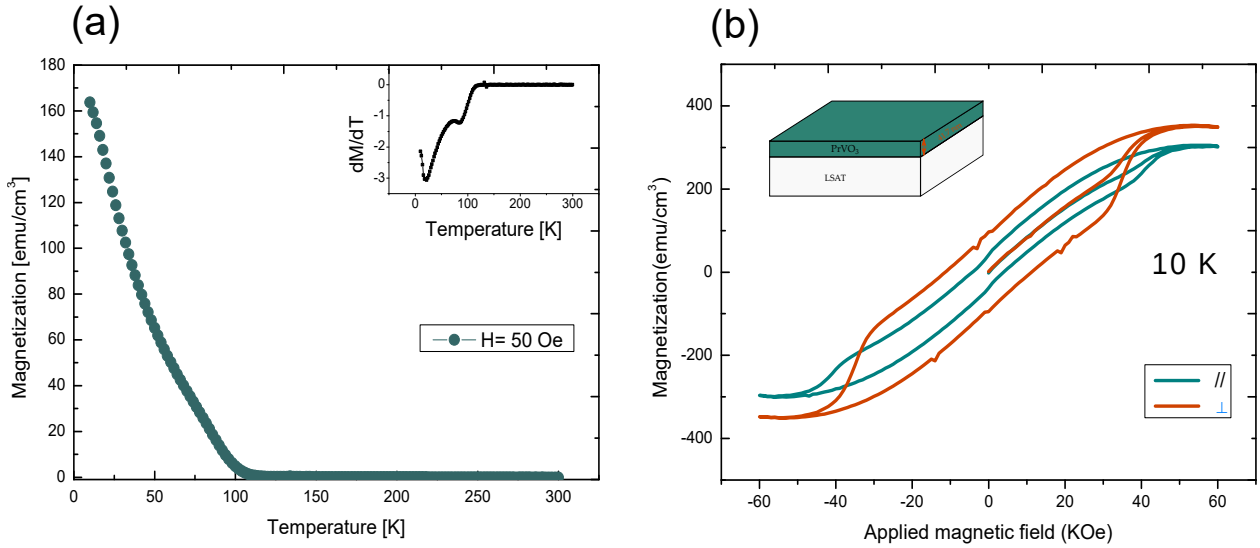

Figure 3.8: :(a) Temperature dependence of the magnetization with a magnetic field of 50 Oe applied in the sample plane for PVO/LSAT. Inset:differentiation of the temperature dependent magnetization. (b) Magnetic hysteresis loops measured at 10K after substracting the diamagnetic substrate contribution of PVO grown on LSAT substrat with a magnetic field applied in (green) and out of the sample plane (orange).

lattice parameter is increased as the in-plane lattice parameter decreases. The latter that tends to match the one of the substrate on account to the compressive feature of the experienced strain. When heating the thin films the in-plane lattice parameter is relaxed enough to return to the bulk values giving rise to a high coercivity. This property would make the PVO films an attractive candidate for applications using magnetostriction effects since their coercivity and magnetization can be tailored via strains.

The temperature dependence of magnetization at an in-plane applied magnetic field of 50 Oe is displayed in Figure 3.9a.. As can be clearly observed, one can see a sharp decrease of magnetization at low temperature and a magnetic transition from paramagnetic (PM) to an antiferromagnetic (AFM) phase transition is occurs at $T_N \approx 125$ K. Such transition is attributed to the beginning of a G-type spin ordering (G-SO)[14]. The differentiation of the temperature-dependent magnetization is displayed in the inset of figure3.9.a where two additional magnetic transitions take place at $T_2 \simeq 20$ K and $T_3 \simeq 80$ K. These transitions were absent in bulk PVO [30] but reported recently in strained PVO films [6] and in doped $Pr_{1-x}Ca_xVO_3$ compound[32].

Upon cooling down to 3 K, the plot of the first derivative of the magnetization temperature dependence exhibits a minimum at very low temperature which could be explained by the polarization of the praseodymium magnetic moments. The newly established order is due to the fact that the antiferromagnetic vanadium sublattice produces an exchange

field that results in a ferrimagnetic structure of Pr sublattice under cooling as already observed in other vanadates[38, 39, 40] This is supported by the presence of a soft component at temperatures below 20 K (see Figure3.11a) and also by the fact that the magnetization saturation reaches 4.86 and 5.54μ_B at 3 K when a magnetic field is applied in and hen a magnetic field is applied in and out-of-plane, respectively. On the other hand, these finding inform us on the contribution of both Pr^{3+} and V^{3+} ions ions to the whole magnetization since the theoretical saturated moment of free $Pr^{3+}$and V^{3+} are 3.22 and 2.12 μ_B , respectively, suggesting that all the praseodymium and vanadium moments are fully aligned parallel to the applied magnetic field.

R.Aeschlimann and al [41]have confirmed recently that the surface overoxidation of DyTiO3 thin films gives rise to a massive paramagnetic response from uncoupled Dy^{3+} ions. This leads to a decrease of the remanent magnetization and an increase of the saturation magnetization which is makedly contrast with the classical ferromagnetic manganite[42, 43]. Usually, in such system we assume that a fraction of the thin film at the surface or near the interface with the substrat is non magnetic using the classical model of dead layer becoming a living layer in that case which help to increase the Ti^{3+} (V^{3+} in PVO) content near the surface resulting in isolated paramagnetic Dy^{3+}.

Magnetic anisotropy

The ZFC,FCW and FCC curves were measured in 50 Oe field from 3 to 300 K as shown in Figure3.9d . The bifurcation between FC and ZFC magnetizations indicates an irreversibility being the charaterestic of a complex system. This difference reflects the impact of the anisotropy on the shapes of ZFC and FC curves below the ordering temperature since the coercivity is related to magnetic anisotropy. The latter plays an important role in determining the magnetization at a given field strength during both the ZFC anf FC processes since it aligns the spins in a preferred direction. During the ZFC process,

the spins are locked in random directions since no magnetic field is applied while cooling the thin films to the desired temperature. When a small magnetic field is applied at temperatures far below T_N and as the system is anisotropic [52], the magnetization decreases to reach negative values indicating a possible competition between antiferromagnetic interactions, a characteristic which is observed in orthovanadate RVO_3 compounds[43, 53] A small negative trapped field in the sample space as well as the coercivity could be responsible for the negative magnetization[54]. During the FC process, the PVO film is cooled under the application of a magnetic field. Consequently, the spins will be alligned in a specific direction depending on the strength of the applied magnetic field. As a result, M_{FC} continuously increases below T_N as the temperature decreases.

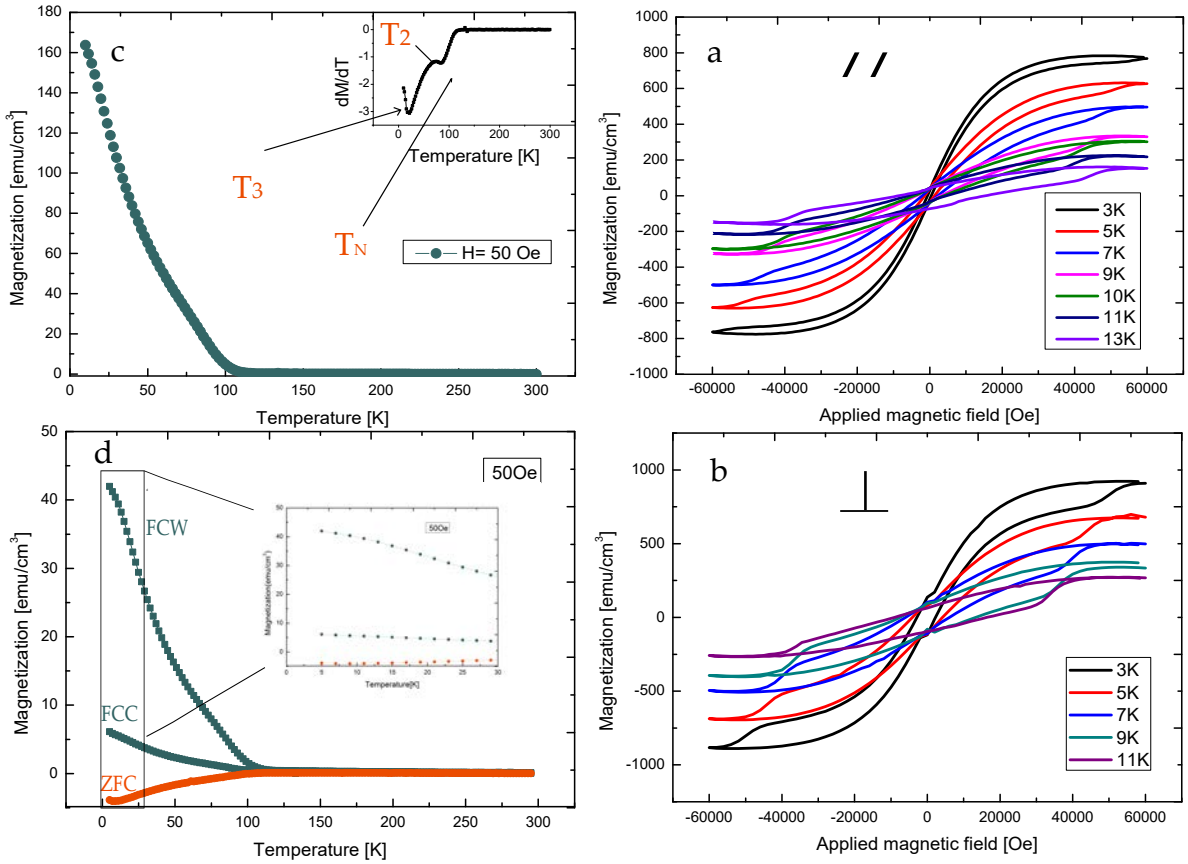

Figure 3.9: Temperature development of isothermal magnetization in the range of 3-13 K with an applied magnetic field in-plane (// symbol, Fig.2.a) and out-of-plane (⊥symbol, Fig.2.b) of PVO film deposited on (001)-oriented LSAT substrate. (c) Temperature dependence of magnetization of thin film PVO at an in-plane applied magnetic field of 50 Oe. Inset: differentiation of the temperature-dependent magnetization. (d) Temperature dependence of magnetization in zero-field-cooling (ZFC), field cooled cooling (FCC) and field cooled warming (FCW) conditions.

3.4.3 Magnetocaloric properties

Magnetic isotherms up collected under magnetic fields going from 0 to 6 T at different temperature are reported in Figure 3.11 for the PVO film deposited on a (001)-oriented LSAT. Except the isothermal magnetization at 3 K which shows a typical behavior of a ferromagnetic material, all the other isotherms follow a sharpe increase when the magnetic field is below 30 kOe indicating a field induced first order metamagnetic transition from AFM to FM state as a result of a strong competition between Pr 4f and V 3d spins. Such competition often leads to a giant MCE in strongly correlated materials[66]. Similar behavior is found in the corresponding arrot plot (M^2 versus H/M) confirming the

first order nature of the transition according to Banerjee [74]criterion as the curves show negative slope at some points as shown in Figure 3.10.

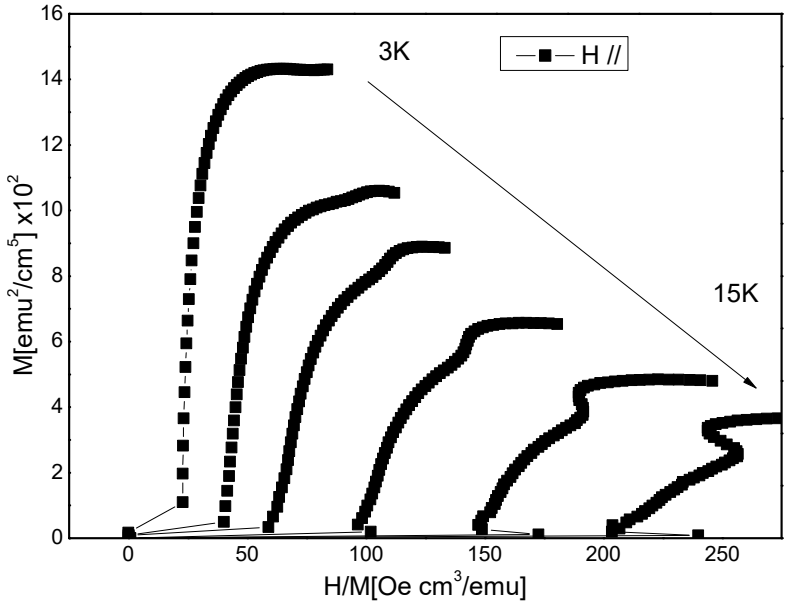

Figure 3.10: Arrott plot of the sample at different temperatures with a magnetic field applied in the sample plan (//)

The large field-induced metamagnetic transition in PVO/LSAT films and the soft component in MH below 30 K are a clear indication of a possible giant magnetic entropy change. In order to explore the magnetocaloric effect in PVO films, magnetic field-induced entropy change $-\Delta S_M$ was calculated using indirect method from the isothermal curves[62], with the following equation based on a Maxwell relation (MR) :

$$\triangle S_M = \int_0^H (\frac{\partial M}{\partial T})_H dH$$

There is a good evidence that the Maxwell relation is also valid near first-order phase transition where it is acceptable to use non-equilibrium data obtained after thermal excursion from the hysteretic regime[9, 64, 65, 63]. Furthermore, it has been demonstrated recently that the magnetocaloric effect in multiferroics could be evaluated perfectly via Maxwell relation[66]. It has been found that entropy change deduced from isotherms data of $EuTiO_3$ fits perfectly with that obtained from specific heat data. In our case, magnetic isotherms of Figure3.11 are used to calculate the entropy change exhibited by the PVO films on LSAT. However, since the entropy change is proportional to the aera between two successive isotherms, ΔS_M, was directly calculated without subtracting the magnetic contribution arising from the substrate as already done in the case of La_2NiMnO_6 thin

films[73]. For PVO/STO, it was difficult to calculate the MCE because of the overlap between M vs H curves at low temperatures (see Figure 3.7).

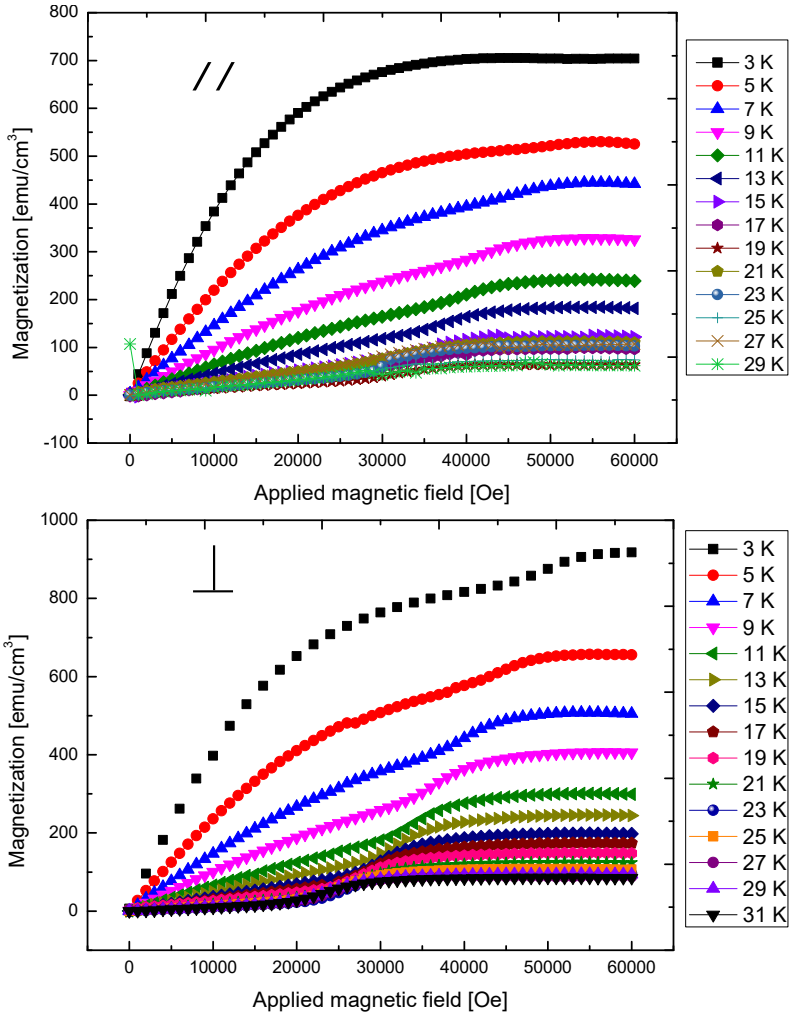

Figure 3.11: Magnetization isotherms of PVO film deposited on a (001)-oriented LSAT substrate in the temperature range of 3-30 K with an interval of 2 K when subjected to in-plane (// symbol, Fig 3.a) and out-of-plane (⊥ symbol, Fig 3.b) magnetic field. . Each loop was measured after a ~30K excursion above T_N to ensure that the demagnetization of the sample is successful and corrected for diamagnetic background signal.

The temperature dependence of the magnetic entropy change unveils larger values at very low temperature for PVO/LSAT films that reach roughly $-\Delta S_M$ = 56.7 J/(kg.K) for a magnetic field changing from 0 to 6 T applied in the sample plane (Figure 4.7a). In a similar field change applied of plane, is slightly lower and found to be about 52.7 J/(kg.K)) when subjected to an out-of plane magnetic field (Figure4.7b). Also, the magnetic entropy change shows a large magnetocaloric effect under relatively low magnetic fields that can be easily reached via permanent magnets. In the magnetic field change of 2 T

applied within and out of thin films plane, $-\Delta S_M$ reaches 19.5 and 16.3 J/(kg.K) , respectively. As shown in Figure4.7, A large magnetocaloric effect can be induced below the AFM transition. This suggests that a major part of the magnetic contribution comes from praseodymium 4f spins.

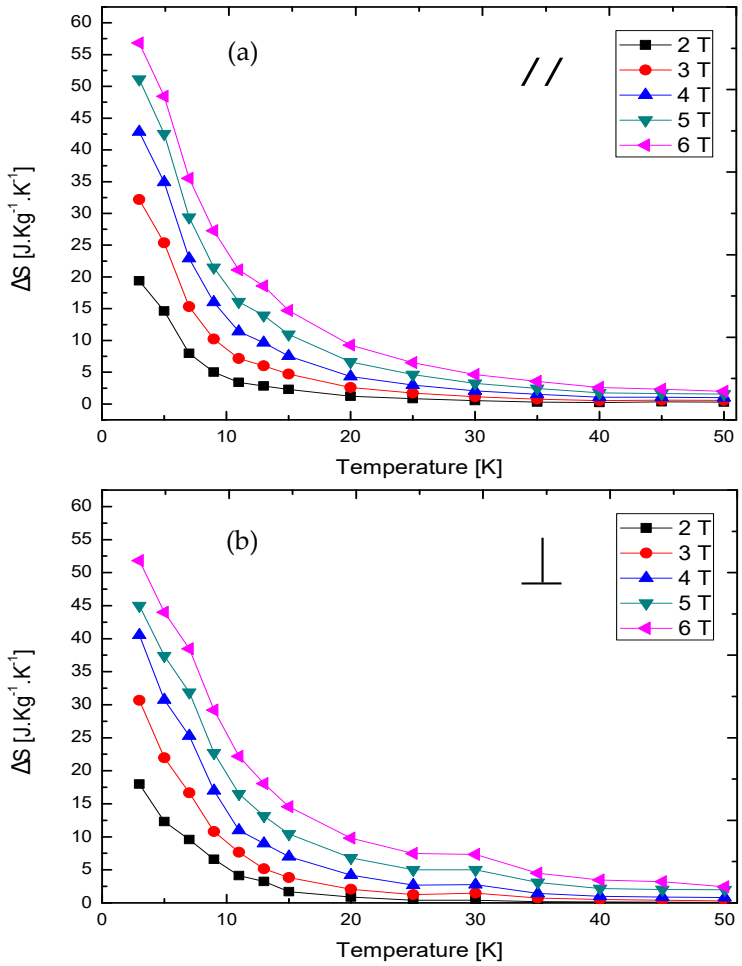

Figure 3.12: Temperature dependence of magnetic entropy change obtained by integrating the MR with magnetic field varying from 2 to 6 T applied in-plane (a) and out-of-plane of the sample (b) for PVO deposited on LSAT substrate

A list of promising materials for magnetic refrigeration application at low temperature regime are reported in Table 3.2 for comparison. The observed value of $-\Delta S_M$ in a strained PVO film is significantly larger than the values reported for several rare-earth metal transition oxides and intermetallic compounds being 63% to the theoretical limit of Rln(2J+1) making the PVO films a potential candidate for low temperature magnetic refrigeration.

Materials	T_0 (K)	$\triangle H_0$(T)	$\triangle S(J.Kg^{-1}.K^{-1}$	Ref
PVO/LSAT (//-⊥)	3	6	56.7 - 52.7	Present work
$GdFeO_3$	2.5	6	43.1	[35]
$EuTiO_3$(SC)	5.6	5	42.4	[39]
$HoVO_3$	15	7	17.2	[14]
$GdCoO_3/LaALoO_3$	3.5	7	58.65	[58]

Table 3.2: Maximum values of the magnetic entropy change $\triangle S_M$ for PVO deposited on LSAT and several other potential magnetic refrigerant materials. SC: single crystal

3.5 Theoretical calculations

3.5.1 Calculations details

THEORY: Based on densit theory, first principles calculations were performed using Vienna Ab Initio simulation Package[67, 68, 69, 70] with the PBE functional used to reproduce the electronic exchange correlation while the projector augmented-wave (PAW) was employed to construct the pseudopotentiel of all species involved. We performed a U correction of 3.5 eV [71, 72] to deal with the strong on-site Coulomb interaction of 3 d electrons. The cut-off energy set to 500 eV and a k-points shell of 6x6x6 according to the Monkhorst-Pack grid was used for orthorhombic structures which is found to yiels a better convergence.

Ion	Name	Site	Position
Pr^{3+}	Pr	4c	(0.9928, 0.0448, 1/4)
V^{3+}	Mn_1	4b	(0.5 0, 0)
O	O_1	4c	(0.0818, 0.4809, 1/4)
O	O_2	8d	(0.7062, 0.2930,0.0429)

Table 3.3: Pbnm cristallographic sites and atomic positions of $PrVO_3$ unit cell

For bulk calculations, all cell parameters and atomic positions are relaxed within Pbnm symmetry. In order to study the effect of epitaxial strain arising from the film/substrate lattice mismatch, bulk geometry has been subjected to an epitaxial constraints on its lattice parameters. Two different growth orientations are considered (see figure3.13), the first growth along the Pbnm [001] direction where the two lattice vectros of the orthorhombic unit cell lie within the substrate plane with a=b=$\sqrt{2}.a_{sub}$ (a_{sub}= Substrate lattice) to preserve the Pbnm symmtry of bulk PVO and the second growth along the orthorhombic [110] direction where the compressive constraint lower the symmtery to $P2_1/m$ resulting

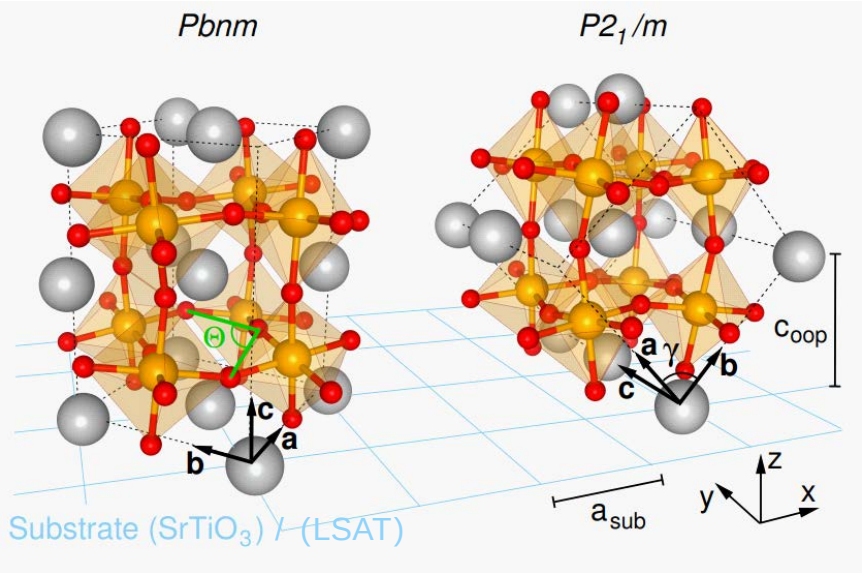

Figure 3.13: Schematic depiction of two different orientations of the bulk crystal structure of $PrVO_3$ relative to a hypothetical square lattice substrate , corresponding to the [001] (left) and the [110] (right) P bnm growth directions. The respective unit cells (dashed lines) and their basis vectors, a, b, and c, are indicated. The gray, golden, and red spheres refer to Pr, V, and O atoms, respectively.

in monoclinic unit cell with $\gamma \neq 90^{\circ}$. The in-plane lattice parameters are set equal to the lattice constant of the subtrate, while the out-of-plane parameter is optimized for each value of the substrate parameter and all the structures are relaxed until the forces on atoms were less than 3 meV/A. Four magnetic states are considered in the simulation (Ferromagnetic, G-type, C-type, and A-type antiferromagnetic). The atomic coordinates for bulk PVO are smmarized in table 3.3.

3.5.2 Electronic and structural properties

Theoretical calculations are important for a better understanding of the fundamental mechanisms behind the physical properties of materials. Ab initio calculations based on density functional theory (DFT) was performed to investigate the bulk and film properties of PVO. In order to check the ground state of bulk PVO, the total energies of four different magnetic ordering configurations are calculated using GGA+U approximation. The ferromagnetic (FM) and the three antiferromagnetic (AFM) structures are shown in Figure3.14(a) and denoted by AF-G , AF-C and AF-A. Our results indicate a ground state magnetic structure where the Vanadium spins forms a C-type AFM structure consistent with previous studies[14, 6]. For thin films calculations, two different orientations have been taken into account. First, we preserve the bulk Pbnm symmetry for a growth along

[001] direction where the two lattice vectros of the orthorhombic unit cell lie within the substrate plane. A second growth along the orthorhombic [110] direction where the compressive constraint lower the symmtery to $P2_1/m$ is also considered. The latter scenario that results in monoclinic unit cell was found to be clearly preferable by comparing the total energy difference between the two symmetries. It yields to a G-type spin ordering for PVO grown on both LSAT and STO substrates.

3.5.3 Magnetic properties

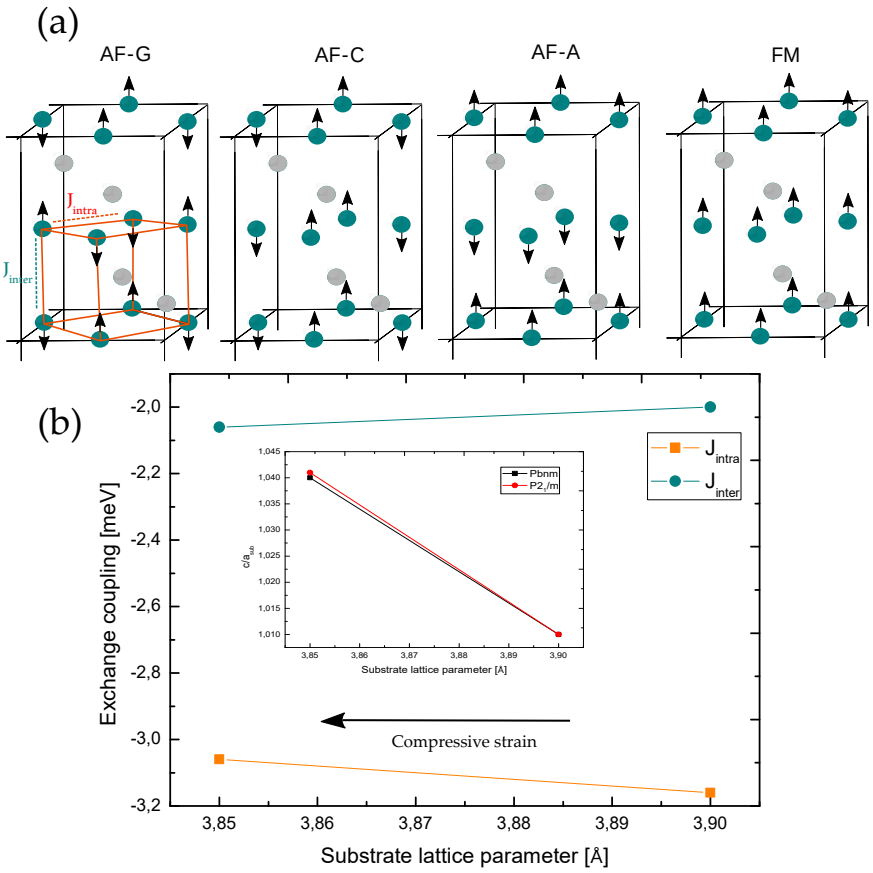

Figure 3.14: The distorted perovskite magnetic structure of $PrVO_3$, in which the pseudocubic cell is shown by orange lines. Four magnetic structures are schematically shown: Ferromagnetic (FM), antiferromagnetic C-type, antiferromagnetic G-type and antiferromagnetic A-type. The grey and green spheres represent Pr and V atoms, respectively.

The enhancement of magnetic interactions under compressive strain is seen using our calculations. The intraplane and interplane magnetic exchange interactions J_{intra} and J_{inter} can be determined from the relation between the exchange parameters$J_{i,j}$ and the magnetic energies $e_{i,j}$ of four magnetic configurations, $e_{i,j} = J_{i,j}.S_i.S_j$ based on the effective

Heisenberg model $H = \sum_{i,j} J_{i,j}.S_i.S$ where S_i takes 1 restricted to nearest neighbor vanadium sites (see Figure 3.14(b)). The intrarplane magnetic exchange interactions increases due to compressive strain in the [110] direction since the film lattice parameters tends to match the one of the substrate leading to an increase in the out-of-plane lattice parameter which is seen when plotting the c/a_{sub} ratio for two orientations as a function of lattice parameter a_{sub} of the substrate (See inet of Figure 3.14(b)).It is worth noting that some of Pr-V pairs are found to interact ferromagnetically confirming the competition between AFM and FM interactions. In addition, the total magnetic moment is found to be 4.1 μ_B using GGA+U which indicate that both Pr and V contribute to the magnetism in $PrVO_3$.

Summary

In summary, we have investigated the magnetic and magnetocaloric properties of $PrVO_3$ thin films grown by pulsed laser depositionin view of their potential application in cryogenic magnetic cooling. The obtained results reveal that the magnetic and magnetocaloric properties of $PrVO_3$ (PVO) compounds can be easy tailored by using the thin films approach. Particularly, the coercive magnetic field was dramatically decreased making from the PVO compound a nearly soft magnet in the region where the magnetic entropy change is released as well as a considerable increase in saturation magnetization. Accordingly, a giant magnetocaloric effect is exhibited by PVO thin films grown on LSAT substrates at low temperatures showing the great impact of strain effects [75]. This finding opens the way for the implementations of PVO thin films in some specific applications such as on-chip magnetic micro-refrigeration and sensor technology. On the other hand, the DFT calculations have confirmed the ground state and the competition between magnetic interactions under compressive strains in PVO thin films. Our result not only suggests that epitaxial PVO thin films is potential for refrigeration at cryogenic temperatures but may also pave the way to create many novel functionalities in perovskite-type transition metal oxides by control of structural aspects.

Bibliography

[1] M. H. Phan and S. C. Yu, J. Magn. Magn. Mater. 308, 325 (2007).

[2] M. Balli, S. Jandl, P. Fournier, and M. M. Gospodinov, Appl. Phys. Lett. 104, 232402 (2014).

[3] M. Balli, B. Roberge, S. Jandl, P. Fournier, T. T. M. Palstra, and A. A. Nugroho, J. Appl. Phys 118, 073903 (2015)

[4] X. Moya, L. E. Hueso, F. Maccherozzi, A. I. Tovstolytkin, D. I. Podyalovskii, C. Ducati, L. C. Phillips, M. Ghidini, O. Hovorka, A. Berger, M. E. Vickers, E. Defay, S. S. Dhesi, and N. D. Mathur, Nat. Mater. 12, 52 (2013)

[5] J. C. Debnath, J. H. Kim, Y. Heo, A. M. Strydom, and S. X. Dou, J. Appl. Phys. 113, 063508 (2013).

[6] V. Suresh Kumar, R. Chukka, Z. Chen, P. Yang, and L. Chen, AIP Adv. 3, 052127 (2013); Q. Zhang, S. Thota, F. Guillou, P. Padhan, V. Hardy, A. Wahl, and W. Prellier, J. Phys.: Condens. Matter 23, 052201 (2011).

[7] Liu, Y. et al. Large reversible caloric effect in FeRh thin films via a dual-stimulus multicaloric cycle. Nat Commun 7, 11614 (2016)

[8] R. A. Rao, D. Lavric, T. K. Nath, C. B. Eom, L. Wu, and F. Tsui ; Appl. Phys. Lett. 73, 3294 (1998)

[9] O. Copie, J. Varignon, H. Rotella, G. Steciuk, P. Boullay, A. Pautrat, A. David, B. Mercey, P. Ghosez, W. Prellier, Advanced Materials 2017, 29, 1604112.

[10] K. Zhang, J. Sunarso, Z. Shao, W. Zhou, C. Sun, and S. Liu: Research progress and materials selection guidelines on mixed conducting perovskite-type ceramic membranes for oxygen production. RSC Adv. 1, 1661–1676 (2011)

[11] V.M. Goldschmidt: Die Gesetze der Krystallochemie, Vol. 14 (Springer-Verlag, Berlin, Germany, 1926).

[12] A.M. Glazer: The classification of tilted octahedra in perovskites. Acta Crystallogr. Sect. B Struct. Crystallogr. Cryst. Chem. 28, 3384–3392 (1972).

[13] J.B. Goodenough: Theory of the role of covalence in the perovskite-type manganites [La,M(II)]MnO3. Phys. Rev. 100, 564–573 (1955).

[14] J. Kanamori: Superexchange interaction and symmetry properties of electron orbitals. J. Phys. Chem. Solids 10, 87–98 (1959).

[15] P.W. Anderson: Antiferromagnetism. Theory of superexchange interaction. Phys. Rev. 79, 350–356 (1950).

[16] S. Jin, T.H. Tiefel, M. McCormack, R.A. Fastnacht, R. Ramesh, and L.H. Chen: Thousandfold change in resistivity in magnetoresistive La–Ca–Mn–O films. Science 264, 413–415 (1994).

[17] P. Lampen, N.S. Bingham, M.H. Phan, H. Kim, M. Osofsky, A. Piqué, T.L. Phan, S.C. Yu, and H. Srikanth: Impact of reduced dimensionality on the magnetic and magnetocaloric response of La0.7Ca0.3MnO3. Appl. Phys. Lett. 102, 062414 (2013).

[18] Z.M. Wang, T. Tang, Y.P. Wang, S.Y. Zhang, and Y.W. Du: Room temperature large magnetoresistance and magnetocaloric properties of La0.78Ag0.22MnO3 film. J. Magn. Magn. Mater. 246, 254–258 (2002)

[19] M. Koubaa, W.C.R. Koubaa, and A. Cheikhrouhou: Magnetocaloric effect and magnetic properties of La0.75Ba0.1M0.15MnO3 (M 5 Na, Ag, and K) perovskite manganites. J. Alloys Compd. 479, 65–70 (2009).

[20] W. Prellier, P. Lecoeur, and B. Mercey: Colossal-magnetoresistive manganite thin films. J. Phys. Condens. Matter 13, R915 (2001)

[21] D.D. Belyea, T.S. Santos, and C.W. Miller: Magnetocaloric effect in epitaxial La0.56Sr0.44MnO3 alloy and digital heterostructures. J. Appl. Phys. 111, 07A935 (2012).

[22] A. Goktas, I.H. Mutlu, and A. Kawashi: Growth and characterization of La1xAxMnO3 (A 5 Ag and K, x 5 0.33) epitaxial and polycrystalline manganite thin films derived by sol–gel dip-coating technique. Thin Solid Films 520, 6138–6144 (2012)

[23] J.B. Puga, B.D. Bordalo, D.J. Silva, M.M. Dias, J.H. Belo, J.P. Araújo, J.C.R.E. Oliveira, A.M. Pereira, and J. Ventura: Novel thermal switch based on magnetic nanofluids with remote activation. Nano Energy 31, 278–285 (2017)

[24] V.S. Kumar, R. Chukka, Z. Chen, P. Yang, and L. Chen: Strain dependent magnetocaloric effect in La0.67Sr0.33MnO3 thin-films. AIP Adv. 3, 052127 (2013).

[25] Giri SK, Dasgupta P, Poddar A, Sahoo RC, Paladhi D, Nath TK (2015) Strain modulated large magnetocaloric effect in Sm0.55Sr0.45MnO3 epitaxial films. Appl Phys Lett 106:023507

[26] Jiang-Heng Jia et al A large magnetocaloric effect of GdCoO3−d epitaxial thin films prepared by a polymer assisted spin-coating methodJ. Mater. Chem. C, ,7, 14970-14976 (2019)

[27] L. D. Tung, Physical Review B 2005, 72, 054414.

[28] F. Wang, J. Zhang, P. Yuan, Q. Yan, P. Zhang, Journal of Physics: Condensed Matter 2000, 12, 3037

[29] Kawano H, Yoshizawa H and Ueda Y 1995 J. Phys. Soc. Japan 63 2857

[30] Zubkov V G, Bazuev G V and Shveikin G P 1974 Sov. Phys.–Solid State 18 1165

[31] Ren Y, PalstraTTM, Khomskii D I, Pellegrin E, Nugroho AA, Menovsky AA and Sawatzky GA 1998 Nature 396 441

[32] M. Uehara, B. Barbara, B. Dieny, and P. C. E. Stamp, Phys. Lett. 114A,23 (1986)

[33] J. M. D. Coey, T. R. McGuire, and B. Tissier, Phys. Rev. B 24, 1261 (1981)

[34] G. Hadjipanayis, D. J. Sellmyer, and B. Brandt, ibid. 23, 3349 (1981)

[35] J. Kushauer, R. van Bentum, W. Klee- mann, and D. Bertrand, ibid. 53, 11647 (1996)

[36] N. V. Baranov, V. I. Pushkarski, A. E. Sviderski, and H. Sassik, J. Magn. Magn. Mater. 157–158, 635 (1996)

[37] V. V. Ustinov, M. A. Milayev, L. N. Romashev, T. P. Krinitsina, A. M.Burkhanov, V. V. Lauter-Pasyuk, and H. J. Lauter, J. Magn. Magn. Mater.300, e281–e283 (2006)

[38] O. Copie, H. Rotella, P. Boullay, M. Morales, A. Pautrat, P.-E. Janolin, I. C. Infante, D. Pravathana, U. Lüders, and W. Prellier, J. Phys.: Condens. Matter 25, 492201 (2013)

[39] S. Chikazumi, Physics of Ferromagnetism, Oxford University Press Inc., New-York, 1991

[40] D. Kumar, A. David, A. Fouchet, B. Domenge's, Phys. Rev. B. B 99, 224405 (2019)

[41] Vailionis A et al 2011 phys rev b 83 064101

[42] N. Anuniwat, M. Ding, S. J. Poon, S. A. Wolf, and J. Lu, J. Appl. Phys. 113, 43905 (2013).

[43] A. Bur, T. Wu, J. Hockel, C. J. Hsu, H. K. D. Kim, T. K. Chung, K. Wong, K. L. Wang, and G. P. Carman, Journal of Applied Physics 109 (12) (2011).

[44] S. Miyasaka, Y. Okimoto, M. Iwama, Y. Tokura, Phys. Rev. B. 2003, 68, 100406

[45] D. Kumar, A. David, A. Fouchet, B. Domenge's, Phys. Rev. B. B 99, 224405 (2019)

[46] M. Reehuis, C. Ulrich, P. M. Abdala, P. Pattison, G. Khaliullin, J. Fujioka, S. Miyasaka, Y. Tokura, B. Keimer, Physical Review B 2016, 94, 104436.

[47] M. Reehuis, C. Ulrich, P. Pattison, B. Ouladdiaf, M. C. Rheinstadter, M. Ohl, L. P. Regnault, M. Miyasaka, Y. Tokura, ¨ and B. Keimer, Phys. Rev. B 73, 094440 (2006).

[48] M. Reehuis, C. Ulrich, P. Pattison, M. Miyasaka, Y. Tokura, and B. Keimer, Eur. Phys. J. B 64, 27 (2008)

[49] R. Aeschlimann, D. Preziosi, P. Scheiderer, M. Sing, S. Valencia, J. Santamaria, C. Luo, H. Ryll, F. Radu, R. Claessen, C. Piamonteze, M. Bibes, Advanced Materials 2018, 30, 1707489

[50] M. Bibes, L. Balcells, S. Valencia, J. Fontcuberta, M. Wojcik, E. Jedryka, S. Nadolski, Phys. Rev. Lett. 2001, 87, 67210

[51] M. Bibes, L. Balcells, S. Valencia, J. Fontcuberta, E. Jedryka, M. Wojcik, S. Nadolski, Thin Solid Films 2001, 400, 85.

[52] P A Joy, P S Anil Kumar‡ and S K Date J. Phys.: Condens. Matter 10 (1998) 11049–11054

[53] L. D. Tung, M. R. Lees, G. Balakrishnan, and D. McK. Paul, Phys. Rev. B 75, 104404 (2007).

[54] N. Kumar and A. Sundaresan, Solid State Commun. 150, 1162 (2010)

[55] G. Zubkov. G. V. Bazuev & G. P. Shveikin, Sov. Phys. Solid Stute 18, 1165 (1974).

[56] J.-Q. Yan, J.-S. Zhou, and J. B. Goodenough Phys. Rev. Lett. 93, 235901

[57] Onoda, Masashige, and Hiroshi Nagasawa. "Magnetic and structural aspects of semiconducting perovskites RVO3." Solid state communications 99.7 (1996): 487-491.

[58] Yan, J-Q., J-S. Zhou, and John B. Goodenough. "Unusually Strong Orbit-Lattice Interactions in the R V O 3 Perovskites." Physical review letters 93.23 (2004): 235901.

[59] Zhang, Q., et al. "Impact of the various spin-and orbital-ordering processes on the multiferroic properties of orthovanadate DyVO 3." Physical Review B 90.2 (2014): 024418.

[60] Das, M., S. Roy, and P. Mandal. Physical Review B 96.17 (2017): 174405.

[61] Cao et al. J. Appl. Phys. 119, 063904 (2016)

[62] Tishin, A. M. & Spichkin, Y. I. The Magnetocaloric Effect and its Applications (Institute of Physics, 2003)

[63] Moore, J. D., Skokov, K. P., Liu, J. & Gutfleisch, O. Procedure for numerical integration of the magnetocaloric effect. J. Appl. Phys. 112, 063920 (2012).

[64] Moya, X., Kar-Narayan, S. & Mathur, N. D. Caloric materials near ferroic phase transitions. Nat. Mater. 13, 439–450 (2014)

[65] Moya, X. et al. Giant electrocaloric strength in single-crystal BaTiO3. Adv. Mater. 25, 1360–1365 (2013)

[66] A. Midya, P. Mandal, K. Rubi, R. Chen, J. S. Wang, R.Mahendiran, G. Lorusso, and M. Evangelisti,Phys.Rev.B93,094422(2016).

[67] Kresse, G. & Hafner, J. Ab initio molecular dynamics for liquid metals. Phys. Rev. B 47, 558–561 (1993)

[68] Blochl, P. E. Projector augmented-wave method. Phys. Rev. B 50, 17953–17979 (1994)

[69] Kresse, G. & Furthmuller, J. Efficient iterative schemes for ab initio total-energy calculations using a plane-wave basis set. Phys. Rev. B 54, 11169–11186 (1996).

[70] Kresse, G. & Joubert, D. From ultrasoft pseudopotentials to the projector augmented-wave method. Phys. Rev. B 59, 1758–1775 (1999).

[71] S. L. Dudarev, G. A. Botton, S. Y. Savrasov, C. J. Humphreys, A. P. Sutton, Physical Review B 1998, 57, 1505.

[72] D.D. Belyea, T.S. Santos, and C.W. Miller: Magnetocaloric effect in epitaxial La0.56Sr0.44MnO3 alloy and digital heterostructures. J. Appl. Phys. 111, 07A935 (2012).

[73] D. Matte, M. de Lafontaine, A. Ouellet, M. Balli, and P. Fournier, Phys. Rev. App. 2018, 9, 054042.

[74] Banerjee, B. K. On a generalised approach to first and second order magnetic transitions. Phys. Lett. 1964, 12, 16.

[75] Bouhani, H.; Endichi, A.; Kumar, D.; Olivier, O.; Zaari, H.; David, A.; Fouchet, A.; Prellier, W.; Mounkachi, O.; Balli, M.; Benyoussef, A.; El kenz, A.; Mangin, S. Engineering the magnetocaloric properties of PrVO3 epitaxial oxide thin films by strain effects. App. Phys. Lett. 2020, 117, 072402.

Chapter 4

Magnetocaloric effect in $HoMn_2O_5$ single crystals

4.1 Introduction

In this chapter, we mainly focus on the electronic, magnetic and magnetocaloric properties of HoMn2O5 single crystals. The aim of this investigations is to explain the reasons behind the large rotating magneto caloric effect recently observed in HoMn2O5 single crystals [1]. Both DFT calculations and Monte Carlo simulation were used in the following study. First, we give in section a short overview about the magnetic transition in the material and discuss the MCE in multiferroic RMn_2O_5. Second, we investigate the electronic and magnetic properties of HoMn2O5 single crystals. Finally, we calculate the magnetocaloric effect in terms of isothermal entropy change and relative cooling power (RCP) confirming the large rotary MCE observed experimentally.

4.2 Why RMn_2O_5

The multiferroic crystals RMn_2O_5 (R = rare earth) was first described in 1964 [2], but its multiferroic properties were discovered only recently. The experimental discovery of remarkable magnetoelectric coupling in $TbMn_2O_5$[3] is one of the reasons that makes the this family exceptional and interesting to study. Since then, RMn_2O_5 have been extensively explored because of their impressive physical properties as well as potential applications in spintronic devices. The strong interplay between magnetism and ferroelectricity provides an additional degree of freedom to controle the magnetic and dielectric properties in these materials. On the other hand, the study of the MC properties has unveiled a great

potential for lowr-temperature cooling application [1, 8].

Vartious intermetallic materials exists with exceptional magnetocaloric effect at low temperature regime. However, their chemical and mechanical instability continue to seriously hinder their use. In fact, one of the main problems with these materials is the decomposition caused by hydrogen absorption [4]. Moreover, the undesirable thermal losses caused by the creation of eddy current during the heating-cooling process present an obstacle towards the implementation in functional devices [5] which could be avoided by using RMn_2O_5oxides which reveal an insulating character combined with high chemical and mechanical stabilities [6]. Interestingly, some the these materials present a possibility to tune their MCE to its maximum when they are rotated around the intermediate axis in constant magnetic field taking advantage of the magnetic anisotropy [1, 7]. Therefore, these new physical phenomena and fascinating MC properties emerging in the this classs of materials need to be understood.

4.3 Common features

4.3.1 Magnetic structure

$HoMn_2O_5$ belongs to the family of RMn_2O_5 compounds (R = rare earth) that have an orthorhombic structure [7] consisting of $Mn^{4+}O_6$ octahedral and $Mn^{3+}O_5$ bipyramids connected by their edges and corners. This structure is illustrated in figure4.1. Perfect knowledge of magnetic orders involving Mn^{3+} and Mn^{4+} ions is essential for a better understanding of multiferroic features in RMn2O5 compounds. Recent studies of RMn_2O_5 compounds show rich magnetic properties [1, 8]. The majority of these materials present at least four magnetic transitions: a first transition occurs at $T_1 = 40 - 45$ K in which the spins of Mn ions adopt a sinusoidal incommensurate (ICM) order (See figure).

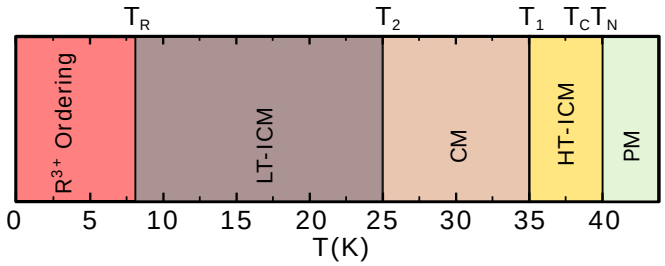

Figure 4.2: Magnetic phase diagram of the RMn_2O_5 compounds. Here, PM, ICM, CM, refer to the abbreviation of paramagnetic, incommensurate magnetic, commensurate magnetic, respectively. Image modified from

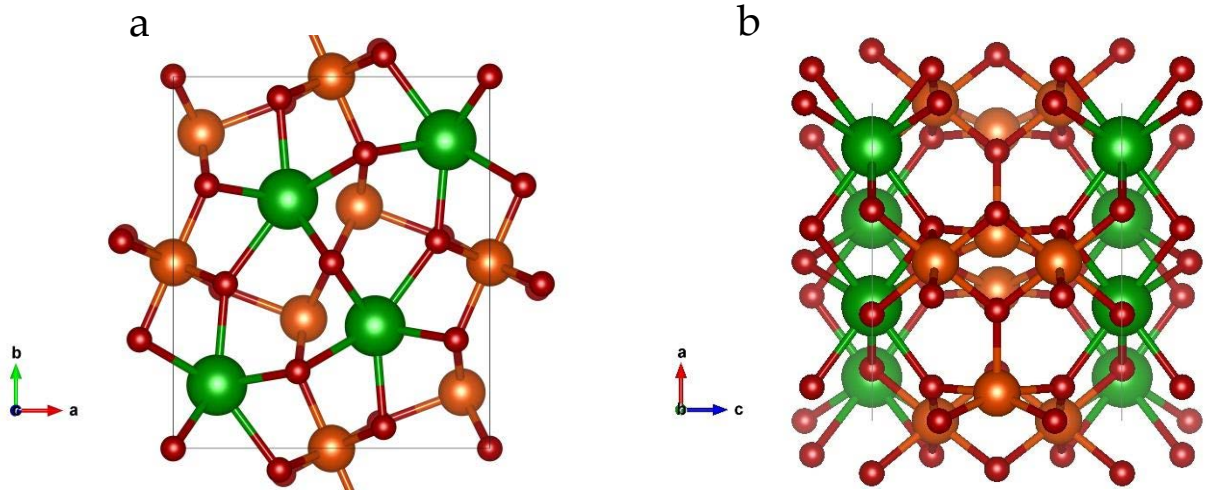

Figure 4.1: a) Side view and (b) top view along b axis of the crystallographic structure of HoMn2O5 single crystals. The green spheres are holmium atoms, the orange stands for the manganese atoms and the red corresponds to oxygen atoms.

Then, another transition takes place at T_2 = 35-41 K where the spins are configured in a commensurate (CM) antiferromagnetic order then a return to sinusoidal incommensurate order below T_2 = 25 K. Below 10 K, the magnetic order of the rare earth ions appears and adopts an incommensurate antiferromagnetic order, becoming commensurate on further cooling [7]. A dielectric constant step is observed at the CM-ICM magnetic phase transition [9] being the key to understand the strong magnetoelectric correlation which is indicated by the modification of dielectric function due to the ordering of Mn spins [10].

4.3.2 Magnetocaloric effect in RMn_2O_5 at low temperature regime

Some studies on RMn_2O_5 oxides (R= rare earth) have shown that there is a huge magnetoelectric effect associated with CM–ICM magnetic phase. In the case of $DyMn_2O_5$, due to the influence of the applied magnetic field, the dielectric constant increases by more than

100%, resulting in a significant magnetodielectric effect ("CMD") [25] In $TbMn_2O_5$ crystals on the other hand, a high electric polarization switch can be obtained by using a relatively low 2T magnetic field. However, magnetocaloric properties have not attracted much interest. Recently, large rotatry MCE at low temperature has been reported in $HoMn_2O_5$ single crystals, which paves the way for the implementation of an efficient magnetic refrigerators. Following the same study, a new concept for the the liquefaction of the helium and hydrogen was also proposed [27]

The recent study in $HoMn_2O_5$ single crystals reported by Balli et al [1] reveals a large magnetic anisotropy as shown in figure 4.3.a with as the easy crystallographic axis along b. The several magnetic easy axis of the $RMn_2O_5$are summarized in table 1.

Magnetic easy axis	R
a	Bi [28], Tb [29]
b	Dy[30], Ho[31]
c	Sm[31, 32], Er[33], Tm [34]and Yb [34]
Magnetically isotropic	Gd[35]

Table 4.1: Magnetic easy axis of the RMn2O5 compounds

By analyzing the magnetization curves, it was found that the the Ho^{3+}magnetic moments order around 10 K, However, due to the high magnetic moment of Ho^{3+}which hides the low weak magnetization caused by Mn moments, the phase transitions related to the Mn sublattice are not clearly visible from the magnetization curves. As reported in Balli et al [1], The antiferromagnetic interactions at high temperatures along the c and a axes are indicated by the inverse magnetic susceptibility while a low antiferromagnetic order or a paramagnetic disorder of Ho^{3+} moments is shown along the axe of easy magnetization b which is in good agreement with early reported neutron diffraction data by Blake et al [7]. Figure 4.3.b shows the magnetocaloric properties of the HoMn2O5 and TbMn2O5single crystal [1, 8] that have been reported in terms of entropy . Following the easy-axis b, –DSmax reaches 3.5 and 13.1 J/kg K in magnetic field changes of 2 and 7 T, respectively. Whereas for or the intermediate a-axis, the maximum of the isothermal entropy change found to be only 5 J/kg K under 7 T. Along the hard-axis c, the obtained MCE is much lower even under high magnetic fields (figure not hsown here). This can be mainly explained by the giant magnetocrystalline anisotropy HoMn2 O5 single crystals as shown in figure 4.3.a. At 2 K, the magnetization along the easy axis reaches 124 Am²/kg for an applied magnetic field of 7 T being only 34 Am²/kg for H //c. The authors make use of the anisotropic MCE observed in $HoMn_2O_5$ single crystals to discover a a large rotating magnetocaloric effect [1]. By rotating the compound in constant magnetic field of 7 T around its a-axis, the obtained entropy change reaches a maximum value of 12.40 J/kg K, being

much higher than the rotating entropy change reported in TbMnO3 [36] and TmMnO3 [37].

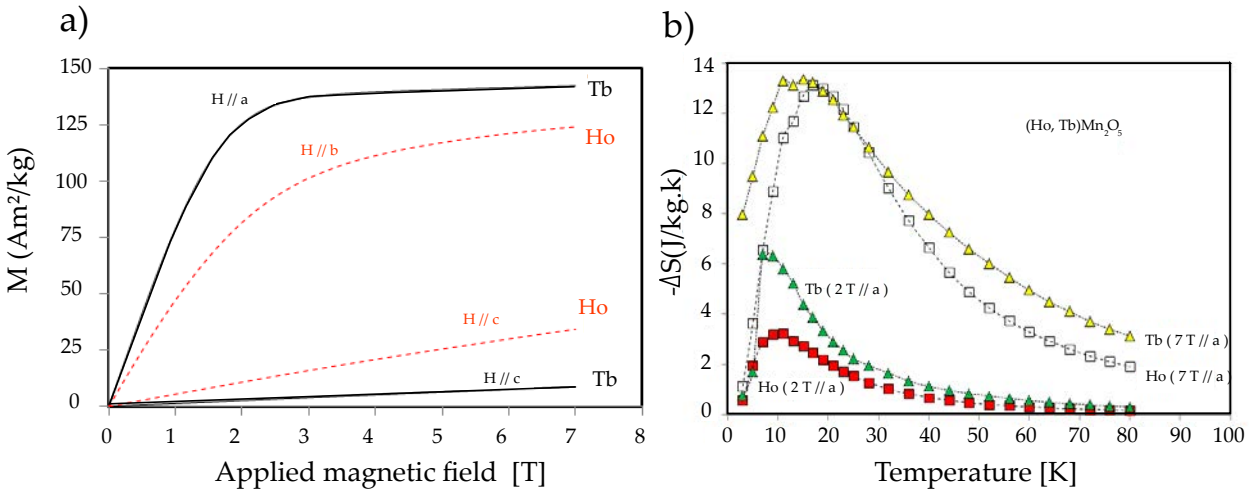

Figure 4.3: (a) Magnetization as a function of an applied magneteic field at 2 K of $RMn_2O_5(R = Ho$ and $Tb)$ single crystals along their easy and hard axes and (b) the isothermal magnetic entropy change under low (2 T) and high (7 T) applied magnetic fields along their easy axes [1, 8]

4.4 Study of $HoMn_2O_5$ single crystals

4.4.1 Computational details

To investigate the electronic, magnetic and magnetocaloric properties of $HoMn_2O_5$ single crystals All calculations were done using the Full Potential Augmented Plane Wave (FP-LAPW) method implemented in WIEN2K code [11] based on density functional theory [12] with the exchange correlation functional treated in the Generalized Gradient Approximations [13] taking into account the spin orbit interactions. The unit cell parmeters are : $a = 7.2643A$, $b = 8.4768A$ and $c = 5.6700A$ and the atomic coordinates are listed in table4.2. To investigate the magnetic properties, we have used 7*6*9 Monkhorst-Pack scheme [14], the total energy was converged to less than 10^{-6} Ryd and the cut-off energy is set to -8.0 Ryd. The radii of the muffin-tin spheres were: $R_{MT}(Ho) = 2.53$, $R_{MT}(Mn1) = 1.86$ and $R_{MT}(O) = 1.67$ a. u (atomic units).

Atom	x	y	z
Ho	0.1367	0.1714	0
Mn_1	0	1/2	0.2611
Mn_2	0.4126	0.3496	1/2
O_1	0	0	0.2702
O_2	0.1637	0.4438	0
O_3	0.1503	0.4300	1/2
O_4	0.3948	0.2063	0.2457

Table 4.2: Structural parameters after the Rietveld refinement of NPD data [44]for $HoMn_2O_5$oxides at room temperature. R and O_2 atoms are at 4g (x, y, 0) positions; Mn_1 at 4f (0, 1/2, z); Mn_2 and O_3 at 4h (x, y, 1/2); O_1 at 4e (0, 0, z) and O_4 at 8i (x, y,z) positions.

Moreover, magnetic anisotropy is calculated using DIPAN program [15, 16] that calculate the dipolar magnetocrystalline anisotropy and the magnetic dipolar hyperfine field by a direct lattice summation over the magnetic moments of all the sites. In order to disentangle the magnetic contribution responsible for the magneto-caloric effect in the material, we have studied the differentiated role of Ho and Mn ions using XMCD and XAS spectrum. Therefore, we calculated, separately, the values of both spin and orbital magnetic moments. XMCD represents the absorption difference between the right circular polarization (μ^+)and the left circular polarization (μ^-). The left and right directions are referenced to the propagation direction of the incident radiation with respect to the axis of the magnetic field. In particular, the photons are polarized left (right). When the direction of propagation is antiparallel, their helicity is ese/Chapitres/Thesis-2020/t2appl.fd ese/Chapitres/Thesis-2020/T2Appl.fd ħ (+-ħ) [17]. The objective of XMCD spectrum is to determine the orbital and spin moment, knowing that there is a relationship between the integral of the XMCD spectrum and the mean value of the projection of the orbital angular momentum on the magnetization axis. This relationship was suggested by TholeCarra and Van Der Laan [18], later, the same authors proposed a second sum rules for spin moment [19].

$$\frac{\int_{j^+} dw(\mu^+ - \mu^-)}{\int_{j^\pm} dw(\mu^+ + \mu^- - \mu^0)} = \frac{1c(c+1) - l(l+1) - 2}{2l(l+1)(4l+2-n)}. < Lz > \tag{4.1}$$

$$\frac{\int_{j^+} dw(\mu^+ - \mu^-) - c(c+1)\int_{j^+} dw(\mu^+ - \mu^-)}{\int_{j^\pm} dw(\mu^+ - \mu^-)} = \frac{l(l+1) - c(c+1) - 2}{3c(4l+2-n)}. < Sz > \tag{4.2}$$

- l = orbital quantum number of the valence state
- c = orbital quantum number of the core state

Direction	En(i)-En(j)
[001]	0.03356
[010]	0.0131
[100]	0.0456
[011]	0.0165

Table 4.3: Difference in energy for different directions in mRy/cell

- $(\mu^+)(\mu^-)$ = absorption spectrum for left (right) circularly polarized light.
- Tz = expectation value of magnetic dipole operator.

The sum rules allow to obtain separately the orbital magnetic moment <Lz> and the spin magnetic moment <Sz> from the integrated XMCD.

For $M_{4,5}$ the transition from 3d (l=2) to 4f (l=3):

$$m_s = (\mu_b/\hbar) < Sz >= \frac{((7\int_{M_5} dw(\mu^+ - \mu^-) - 6\int_{M_4} dw(\mu^+ - \mu^-))}{(\int_{M_4+M_5} dw(\mu^+ + \mu^-)) \times (14 - n_{4f})(1 + 10(< Tz > / < Sz >))^{-1}} \tag{4.3}$$

$$m_L = (\mu_b/\hbar) < Lz >= \frac{-2((\int_{M_4+M_5} dw(\mu^+ - \mu^-))}{\int_{M_4+M_5} dw(\mu^+ + \mu^-)) \times (14 - n_{4f})} \tag{4.4}$$

A strong magneto-crystalline anisotropy is experimentally observed in $HoMn_2O_5$ single crystals where the magnetization tends to orient preferentially along the b-axis [1]. In order to get more insight on the gigantic anisotropy shown in this material, the energy of the system following 001, 010, 100 and 011 direction has been calculated using DIPAN program and presented in Table4.3 The minimum energy found corresponds to 010 direction in good agreement with experimental measurement.

4.4.2 Electronic properties

We have displayed the density of state using GGA approximation to describe the magnetic and electronic properties shown in figure4.4. The main contribution to the magnetism comes from 4f states of Holmium which is responsible for the magnetic moment formation on Holmium atoms. The oxygen-manganese molecular bond is formed by p electrons of oxygen and s electrons of manganese. Each oxygen atom is twice ionized, involving two electrons in its p orbitals. The ionization of the manganese atom depends on the chemical formula of the compound: Mn is 4 times ionized, Mn^{3+} and Mn^{4+} are deficient in electrons, respectively involving 4 and 3 electrons in its d layers.

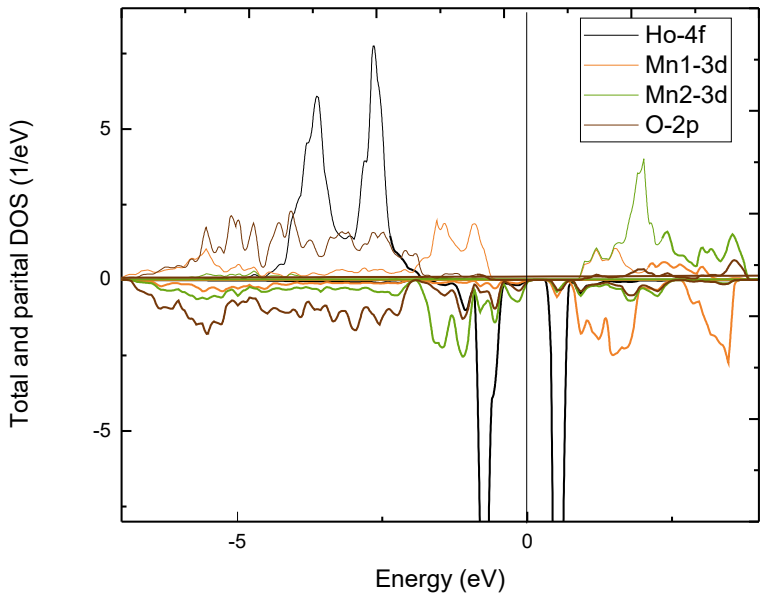

Figure 4.4: Total and partial density of states obtained within (GGA þ Spin Orbit)

In the absence of perturbation, the manganese d orbitals are degenerate but in a crystal field of given symmetry. The crystal matrix favors an arrangement of some orbitals by partially lifting their degeneration. For $HoMn_2O_5$compound, Mn occupies two sites of different symmetry: Mn^{4+}at the center of an octahedron and Mn^{3+} at the center of a pyramid. Each symmetry acts differently on the distribution of the electronic levels of Mn. The d orbitals are divided into two sub-groups for octahedral and tetragonal symmetries: at t2g level of low triple-degenerate and another level doubly degenerate Eg. As expected, we can see that the degeneracy of its d orbital is lifted especially in d_{z^2} lodge. This anomaly is known as the crystal field deformation or Jahn Teller effect [21]. One can also notice that 4f Holmium orbitals favors the spin orbit coupling effect while the 3d orbitals of manganese favors the crystalline field. t2g levels have d_{xy}, d_{yz} and d_{xz} orbital character lying on the same level while there is separation in energy between the e2g pics which indicate a deformation field or splitting in Mn1. In the contrary, the partial density of states for Mn2 shows a t2g splitting with a 2/3 filled band while there is no e2g splitting as shown in figure 4.5.

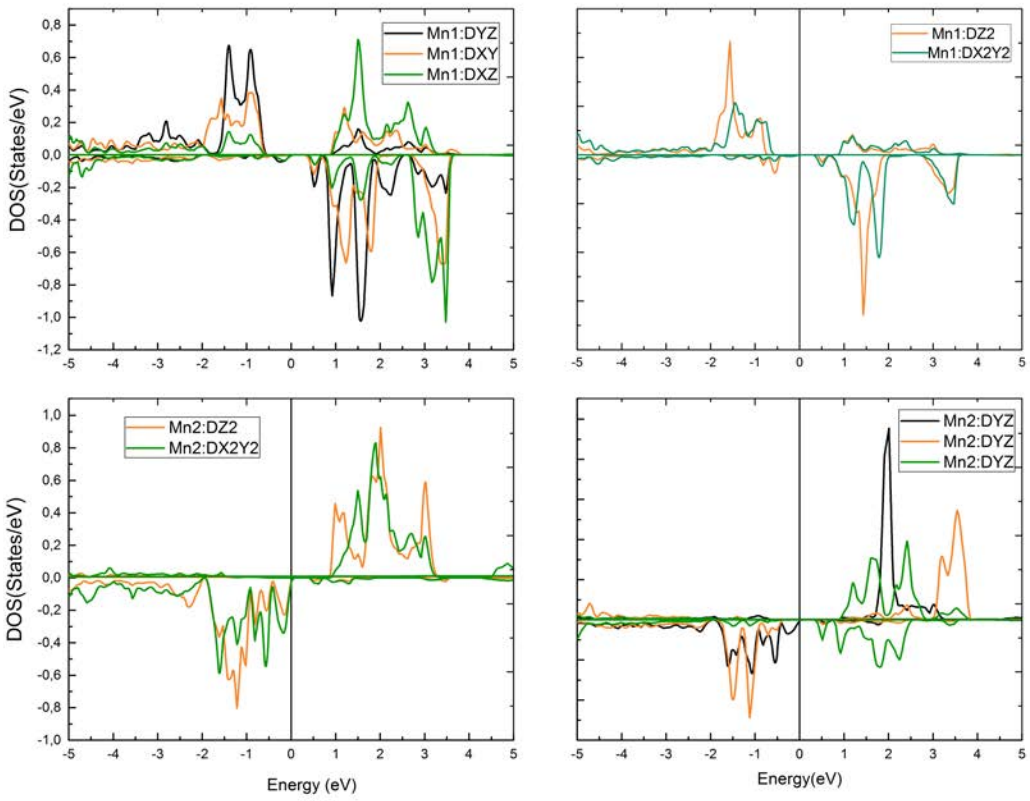

Figure 4.5: Partial density of states for Mn1 (3d) and Mn2 (3d)

4.4.3 Magnetic properties

As mentioned in the introduction, $HoMn_2O_5$single crystals show interesting magnetic properties following a specific direction. Indeed, the calculation of the energy of each axis demonstrates that this system has its lowest energy following the b-axis being in fair agreement with recently reported experimental data [1]. The high magnetic moment of holmium atoms makes the compound an excellent candidate for MCE applications. In the following section we calculate spin and orbital magnetic moments, separately, using XMCD spectrum aiming to disentangle the magnetic contribution responsible for the MCE in this material.

4.4.3.1 XMCD at the Ho $M_{4,5}$edge

The absorption edge that provides the most direct information on the rare earth 3d-4f transitions is the M4,5 edge. The theoretical treatment of that edge is generally done using a model where the interactions with the environment such as the crystal field are considered to be of weak perturbation except for systems where the rare earth exhibits valence

Ion	Ho^{3+}	Mn^{4+}	Mn^{3+}
Electronic configuration	$4f^{10}$	$3d^3$	$3d^4$
Spin magnetic moment (S)	2	2	3/2
Orbital magnetic moment (L)	6	0	0
Total magnetic moment (J)	8	2	3/2
Effective magnetic moment (μ_b)	10.61	4.89	3.87

Table 4.4: Electronic configuration, spin, angular and total magnetic moment as well as the effective magnetic moment for all the three ions

instability or mixed valence [19]. This approach is valid due to localized Ho 4f electrons and there is therefore no overlap between the 4f levels of two neighboring atoms.

In figure 4.6a, the Ho 3d-4f absorption spectrum is characterized by M4 and M5 that are separated in energy by the strong spin-orbit effect. At M_5 edge, the intensity is very high compared to M_4 edge indicating a large contribution of the orbital moment. We calculated, therefore, the spin and orbital magnetic moment. The values are as follows: The expected value of a free Ho^{3+} ($4f^{10}$) magnetic moment with respect to hund's rule ground state ($J = 8$, $S = 2$ and $L = 6$) is 10.61 μ_B taking into consideration that the atom is considered as isolated whereas, it is necessary to take into account the atomic environment. The values of the magnetic moment for the manganese free ions are summarized in table 4.4.

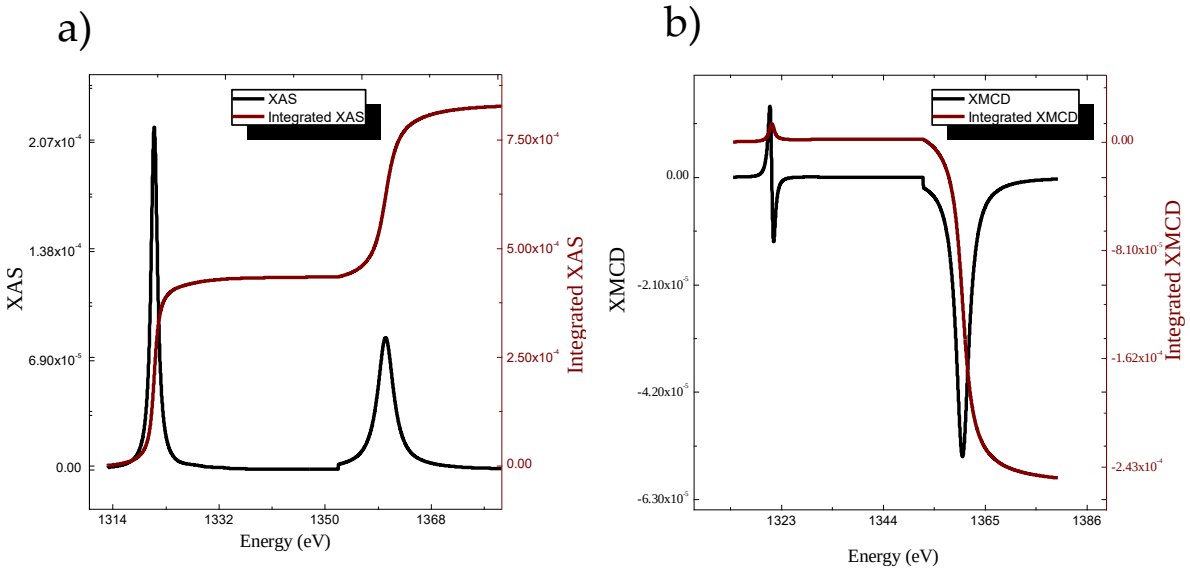

Figure 4.6: XAS spectra representing M4.5 (wine line) and the integral of the spectra (black line) within GGA approximation and (b) XMCD spectra representing M4.5 (wine line) and the integral of the spectra (black line) within GGA approximation.

The negative (positive) signal indicates a parallel alignment of Ho magnetic sublattice to the applied magnetic field and may refer to a double transition: 3d to 4f and 4f to 5s

known as the quadrupole tran- sition. Figure 4.6b represents the integral of XAS (XMCD) that allow the calculation of the spin and orbital magnetic moment.

	XMCD			Experimental
	Ho	Mn_1	Mn_2	
Spin moment	7.77			
Orbital moment	2.44	0.066	-0.14	
Total moment	10.21	2.79	-2.58	10.3 [24]

Table 4.5: Spin, orbital and total magnetic moment for Ho, Mn1 and Mn2. XMCD

4.4.3.2 XMCD at the Mn $L_{2,3}$ edge

We tried now to acquire in depth information about the magnetic contribution from the Mn ions. The results shown in Table 1, indicates that only a small magnetic moment is induced within the antiferro-magnetic cycloidal configuration confirming that along the easy axis b, the contribution of the Mn lattice to the full magnetization is negligible and mainly originates from the Ho^{3+} sublattice.

4.4.4 Magnetocaloric properties

To investigate the magnetocaloric effect in $HoMn_2O_5$ single crystals, a classical model that combines both Ising and XY models was proposed to deal with the anisotropy since the manganese spin's components can be oriented in any direction in a two-dimensional plane while the holmium's spin components direction are either parallel or antiparallel. Indeed, the spins are represented by two-component vectors that satisfy the $\sigma_i^2 = \sigma_{ix}^2 + \sigma_{iy}^2$ constraint.

The proposed Hamiltonian is:

$$H = -J_1 \sum_{<i,j>} \overrightarrow{\sigma_i^1}\overrightarrow{\sigma_j^1} - J_2 \sum_{<i,j>} \overrightarrow{\sigma_i^1}\overrightarrow{\sigma_j^1} - J_3 \sum_{<i,j>} \overrightarrow{\sigma_i^1}\overrightarrow{\sigma_j^1} - J_4 \sum_{<i,j>} \overrightarrow{\sigma_i^1}\overrightarrow{\sigma_j^1} - -J_1 \sum_{<i,j>} \overrightarrow{\sigma_i^1}\overrightarrow{\sigma_j^1} \tag{4.5}$$

where :

S_{iy}: Holmium spin, σ_1 : Manganese Mn^{4+} spin and σ_2 : Manganese Mn^{3+} spin J_1: Interaction coupling between first Mn^{4+} nearest neighbors J_2: Interaction coupling between first Mn3þ nearest neighbors J_3: Interaction coupling between first Mn^{4+} - Mn^{3+}nearest neighbors J_4: Interaction coupling between second Mn^{4+}- Mn^{3+} nearest neighbors J_5: Interaction coupling between first Ho^{3+} -Mn^{3+} nearest neigh- bors J_6: Interaction coupling

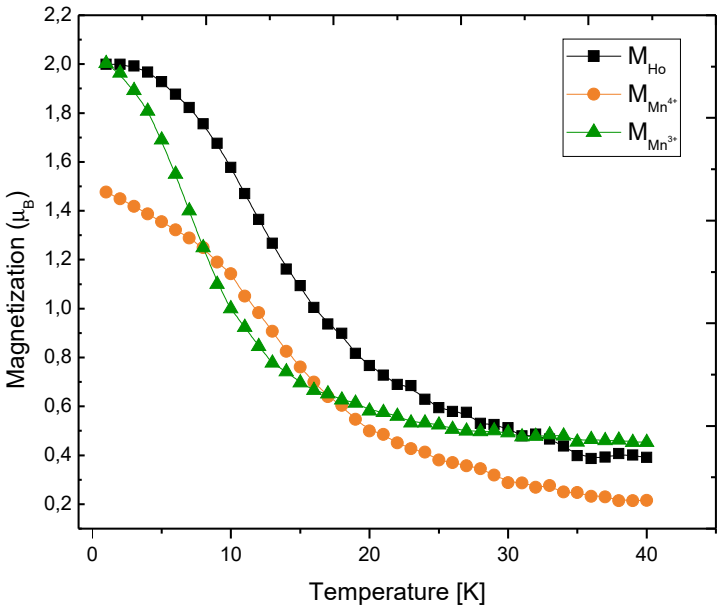

Figure 4.7: Temperature dependence of magnetization following y axis for HoMn2O5 (b) Isothermal magnetic entropy change for different applied mag- netic field along the same axis.

between first Ho^{3+}- Mn^{4+} nearest neighbors J_7: Interaction coupling between first Ho^{3+} nearest neighbors J_8: Interaction coupling between second Ho^{3+}nearest neighbors

With $\overrightarrow{\sigma_i^1} = \begin{pmatrix} \sigma_{ix}^1 \\ \sigma_{iy}^1 \end{pmatrix}$,$\overrightarrow{\sigma_i^2} = \begin{pmatrix} œ_{\text{ix}}^2 \\ œ_{\text{iy}}^2 \end{pmatrix}$, and h: external magnetic field

The MCE is studied based on Monte Carlo simulations using the Hamiltonian given by Eq 4.5where random spins were chosen and then flipped with Boltzmann based probability using Metropolis algorithm [23] $P_{MET} = \exp.\left(-\frac{\triangle E}{K_B.T}\right)$). The equilibrium properties are reached when averaging the generated configuration starting from different initial conditions. The data generated with 106 steps per spin discarding the first 104 generated configurations, our calculations were performed for a system with N = 60.

The program used for calculations predicts the following thermodynamic quantities: the magnetization, specific heat and the susceptibility which are given respectively by:

$$M_s = \frac{1}{N}\sum_{i=1}^{N} S_{iy} \tag{4.6}$$

$$M_{xy} = \frac{1}{N}\sqrt{M_x^2 + M_y^2} \tag{4.7}$$

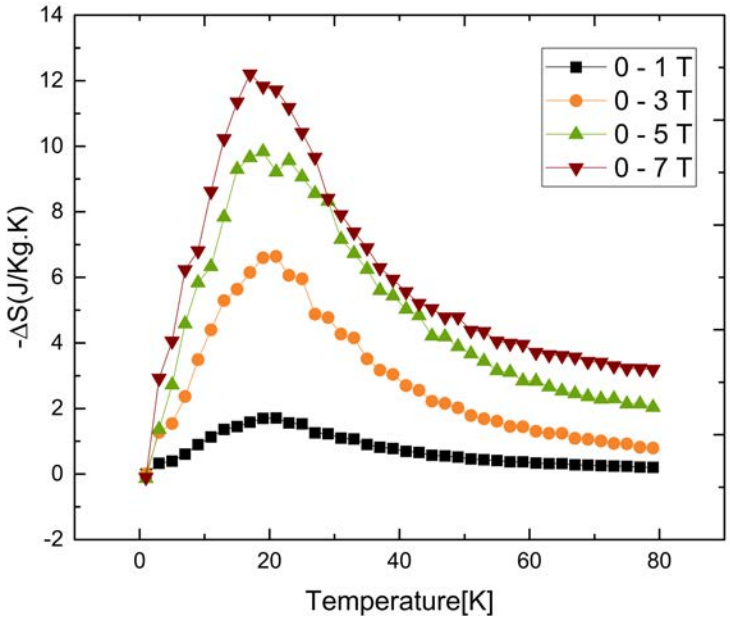

Figure 4.8: Temperature dependence of magnetization following y axis for HoMn2O5 (b) Isothermal magnetic entropy change for different applied mag- netic field along the same axis.

$$\chi = \frac{N}{K_b T}[< M^2_{total} > - < M_{total} >^2] \tag{4.8}$$

$$C_v = \frac{1}{K_b T^2}[< E^2 > - < E >^2] \tag{4.9}$$

Where E is the internal energy of the system, Kb is the Boltzmann con- stant and N is the number of spins in each sublattice. The isothermal magnetic entropy change was calculated using an integral version of Maxwell's relation:

$$\triangle S_M(T, \triangle H) = \int_0^{H_1} \left(\frac{\partial M(T,H)}{\partial T}\right)_H dH \tag{4.10}$$

where SM, M, H and T are the magnetic entropy, magnetization, applied magnetic field, and the temperature, respectively.

Figure4.7 Presents the temperature dependence of magnetization following the b-axis for Ho^{3+}, Mn^{3+} and Mn^{4+}. |DS| values are shown in figure4.8 for several magnetic fields. The magnetic field variation from 0 to 7 T yields to a maximum entropy change of 12.20 J/kg K close to the value reported by Balli et al. [1] which is about 13.1 J/kg K. The maximum of |DS| increases with increasing the external magnetic field since the magnetic

moments are governed by exchange interactions between ions in a magnetic structure that moves to a disordered magnetic configuration (paramagnetic region). Another important parameter that is usually used to compare the MCE is the relative cooling power (RCP) which is defined as the product of the maximum isothermal magnetic entropy and the full width at half maximum and is given in figure4.10 as a function of magnetic field. The RCP reaches 353 J/kg for an applied magnetic field of 7 T. These results are comparable with those reported in literature [1]. By comparing with materials performing in the same range of temperature, the RCP of the HoMn2O5 oxide (225 J/kg for 5 T) obtained for the b axis is higher than that reported in $HoMnO_3$ oxide (120 J/kg for 5 T) [38], and in the intermetallics $ErRu_2Si_2$ (196.5 J/kg for 5 T) [39] and DySb (144 J/kg for 5 T) [40].

Material	T(K)	$H(T)$	$\triangle S_M$
$GdMnO_3$	7	7	31.8 [41]
$DyMnO_3$	5	7	18.3 [41, 42]
$TbMn_2O_5$	13	7	13.8 [8]
$HoVO_3$	15	7	17.2 [43]

Figure 4.9: Maximum entropy change of some oxides under an applied magnetic field of T along their easy axis at low temperature regime

The large values of the magnetocaloric parameters suggest that $HoMn_2O_5$ can be used as a potential refrigerant in low temperature magnetic refrigeration technology, such hydrogen liquefaction in fuel industry. Moreover, the high chemical stability, the existence of both order-disorder and rotating MCEs, together with the absence of thermal hysteresis and field hysteresis losses, allow the material to meet the requirement of a good magnetic refrigerant.

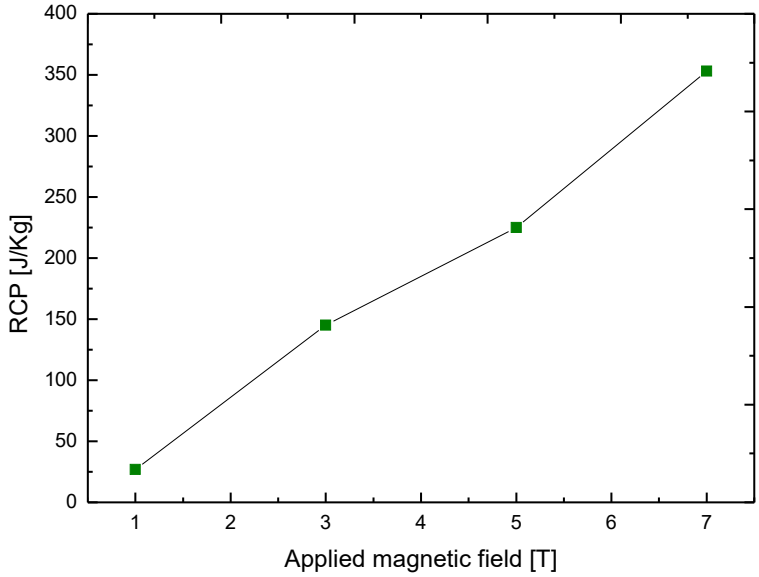

Figure 4.10: Relative cooling power (RCP) as a function of the applied magnetic field.

4.4.5 Summary

In this chapter, we have theoretically investigated the electronic, magnetic and magnetocaloric properties of $HoMn_2O_5$ single crystals using First prinples calculations and Monte Carlo simulation [45]. the DFT study reveal that the saturation magnetization reaches it maximum following the easy axis b. The same calculations show that the main contribution to the MCE comes from Ho ions. The MCE effect in $HoMn_2O_5$ is studied based on Monte Carlo simulations giving similar results compared to experimental study. This work confirms that the use of the intrinsic anisotropic properties is a promising way to optimize the MCE for magnetic refrigeration application at low temperature regime as well as the implementation of compact and efficient rotary magnetic refrigerators.

Bibliography

[1] M.Balli, M.; Jandl, S.; Fournier, P.; Gospodinov, M.M. Anisotropy-enhanced giant reversible rotating magnetocaloric effect in HoMn2O5 single crystals. Appl. Phys. Lett. 2014, 104, 232402

[2] W. Prellier, M. P. Singh, and P. Murugavel. "The single-phase multiferroic oxides: from bulk to thin film." In: J. Phys. Condens. Matter 17.30 (2005), R803

[3] N. Hur, S. Park, P. A. Sharma, et al. "Electric polarization reversal and memory in a multiferroic material induced by magnetic field." In: Nature 429.6990 (2004), pp. 392–395.

[4] Numazawa, T.; Kamiya, K.; Utaki, T.; Matsumoto, K. Magnetic refrigerator for hydrogen liquefaction. Cryogenics 2014, 62, 185–192.

[5] Balli, M.; Mahmed, C.; Bonhote, P.; Sari, O. On the magnetic forces in magnetic cooling machines: Numerical calculations and experimental investigations. IEEE Trans. Magn. 2011, 47, 3383–3386.

[6] Phan, M.H.; Yu, S.C. Review of the magnetocaloric effect in manganite materials. J. Magn. Magn. Mat 2007, 308, 325–340.

[7] G.R. Blake, L.C. Chapon, P.G. Radaelli, S. Park, N. Hur, S.-W. Cheong, J. Rodríguez-Carvajal, Spin structure and magnetic frustration in multiferroic RMn2O5 (R¼\ Tb, Ho,Dy), Phys. Rev. B 71 (2005) 214402

[8] M. Balli, S. Jandl, P. Fournier, D.Z. Dimitrov, Giant rotating magnetocaloric effect at low magnetic fields in multiferroic TbMn2O5 single crystals, Appl. Phys. Lett. 108 (2016) 102401

[9] K. Cao, G.-C. Guo, D. Vanderbilt, L. He, First-principles modeling of multiferroic RMn2O5, Phys. Rev. Lett. 103 (2009) 257201

[10] I. Radulov, V.I. Nizhankovskii, V. Lovchinov, D. Dimitrov, A. Apostolov, Colossal magnetostriction effect in HoMn2O5, Eur. Phys. J. B. 52 (2006) 361–364

[11] P. Blaha, P. Blaha, K. Schwarz, G.K.H. Madsen, D. Kvasnicka, J. Luitz, WIEN2k_7.3, an Augmented Plane Wave þ Local Orbitals Program for Calculating Crystal Properties, Karlheinz Schwarz, Techn, Uni- versitd'at Wien, Austria, 2007.

[12] P. Hohenberg, W. Kohn, Inhomogeneous electron gas, Phys. Rev. 136 (1964) B864–B871

[13] J.P. Perdew, K. Burke, M. Ernzerhof, Generalized gradient approximation made simple, Phys. Rev. Lett. 77 (1996) 3865–3868

[14] H.J. Monkhorst, J.D. Pack, Special points for Brillouin-zone integrations, Phys. Rev. B 13 (1976) 5188–5192

[15] P. Novak', Inst. Of Physics, Acad.Science, Prague, Czeck Republic, 2019.

[16] Peter Blaha, Karlheinz Schwarz, Georg K. H. Madsen, Dieter Kvasnicka, Joachim Luitz, Robert Laskowski, Fabien Tran, Laurence D. Marks: WIEN2k an Augmented Plane Wave þ Local Orbitals Program for Calculating Crystal Properties Revised Edition WIEN2k 18.2 (Release 07/17/2018)

[17] B.T. Thole, P. Carra, F. Sette, G. van der Laan, X-ray circular dichroism as a probe of orbital magnetization, Phys. Rev. Lett. 68 (1992) 1943–1946

[18] P. Carra, B.T. Thole, M. Altarelli, X. Wang, X-ray circular dichroism and local magnetic fields, Phys. Rev. Lett. 70 (1993) 694–697

[19] R. Wu, A.J. Freeman, Limitation of the magnetic-circular-dichroism spin sum rule for transition metals and importance of the magnetic dipole term, Phys. Rev. Lett. 73 (1994) 1994–1997

[20] M. Balli, P. Fournier, S. Jandl, S. Mansouri, A. Mukhin, Y. V Ivanov, A. M. Balbashov, Comment on "Giant anisotropy of magnetocaloric effect in TbMnO3 single crystals", Phys. Rev. B 96 (2017) 146401

[21] T.-R. Chang, H.-T. Jeng, C.-Y. Ren, C.-S. Hsue, Charge-orbital ordering and ferroelectric polarization in multiferroic TbMn${ }_{2}$O${ }_{5}$ from first principles, Phys. Rev. B 84 (2011) 24421

[22] I.M. Band, K.A. Kikoin, M.B. Trzhaskovskaya, D.I. Khomskii, Atomic mechanisms for the appearance of mixed valence states in lanthanides and actinides Zh, Eksp. Teor. Fiz. 94 (1988) 79–95.

[23] N. Metropolis, A.W. Rosenbluth, M.N. Rosenbluth, A.H. Teller, E. Teller, Equation of state calculations by fast computing machines, J. Chem. Phys. 21 (1953) 1087–1092

[24] Jens Jensen, Allan R. Mackintosh, Rare Earth Magnetism, 1991

[25] Hur, N.; Park, S.; Sharma, P.A.; Guha, S.; Cheong, S.W. Colossal Magnetodielectric Effects in DyMn2 O5 , Phys. Rev. Lett. 2004, 93, 107207

[26] Hur, N.; Park, S.; Sharma, P.A.; Ahn, J.S.; Guha, S.; Cheong, S.W. Electric polarization reversal and memory in a multiferroic material induced by magnetic fields. Nature 2004, 429, 392–395.

[27] Balli, M.; Jandl, S.; Fournier, P.; Gospodinov, M.M. Anisotropy-enhanced giant reversible rotating magnetocaloric effect in HoMn2O5 single crystals. Appl. Phys. Lett. 2014, 104, 232402.

[28] J. W. Kim, S. Y. Haam, Y. S. Oh, et al. "Observation of a multiferroic critical end point." In: Proc. Natl. Acad. Sci. 106.37 (2009), pp. 15573–15576.

[29] N. Hur, S. Park, P. A. Sharma, et al. "Colossal Magnetodielectric Effects in DyMn2O5 ." In: Phys. Rev. Lett. 93.10 (2004), p. 107207

[30] S. Chattopadhyay, S. Petit, E. Ressouche, et al. "3d-4f coupling and multiferroicity in frustrated Cairo Pentagonal oxide DyMn2O5 ." In: Sci. Rep. 7.1 (2017), p. 14506

[31] N. Hur, S. Park, P. A. Sharma, et al. "Colossal Magnetodielectric Effects in DyMn2O5 ." In: Phys. Rev. Lett. 93.10 (2004), p. 107207.

[32] G. Yahia, F. Damay, S. Chattopadhyay, et al. "Recognition of exchange striction as the origin of magnetoelectric coupling in multiferroics." In: Phys. Rev. B 95.18 (2017), p. 184112.

[33] Y. Koyata and K. Kohn. "Low-temperature phase transition in ErMn2O5 ." In: Ferroelectrics 204.1 (1997), pp. 115–124

[34] Y. Koyata, H. Nakamura, N. Iwata, et al. "Electric and Magnetic Low-Temperature Phase Transitions of YbMn2O5 ." In: J. Phys. Soc. Japan 65.5 (1996), pp. 1383–1386.

[35] N. Lee, C. Vecchini, Y. J. Choi, et al. "Giant tunability of ferroelectric polarization in GdMn2O5 ." In: Phys. Rev. Lett. 110.13 (2013), pp. 2–5.

[36] Jin, J.L.; Zhang, X.Q.; Li, G.K.; Cheng, Z.H.; Zheng, L.; Lu, Y. Giant anisotropy of magnetocaloric effect in TbMnO3 single crystals. Phys. Rev. B 2011, 83, 184431

[37] Jin, J.L.; Zhang, X.Q.; Ge, H.; Cheng, Z.H. Rotating field entropy change in hexagonal TmMnO3 single crystal with anisotropic paramagnetic response. Phys. Rev. B 2012, 85, 214426

[38] A. Midya, P. Mandal, S. Das, S. Banerjee, L. S. S. Chandra, V. Ganesan, and S. R. Barman, Appl. Phys. Lett. 96, 142514 (2010).

[39] T. Samanta, I. Das, and S. Banerjee, Appl. Phys. Lett. 91, 152506 (2007).

[40] W. J. Hu, J. Du, B. Li, Q. Zhang, and Z. D. Zhang, Appl. Phys. Lett. 92, 192505 (2008).

[41] Wagh, A.A.; Suresh, K.G.; Kumar, P.A.; Elizabeth, S. Low temperature giant magnetocaloric effect in multiferroic GdMnO3 single crystals. J. Phys. D 2015, 48, 135001.

[42] Balli, M.; Jandl, S.; Fournier, P.; Mansouri, S.; Mukhin, A.; Ivanov, Y.V.; Balbashov, A.M. On the magnetocaloric effect in the multiferroic hexagonal DyMnO3 single crystals. J. Magn. Magn. Mat. 2015, 374, 252–257

[43] Balli, M.; Roberge, B.; Jandl, S.; Fournier, P.; Palstra, T.T.M.; Nugroho, A.A. Observation of large refrigerant capacity in the HoVO3 vanadate single crystal. J. Appl. Phys. 2015, 118, 073903.

[44] Alonso, J. A., Casais, M. T., Martínez-Lope, M. J., Martínez, J. L., & Fernández-Díaz, M. T. (1997). A structural study from neutron diffraction data and magnetic properties of (R = La, rare earth). Journal of Physics: Condensed Matter, 9(40), 8515–8526.

[45] Bouhani, H.; Endichi, A.; Zaari, H.; Benyoussef, A.; Hamedoun, M.; Balli, M.; El kenz, A.; Mounkachi, O. On the origin of the giant magnetocaloric effect in HoMn2O5 single crystals: First principles study and Monte Carlo simulations. Mat. Chem. Phys. 2019, 231, 366–371.

Chapter 5

General conclusions and future challenges

During the United Nations conference on climate change Paris 2015, the world leaders negotiated to limit climate warming to less than 2řC by 2100. The discussions aimed at avoiding the serious climatic catastrophes in the world and the participants sought to retard greenhouse effect by increasing the use of technologies with zero carbon. One of theses technologies is the magnetic refrigeration which is an emergent, innovating and potentially low carbon technology. In this thesis, we have experimentally and theoretically investigated the potential of oxide-based materials for magnetic refrigeration application. First, we aimed at gaining insights into the underlying mechansim of the magnetic refrigeration based on the magnetocaloric effect (MCE). Second, we were interested in exploring the magnetic and magnetocaloric effect in highly frustrated RVO_3 multiferroics oxide thin films as well as investigating the physics behind the recent giant rotary MCE observed recently in $RMn2O_5$ family. We present here a summary of the results obtained in this thesis.

Recently, The magnetocaloric effect in manganite-based perovskites exhibiting multiferroic behaviors have become an interesting topic because of the potential application of these oxides in some specific applications such as the liquefaction of hydrogen and and space industry. These manganite perovskites oxides fulfill the necessary conditions for practical applications as they unveil a large corrosion resistance, high eletric resistance, low hysteresis and mechanical stability, On the contrary, the magnetocaloric potential of the RVO_3 vanadates has not yet been explored except for the bulk $HoVO_3$. However, perovskite-type vanadium oxides RVO_3 display a great variety of phase transitions associated with a series of charge, spin and orbital ordering phenomena making them interesting candidates from a magnetocaloric point of view. Today's research activity in magnetic

refrigeration is focused more on the exploration of micro and nanostructuring in order to open a wide range of new applications such as ,as on-chip magnetic cooling of a nano-electronic device and sensor technology. This in particular motivated us to investigate the MCE in RVO_3 thin films since their behavior strongly depends on the cooperative nature of the Jahn-Teller distortion making them sensitive to strain effects including the induced biaxial strain due to the lattice mismatch between the substrate and the film. Such structural effects tends to play an important role in tuning the film properties. In this work, we mainly focused on exploring and tuning the magnetic and magnetocaloric properties of high quality epitaxial $PrVO_3$ (PVO) thin films by applying a compressive strain via a proper choice of substrate.

Despite the fact that the magnetism of $PrVO_3$ in its bulk form is quit complex and shows unusual features at low temperatures such as stairlike behavior in the hysteresis loops with a high coercivity that reach 2.4 T as well as, a relatively high values of remanent magnetization (M_r) and low values of saturation magnetization (M_s) being less viable from a magnetocaloric point of vue, we have demonstrated that the magnetic and magnetocaloric properties $PrVO_3$ compounds can be easy tailored by using the thin films approach giving rise to giant magnetocaloric effect at low temperatures regime in compressively strained thin films.

It was shown in previous studies that monitoring the concentration of oxygen vacancies in PVO perovskite thin films through the controle of deposition parameters can produce a substantial macroscopic tensile strain which affects the exchange interactions manisfesting in a nontrivial evolution of Néel temperature in a range of 30 K. Hence, we studied the effect of size and physical strain induced by the substrat on magnetic and magnetocaloric properties of highly epitaxial PVO films. First, we have grown a 100 nm thick of PVO/STO using pulsed laser deposition. Magnetic measurements shows a hard ferromagnetic behabvior at low temperatures and the hysteresis is characterized by a large coercivity of 2.8 T and low saturation magnetization. We observed a decrease of T_N compared to bulk PVO ($T_N \simeq 140$ K) being 85 K which could be explained by the distortion of the film lattice caused by the oxygen vacancies while no recognizable anisotropy can be seen in our measurements.

Further, We have deposited PVO film on a (001)-oriented LSAT substrate with a thickness of 41,7 nm. Suprisingly, a strong magnetic anisotropy is observed together with a significant increase in M_s from 0.291 μ_B/f.u at 10 K observed in 100 nm thick PVO/STO to 1.89 μ_B/f.u in PVO /LSAT films under amagnetic field applied within the sample plan, as well as a decrease in M_r and most importantly, a markedly decrease in H_c from 2.4 T observed in PVO films deposited on STO to reach only 0.1 T at 10 K. More surprisingly,

the coercive field decreases dramatically at 3 K reaching only 0.05 T for magnetic fields applied within the films plane while M_s reachs its high value of 4.86 $\mu_B/f.u$ at 3 K (H//). This inform us on the contribution of both $Pr^{3+}$and V^{3+}ions to the whole magnetization suggesting that all the praseodymium and vanadium moments are fully aligned parallel to the magnetic field.

Magnetic isotherms collected under magnetic fields going from 0 up to 6 T at different temperatures to understand the evolution of the magnetization and the entropy change with the application of magnetic field in PVO films revealing a metamagnetic phase transition from an antiferromagnetic to a ferromagnetic configuration of spins at temperatures below 30 K as a result of a strong competition between Pr 4f and V 3d spins. For PVO/STO, it was difficult to calculate the MCE because of the overlap between M vs H curves and the small magnetic signal at low temperatures. The temperature dependence of the magnetic entropy change unveils larger values at very low temperature for PVO/LSAT films that reach roughly $-\Delta S_M$ = 56.7 J/(kg.K) for a magnetic field changing from 0 to 6 T applied in the sample plane. In a similar field change applied of plane, is slightly lower and found to be about 52.7 J/(kg.K) when subjected to an out-of plane magnetic field. Also, the magnetic entropy change shows a large magnetocaloric effect under relatively low magnetic fields that can be easily reached via permanent magnets. In the magnetic field change of 2 T applied within and out of thin films plane, $-\Delta S_M$ reaches 19.5 and 16.3 J/(kg.K), respectively.

Theoretical calculations were also perfored in order to gain more insight into the microscopic properties of the thin films. Density functional theory calculations confirms the ground state and the competition between the magnetic interactions when the films are under compressive strain for two different orientations. First, we preserve the bulk Pbnm symmetry for a growth along [001] direction where the two lattice vectors of the orthorhombic unit cell lie within the substrate plane. We adopt a second growth along the orthorhombic [110] direction where the compressive constraint lower the symmtery to $P2_1/m$ resulting in monoclinic unit cell which we found to be clearly preferable by comparing the total energy difference between the two symmetries yielding a G-type spin ordering for PVO grown on both LSAT and STO substrates.

Our result not only suggests that epitaxial PVO thin films present a non-negligible potential is for refrigeration at cryogenic temperatures but may also pave the way for new applications taking for example advantage of the possibility to tailor the magnetic coercivity in PVO thin films and exploiting multiple instabilities in strongly correlated materials to explore new magnetocaloric materials. However, we are aware that the reported entropy change values in PVO thin films are too large when compared to the best

magnetocaloric materials working in a similar working temperature range. The necessary was done to reasonably evaluate the MCE in term of the entropy change by considering the impact of hysteretic phenomena. However, in order to accurately estimate DS, the measurements of specific heat in equilibrium conditions are highly required. This point will be certainly addressed in the future

On the other hand, we have theoretically investigated the electronic, magnetic and magnetocaloric properties of $HoMn_2O_5$ single crystals which is another oxide of RMn_2O_5 family using First prinples calculations and Monte Carlo simulation. The DFT study reveal that the saturation magnetization reaches it maximum following the easy axis b. The same calculations show that the main contribution to the MCE comes from Ho ions by performing XMCD spectrum calculations. The MCE effect in the material is studied based on Monte Carlo simulation giving similar results compared to experimental study. These results contribute to a deeper understanding of the physics behind the giant magnetocaloric effect in $HoMn_2O_5$ single crystals confirming that the use of the intrinsic anisotropic properties is a promising way to optimize the MCE for magnetic refrigeration application at low temperature regime as well as the implementation of compact and efficient rotary magnetic refrigerators.

Publications

- Engineering the magnetocaloric effect of epitaxial oxide thin films by strain effects, H.Bouhani et al, Applied Physics Letters Vol 117, 2020.
- On the origin of the giant magnetocaloric effect in $HoMn_2O_5$ single crystals: First principles study and Monte Carlo simulations, H.Bouhani et al, Materials and Chemistry of Solids, Vol 231, 2019
- Magnetocaloric effect in ternary ErAgAl: Ab initio, mean field and Monte Carlo approaches, H.Bouhani et al, Results in Physics Vol 10, 2018.
- Electronic and magnetic properties of the multiferroic $TbMn_2O_5$, A. ENDICHI et al, Applied Physics A, Vol 126, 410. 2020.

Résumé en Francais

Couches minces à base d'oxyde multiferroïque appliquées à la réfrigération magnétique

Lors de la conférence des Nations Unies sur le changement climatique Paris 2015, les dirigeants mondiaux se sont engagées à prendre des mesures ambitieuses pour maintenir le réchauffement climatique à moins de 2°C d'ici 2100. Les discussions visaient à éviter les graves catastrophes climatiques dans le monde et les participants ont cherché à limiter les gaz à effet de serre en augmentant l'utilisation de technologies à zéro carbone. L'une de ces technologies est la réfrigération magnétique qui est une technologie émergente, innovante et potentiellement à faible émission de carbone. Dans cette thèse, nous avons étudié expérimentalement et théoriquement le potentiel des matériaux à base d'oxyde multiferroïque pour l'application de la réfrigération magnétique. Tout d'abord, nous avons cherché à comprendre le mécanisme de la réfrigération magnétique basée sur l'effet magnétocalorique (EMC) et a discuter les différents défis à relever avant d'avoir des dispositifs qui sont compétitifs avec des réfrigérateurs à compression de vapeur. Deuxièmement, nous nous intéressions à l'exploration et l'amélioration de l'effet magnétique et magnétocalorique dans des films minces d'oxyde multiferroique RVO_3 fortement corrélés à structure pérovskite déposés par ablation laser, ainsi qu'à l'étude de la physique derrière l'EMC rotatif géant observé récemment dans la famille RMn_2O_5. Nous présentons ici un résumé des résultats obtenus dans cette thèse.

Récemment, l'effet magnétocalorique dans les perovskites à base de manganite présentant un comportement multiferroïque est devenu un sujet intéressant dans la technologie de la réfrigération magnétique à trés basse température comme la technologie cryogénique, la liquéfaction de l'hydrogène et la recherche en science spatiale. Ces oxydes de perovskites de manganite remplissent les conditions nécessaires pour des applications pratiques car ils dévoilent une grande résistance à la corrosion, une résistance élétrique élevée, une faible hystérèse et une stabilité mécanique. Au contraire, le potentiel magnétocalorique des vanadates RVO_3 n'a pas encore été explorée, à l'exception de $HoVO_3$ dans son état massif. Cependant, les oxydes de vanadium de type perovskite présentent une grande variété de transitions de phase associées à une série de phénomènes de charge, de spin et d'ordre orbitale ce qui en fait des candidats intéressants d'un point de vue magnétocalorique.

L'activité de recherche d'aujourd'hui dans la réfrigération magnétique portent principalement sur les structures en couches minces en vue de créer de nouveaux domaines d'applications tels que la microréfrigération, les pompes microfluidiques et les dispositifs multiferroiques ce qui nous a particulièrement motivé pour enquêter sur l'EMC dans les films minces RVO_3 puisque leur comportement dépend fortement de la nature coopérative de la distorsion Jahn-Teller qui les rend sensibles à la déformation. Ces effets de structure ont tendance à jouer un rôle important dans l'amélioration des propriétés magnétocaloriques des film minces. Par conséquent, nous nous sommes concentrés principalement sur l'exploration et l'amélioration des propriétés magnétiques et magnétocaloriques des films minces de $PrVO_3$ en appliquant une contrainte de compression par l'intermédiaire d'un bon choix de substrat ainsi que l'étude de l'effet de taille sur ces proprietés.

Malgré le fait que le magnétisme de $PrVO_3$ (PVO) dans son état massif est bien complexe et montre des caractéristiques inhabituelles à basse température comme l'évolution

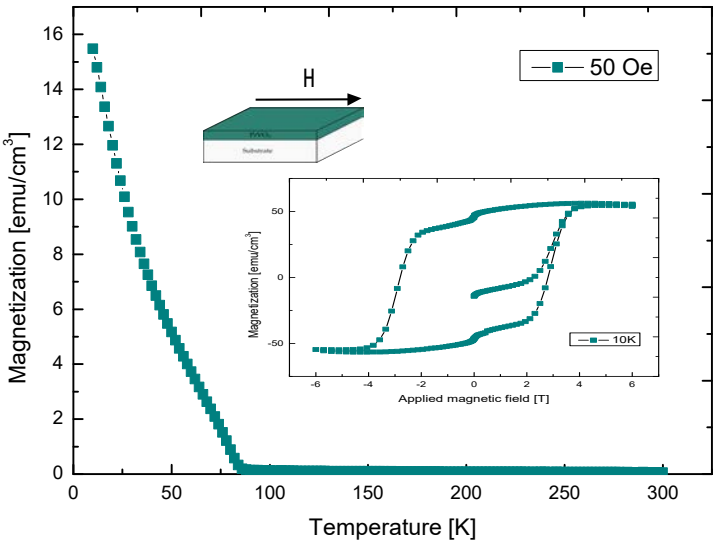

Figure 5.1: Magnetization dependence of temperature for PVO film on STO substrate performed at an in-plane applied magnetic field of 50 Oe. Inset displays the magnetic hysteresis loops measured at 10 K after substracting the diamagnetic contribution of the substrate and the holder.

en escalier des boucles d'hystérésis avec une forte coercivité qui atteint 2,4 T en raison du ń pinning ż des parois de domaines ainsi que des valeurs relativement élevées de l'aimantation rémanente M_r et de faibles valeurs de l'aimantation de saturation M_s les rendant moins viables pour desapplications de la réfrigération magnétique, nous avons démontré que le magnétisme et les propriétés magnétocaloriques des composés PVO peuvent être facilement modulées en utilisant l'approche des couches minces donnant lieu à un effet magnétocalorique géant à trés basses températures dans des films minces en compression.

Il a été démontré dans des études précédentes que le controle de la concentration des sites vacants d'oxygène dans les films minces perovskite (PVO) à travers le contrôle des paramètres de dépôt peut produire une contrainte macroscopique importante qui affecte les interactions d'échange qui se manifeste par une évolution non triviale de la température de Néel dans une gamme de 30 K. Par conséquent, nous avons étudié l'effet de la taille et la contrainte physique induite par le substrat sur les propriétés magnétiques et

magnétocaloriques de films minces épitaxiés. Tout d'abord, nous avons déposé un film mince de 100 nm d'épaisseur de PVO sur un subtrat STO par ablation laser pulsée. Les mesures magnétiques montrent un comportement ferromagnetique dur à basse température accompagné par une grande coercivité de 2,8 T et une faible aimantation à saturation, comme le montre la figure 5.1. Nous avons observé une diminution de T_N par rapport au PVO en état massif ($T_N \simeq 140$ K) étant de 85 K, ce qui pourrait s'expliquer par la distorsion du réseau cristallin du film causée par les sites vacants de l'oxygen. Aucune anisotropie reconnaissable ne peut être vu dans nos mesures.

En outre, nous avons déposé une couche de PVO sur un substrat LSAT orienté (001) d'une épaisseur de 41,7 nm. Étonnamment, une forte anisotropie magnétique est observée avec une augmentation significative de M_s de 0.291 μ_B/f.u à 10 K observé dans PVO/STO à 1.89 μ_B/f.u dans les films PVO /LSAT pour un champ magnétique appliqué dans le plan de l'échantillon (voir figure 5.2), ainsi qu'une diminution de M_r et, surtout, une diminution marquée deH_c de 2,4 T observés dans les films minces de PVO/STO pour atteindre seulement 0,1 T à 10 K. Plus surprenant, le champ coercitif diminue considérablement à 3 K atteignant seulement 0,05 T pour les champs magnétiques appliqués dans le plan des films tandis que M_s atteint sa valeur élevée de 4.86μ_B/f.u à 3 K (H//). Cela nous informe sur la contribution des deux ions Pr^{3+}et V^{3+} à l'ensemble de l'aimantation suggérant que tous les moments de praseodymium et de vanadium sont entièrement alignés parallèlement au champ magnétique.

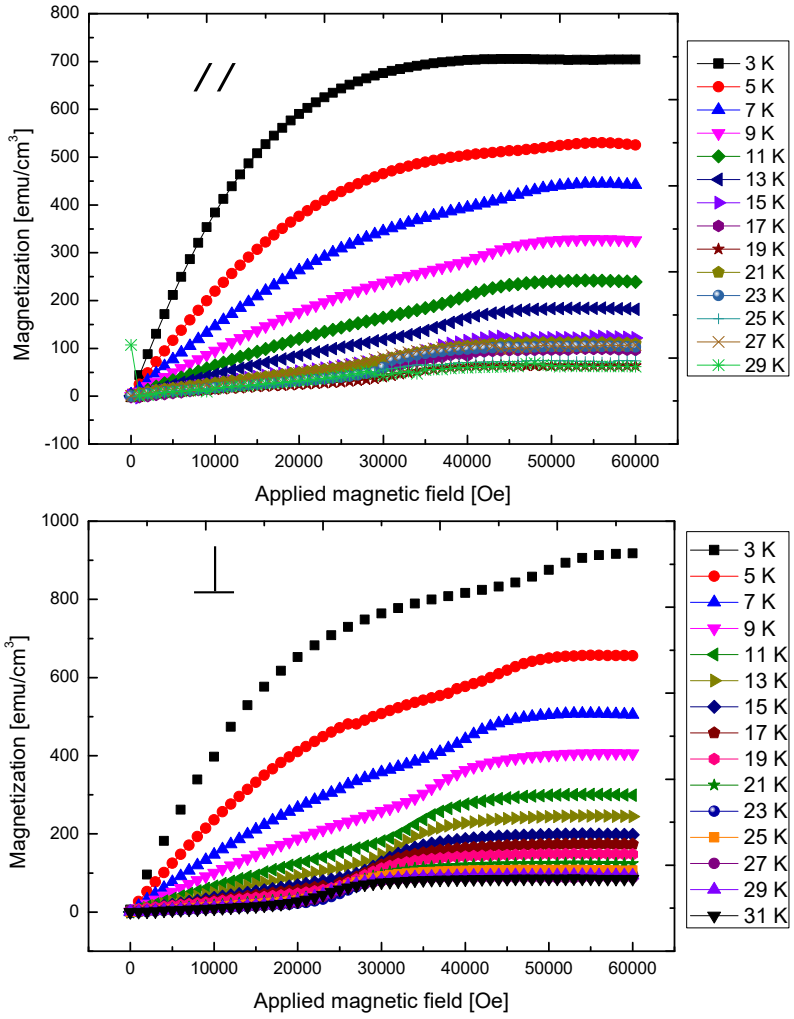

Figure 5.2: Magnetization isotherms of PVO film deposited on a (001)-oriented LSAT substrate in the temperature range of 3-30 K with an interval of 2 K when a magnetic field is applied in and out of the sample plane. . Each loop was measured after a 30K excursion above T_N to ensure that the demagnetization of the sample is successful and corrected for diamagnetic background signal.

L'aimantation isothermale jusqu'à 6 T à une température différente a été mesurée afin de comprendre l'évolution de la l'aimantation et le changement d'entropie avec l'application du champ magnétique dans les films PVO révélant une transition de phase métamagnétique d'une configuration de spins antiferromagnetique à une configuration ferromagnetique à des températures inférieures à 30 K comme le montre la figure 2,en raison de la forte compétition entre les spins de la couche 4f de Praseodymium et ceux de la

couche 3d de Vanadium. Pour PVO/STO, il était difficile de calculer l'EMC en raison du chevauchement entre les courbes M vs H et le faible signale magnétique à basse températures. L'évolution de la variation de l'entropie magnétique en fonction de la température révèle des valeurs élevées à basse température pour les films minces de PVO/LSAT qui atteignent environ $-\Delta S_M = 56.7$ J/(kg.K) pour un changement de champ magnétique de 0-6 T appliqué dans le plan d'échantillon et 52,7 J/(kg. K) lorsqu'il est soumis à un champ magnétique appliqué hors du plan comme le montre la figure 5.3. En outre, le changement magnétique entropie montre un grand effet magnétocalorique dans des champs magnétiques relativement faibles qui peuvent être facilement accessible par des aimants permanents. Pour un champ magnétique de 2 T appliqué // et $\perp$, l'entropie magnétique atteint 19,5 et 16,3 J/(kg. K), respectivement.

Des calculs théoriques ont également été perfomrés afin d'obtenir une meilleure compréhension des propriétés microscopiques des couches minces. Les calculs de la théorie de la fonctionnelle de la densité confirment l'état fondamental et la compétition des interactions magnétiques par la contrainte en compression pour deux orientations différentes. D'abord, nous préservons la symétrie de Pbnm pour une croissance le long de la direction [001] où les deux vectros le la maille unitaire orthorhombique se trouvent dans le plan de substrat (voir la figure 5.4).

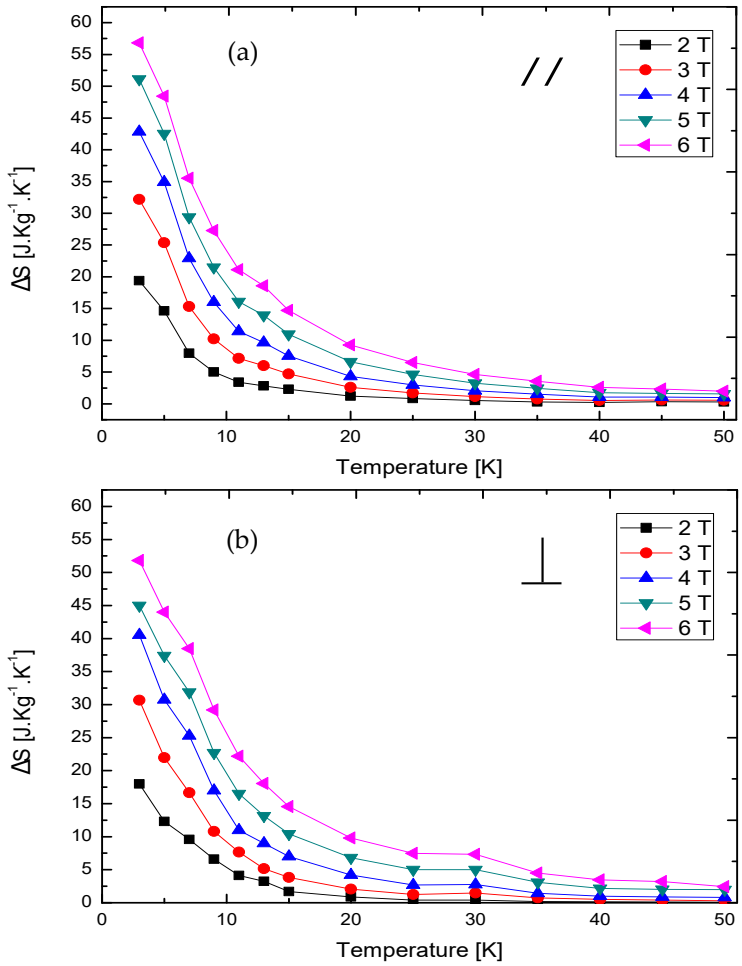

Figure 5.3: Temperature dependence of magnetic entropy change obtained by integrating the Maxwel Relation with a magnetic field varying from 2 to 6 T applied in-plane (a) and out-of-plane of the sample (b) for PVO deposited on LSAT substrate

.Nous adoptons une deuxième croissance le long de la direction orthorhombic [110] où la contrainte en compression ce qui brise la symétrie à $P2_1/m$ (cellule monoclinique) que nous avons trouvé clairement préférable en comparant la différence totale d'énergie des deux orientations donnant un ordre de spin de type G pour PVO deposé sur les deux substrats.

Notre résultat suggère non seulement que les couches minces épitaxiales de PVO sont potentielles pour la réfrigération aux températures cryogéniques mais peuvent également ouvrir la voie à créer de nombreuses nouvelles fonctionnalités dans les oxydes perovskite

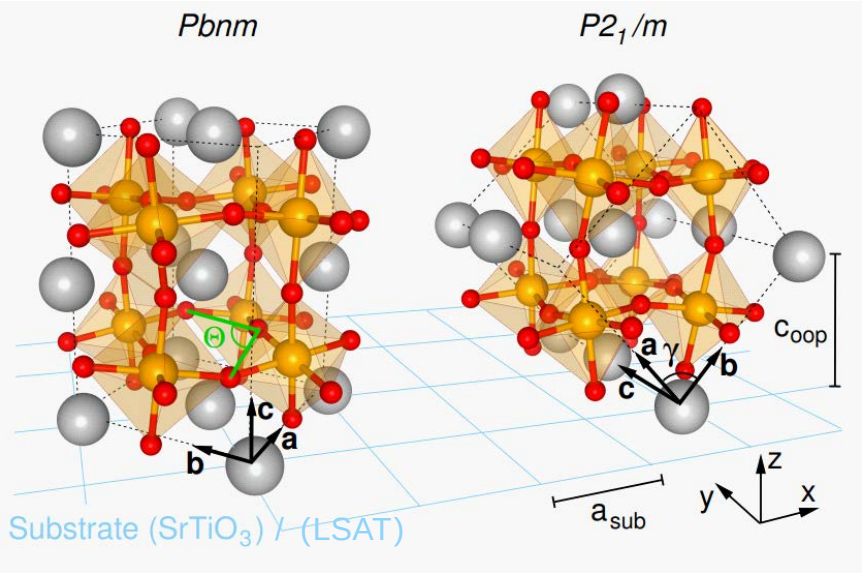

Figure 5.4: Schematic depiction of two different orientations of the bulk crystal structure of $PrVO_3$ relative to a hypothetical square lattice substrate , corresponding to the [001] (left) and the [110] (right) P bnm growth directions. The respective unit cells (dashed lines) and their basis vectors, a, b, and c, are indicated. The gray, golden, and red spheres refer to Pr, V, and O atoms, respectively.

par le contrôle des aspects structurels et exploiter plusieurs instabilités des matériaux fortement corrélés pour la découverte de nouveaux matériaux magnétocaloriques. Cependant, nous sommes conscients que les valeurs de la variation d'entropie rapportées dans les films minces de $PrVO_3$ sont trop grandes par rapport aux meilleurs matériaux magnétocaloriques travaillant dans une gamme de température de travail similaire. Le nécessaire a été fait pour évaluer raisonnablement l'effet magnétocalorique en terme de ΔS_M en considérant l'impact des phénomènes d'hystérèsis. Toutefois, afin d'estimer avec précision la variation de l'entropie magnétique, les mesures de chaleur spécifique dans des conditions d'équilibre sont très nécessaires. Ce point sera certainement abordé dans l'avenir. Ainsi, nous sommes entrain de développer un modèleăthéorique qui décrit le mieux le système en introduisant l'aspect non colinéaire dans l'hamiltonien du système qui nous permettra ensuite, d'étudier les propriétés magnétique et magnétocaloriques des couches minces de $PrVO_3$ăpar la simulation Monte Carlo ainsi que pour d'autres vanadates dont

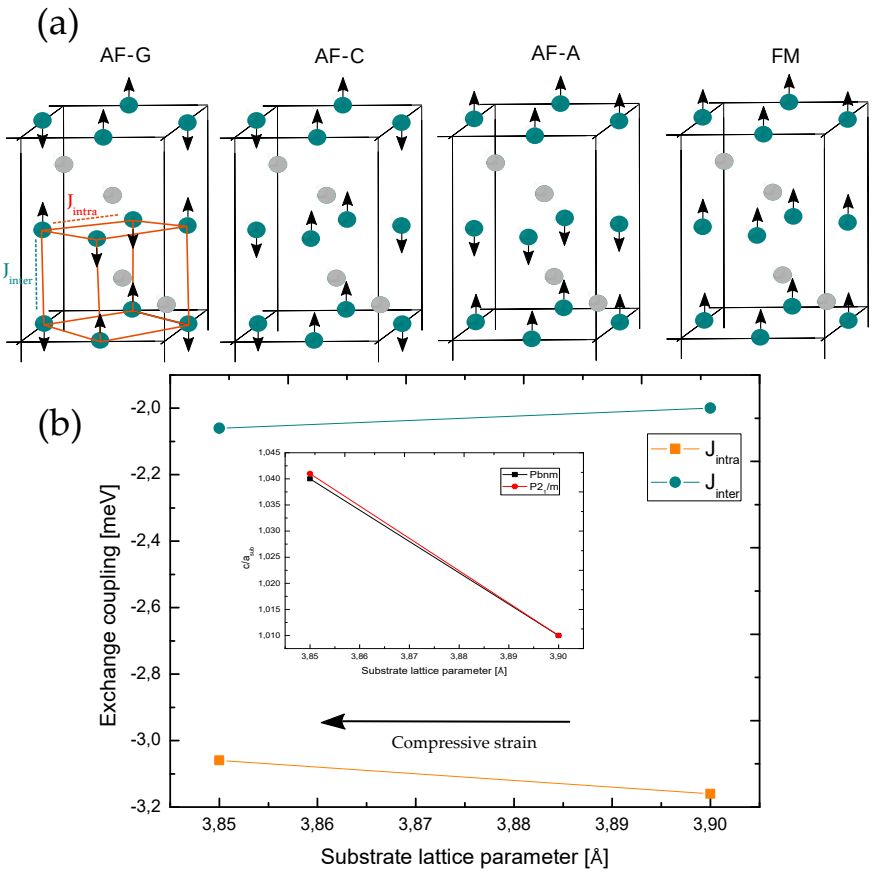

Figure 5.5: The distorted perovskite magnetic structure of $PrVO_3$, in which the pseudocubic cell is shown by orange lines. Four magnetic structures are schematically shown: Ferromagnetic (FM), antiferromagnetic C-type, antiferromagnetic G-type and antiferromagnetic A-type. The grey and green spheres represent Pr and V atoms, respectively

le moment magnétique est plus grand telles que le $GdVO_3, TbVO_3$et le $HoVO_3$.

D'autre part, nous avons théoriquement étudié les propriétés électroniques, magnétiques et magnétocaloriques des mono-cristaux $HoMn_2O_5$ qui est un autre oxyde multifferoique de la famille RMn_2O_5 en utilisant les calculs DFT et la simulation de Monte Carlo. L'étude DFT révèle que l'aimantation à saturation atteint son maximum suivant l'axe de facile aimantation b en comparant l'énergie relative aux différentes directions. Les calculs de la densité d'états et de spectre XMCD montrent que la principale contribution au magnétisme provient des ions Ho. De plus, l'effet MCE dans le matériau est étudié à l'aide de la simulation Monte Carlo. La valeure de l'entropie magnétique pour

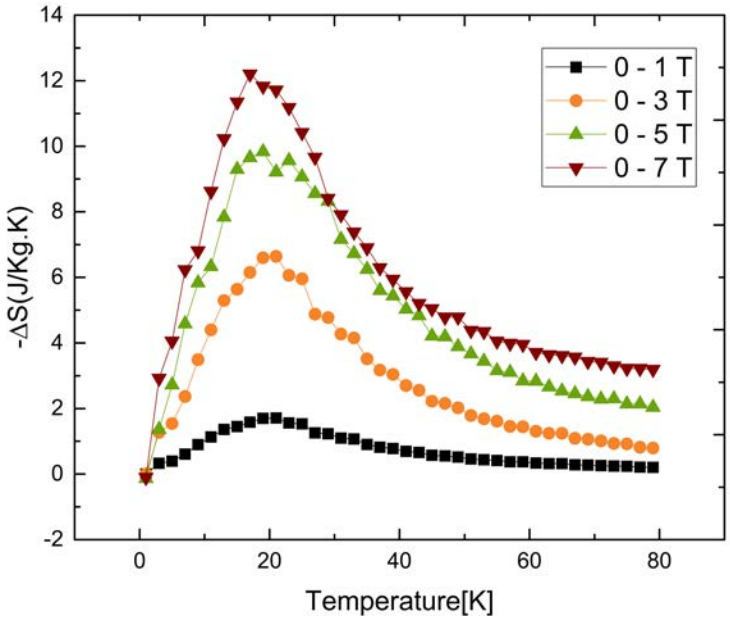

Figure 5.6: Temperature dependence of magnetization following y axis for HoMn2O5 (b) Isothermal magnetic entropy change for different applied mag- netic field along the same axis.

un champ magnétique qui varie entre 0 et 7 T est de 12.20 J/(kg,K) à 18 K comme le montre la figure 5.6, proche de la valeure expérimentale rapportée dans la littérature.

Ces résultats contribuent à une compréhension plus profonde de la physique derrière l'effet magnétocalorique géant dans les mono-cristaux $HoMn_2O_5$, confirmant que l'utilisation des propriétés anisotropes intrinsèques est un moyen prometteur pour optimiser le EMC pour la réfrigération magnétique à trés basse température ainsi que la mise en ¡uvre de réfrigérateurs magnétiques rotatifs compacts et efficaces.